Causal Tracking Control of a Non-Minimum Phase HIL Transmission Test System

Wang, Pengfei

Award date:
2009

Awarding institution:
University of Bath

CAUSAL TRACKING CONTROL OF A NON-MINIMUM PHASE HIL TRANSMISSION TEST SYSTEM

Pengfei Wang

A thesis submitted for the degree of Doctor of Philosophy

University of Bath
Department of Mechanical Engineering

December 2009

Summary

The automotive industry has long relied on testing powertrain components in real vehicles, which causes the development process to be slow and expensive. Therefore, hardware in the loop (HIL) testing techniques are increasingly being adopted to develop electronic control units (ECU) for engine and other components of a vehicle.

In this thesis, HIL testing system is developed to provide a laboratory testing environment for continuously variable transmissions (CVTs). Two induction motors were utilized to emulate a real engine and vehicle. The engine and vehicle models, running in real-time, provide reference torque and speed signals for input and output dynamometers, respectively. To design torque and speed tracking controllers, linear models of the motor and drive systems were firstly identified from the test results. Feedforward controllers were then designed according to the inverse dynamics of the identified models. Because of the existence of unstable zeros in the model, design effort was focused on the stability and causality of the inverse process. Digital preview filters were formulated to approximate the stable inverse of unstable zeros as part of the feedforward controller. Normally, future information of input trajectory is required when implementing the digital preview filters, which makes the feedforward controller non-causal. Since the engine and vehicle model require current information to calculate the next output and no future value can be provided in advance, the application of non-causal digital controllers was limited. A novel method is proposed here to apply non-causal digital controllers causally. Robustness of the controllers is also considered when the two motors are coupled and the gear ratio between them was changed.

The proposed coupled control method was tested and verified experimentally by using a manual gearbox before recommending its use for a CVT testing. A multi-frequency test signal as well as simulation results of a whole vehicle model were used as torque and speed demand signals in the experiments. A HIL testing case was also presented. Frequency and time domain results showed the effectiveness of the

method under both testing procedures to fully compensate for the dynamics of both actuators.

Acknowledgements

I would like to give my appreciation to everyone who has been supporting me in all these three tough years.

Very special thanks to my supervisors Dr. Necip Sahinkaya and Dr. Sam Akehurst. I can never finish my PhD without your expertise, guidance and patience.

Many thanks to the technicians for your assistance on the test rig.

谨以此论文献给我最亲爱的父母，你们的支持和信任永远是我最大的动力。

Contents

Notations

A	Vehicle frontal area
$\mathbf{A}$	Matrix as a function of θ
$\mathbf{A}_1, \mathbf{A}_2$	Matrices calculated from the weighting function w
A_k	Amplitude of harmonic component
B_I	Combined damping ratio of input dynamometer and shaft
B_M	Motor damping ratio
B_N	Nominal damping ratio
B_O	Combined damping ratio of output dynamometer and shaft
$\mathbf{C}$	Vector of transfer function coefficients
C_D	Drag coefficient
D	Number of preview steps required for feedforward controller
$DPF(z^{-1})$	Transfer function of digital preview filter
$DPF_A(z^{-1})$	Transfer function of digital preview filter for gain compensation
$DPF_\Phi(z^{-1})$	Transfer function of digital preview filter for phase compensation
F	Complex measurement variable
$\mathbf{F}_L$	Measurement vector used in the Least Square Estimation
F_t	Engine driving force
$G(s)$	Continuous-time transfer function of the plant
$G_{close}(s)$	Continuous-time transfer function of closed loop speed control
$G_{I\_Dyno}(s)$	Motor and drive system transfer function of input dynamometer
$G_{O\_Dyno}(s)$	Motor and drive system transfer function of output dynamometer
$G_{PID}(s)$	Transfer function of PID controller
$G_{Ratio\_cmp}(s)$	Transfer function of gear ratio compensator
$G_{Speed}(s)$	Transfer function of output dynamometer speed control

$G_{Torque}(s)$	Transfer function of input dynamometer torque control
$H(z^{-1})$	Discrete-time transfer function of the plant
$H_a(z^{-1})$	Stable (acceptable) part of $H(z^{-1})$
$H_{Close}(z^{-1})$	Discrete-time equivalent of $G_{close}(s)$ with ZOH
$H_{M\&L}(z^{-1})$	Discrete-time equivalent of $G_{O\_Dyno}(s) \times L_{O\_Dyno}(s)$ with ZOH
$H_{PID}(z^{-1})$	Discrete-time equivalent of $G_{PID}(s)$ with ZOH
$H_{Speed}(z^{-1})$	Discrete-time equivalent of $G_{Speed}(s)$ with ZOH
$H_{Torque}(z^{-1})$	Discrete-time equivalent of $G_{Torque}(s)$ with ZOH
$H_u(z^{-1})$	Unstable (unacceptable) part of $H(z^{-1})$
J_I	Combined inertia of input dynamometer and shaft
J_M	Motor inertia
J_N	Nominal inertia
J_O	Combined inertia of output dynamometer and shaft
J_{Sh}	Shaft inertia
K	Number of frequency components
$L_{I\_D\&Shs}(s)$	Load transfer function of input dynamometer and shafts
$L_{I\_Dyno}(s)$	Load transfer function of input dynamometer
$L_{I\_Shaft}(s)$	Load transfer function of input shaft
$L_{O\_Dyno}(s)$	Load transfer function of output dynamometer
$L_{O\_Shaft}(s)$	Load transfer function of output shaft
N	Number of preview steps for $DPF(z^{-1})$
P	Number of unstable zeros in $H(z^{-1})$
P_1, P_2	Number of real and complex zeros in $H(z^{-1})$
P_k	Ratio of power to the total power
$Q(z^{-1})$	Transfer function of feedforward controller
R	Relative order of the estimated transfer function $(m-n)$
R^2	Goodness of fit measurement
$R(s)$	Generic output signal

$R(z^{-1})$	Ratio transfer function
T_g	Generated torque
T_m	Measured torque
T_s	Sampling time
$Y(s)$	Generic output signal
$\mathbf{Z}$	Complex measurement vector for a single frequency
$\mathbf{Z}_L$	Measurement matrix used in the Least Square Estimation
a	Vehicle acceleration
a_i	Parameters for denominators of the estimated transfer function
b_i	Parameters for numerators of the estimated transfer function
e	Residual
g	Gravity acceleration
i, k	Integers
m	Order of the denominator of the estimated transfer function
m_v	Vehicle mass
n	Order of the numerator of the estimated transfer function
p	Number of data points
p_k	Power spectrum
q	Number of estimated coefficients
r	Plant input signal
r_c	Rolling resistance coefficient
s	Laplace transform operator
v	Residual degrees of freedom
v_v	Vehicle speed
w	Weighting function
y	Plant output signal
y_d	Desired signal
y_f	Delayed output signal
z	Discrete z-transform operator

z_i	Unstable zeros
$\Gamma(\alpha,\lambda)$	Lagrange transfer function
$\boldsymbol{\alpha}$	Vector of coefficients of DPF_A
α_i	Coefficients of DPF_A
$\boldsymbol{\beta}$	Vector of constants
γ	Covariance matrix
$\boldsymbol{\gamma}$	Vector of coefficients of zero phase filter
γ_i	Coefficients of zero phase filter
η,ξ	Coefficients of $R(z^{-1})$
θ	Normalized frequency
θ_1,θ_2	Lower and upper limits of normalized frequency
θ_r	Road gradient
λ	Lagrange multiplier
ρ	Air density
σ^2	Mean Square Residual
τ	Gear ratio between output and input dynamometers
ϕ_k	Phase of k_{th} frequency component in SPHS signal
ω	Frequency
ω_0	Fundamental frequency
ω_M	Motor speed
$(\cdot\cdot)$	Derivatives
$(\bar{\ })$	Complex conjugate
$(\hat{\ })$	Estimation
$(\ )^{-1}$	Inverse

Chapter 1 Introduction

In this chapter, a general introduction to continuously variable transmissions (CVTs) and hardware in the loop (HIL) testing techniques is presented as the background of this research. To assist the CVT calibration and development processes, a HIL test facility is developed in a laboratory environment using two electric motors as prime movers and absorbers. The vital part in the HIL testing is to control the torque and speed of these motors to track the engine torque and vehicle speed calculated from the real-time simulation models. To achieve a perfect tracking, a feedforward control is normally used, in addition to a feedback control. Inverse techniques for the design of feedforward controllers are presented. Background on the concepts of minimum and non-minimum phase systems is introduced, and stable inverse techniques for non-minimum phase systems are reviewed. A scope of the thesis is also given at the end of the chapter.

1.1 CVT

Currently, most vehicles use either conventional manual transmissions or automatic transmissions configured with multiple planetary gear sets that use integral clutches and bands to achieve discrete gear ratios. The way continuously variable transmission (CVT) differs from manual and automatic transmissions is that the gear ratio is not discretized and can thus be changed continuously between the minimum and maximum values.

1.1.1 Introduction of CVT

Configuration of CVT

The most common configuration of CVTs applied in automotive industry is the pushing metal belt CVT. The feature that characterizes this type of CVT is the

variable-diameter pulleys. Each pulley is made of two cones facing each other. A belt rides in the groove between the two cones. The variable-diameter pulleys must always come in pairs. One of the pulleys, known as the drive or primary pulley, is connected to the crankshaft of the engine. The second pulley is called the driven or secondary pulley which transfers energy to the vehicle driveshafts. The components are shown in Figure 1-1.

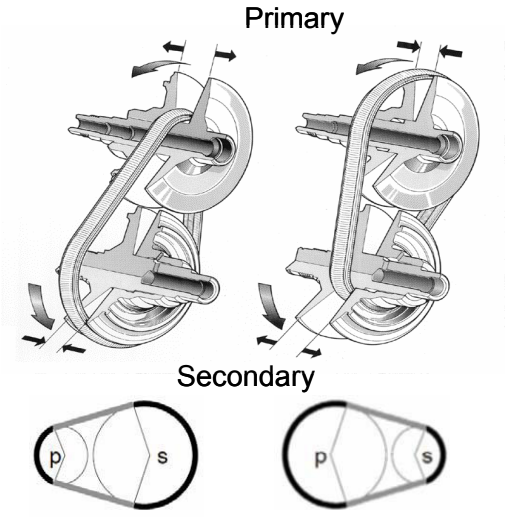

Figure 1-1 Configuration of push belt CVT

The distance between the centres of the pulleys to where the belt makes contact in the groove is known as the pitch radius, shown in Figure 1-1 as *p* and *s*. Since the pulley centre distance is fixed and the belt length is constant, when the radius of one pulley is increased, the radius of the other pulley must be decreased to keep the belt tight. The force can be created from hydraulic pressure, centrifugal force or spring tension to adjust the pulley haves. As the two pulleys change their radii relative to one another, an infinite number of gear ratios is created from low to high and everything in between.

There are also other configurations for CVT, such as toroidal CVTs [1,2] and hydrostatic CVT [3,4]. Although different in components and configuration, all the CVTs have the capability of changing the gear ratio continuously.

Function of CVT

The major advantage of CVT technology is that it allows the engine to operate in a more fuel efficient manner. Unlike other transmissions which only allow a few discrete gear ratios, CVT essentially enable an infinite number of ratios available

within a finite range, so the relationship between the speed of a vehicle, the equivalent road load torque, and the engine speed and torque can be selected within a continuous range. This gives the freedom to operate an engine at speeds that are not fixed in relation to the vehicle speed. In addition, the use of electronic engine control allows the engine torque output to be set by the control strategy rather than the driver. When used together, these two features allow the driver's power demand to be implemented in the most advantageous manner. This has been traditionally demonstrated as a means to optimise fuel economy by running the engine along a line of minimum brake specific fuel consumption (BSFC), usually called an economy line (E-line) [5], shown in Figure 1-2. There is another line (D-line) shown in the figure, which will be further explained later.

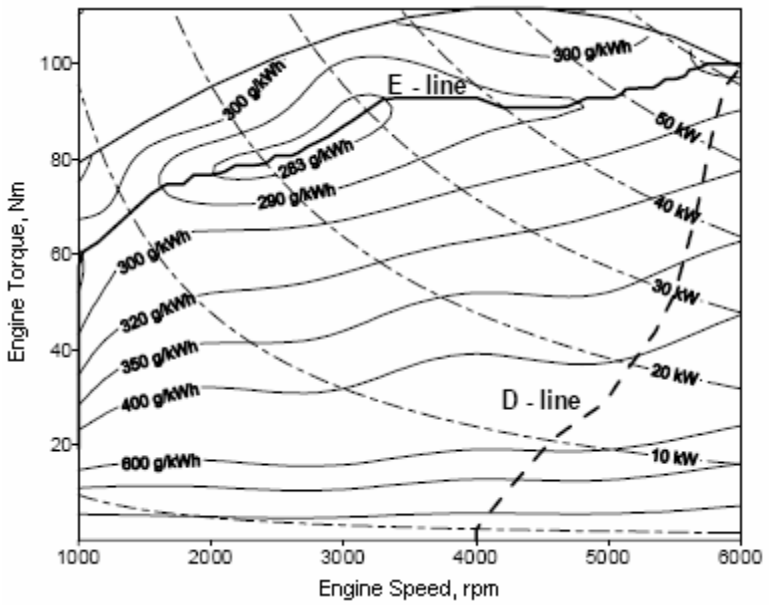

Figure 1-2 Economic and dynamic operating line in engine map

The function of CVT is to make engine operate along the determined E-line to save fuel, in dependent of vehicle speed. Figure 1-3 shows one way to generate the target engine torque and target CVT ratio under the steady state operation. The engine power demand was firstly calculated as the product of the target driving force and vehicle speed, the intersection of iso-horsepower and the target engine operating line (E-line) was selected as the ideal operating point defining the target engine torque and engine speed for this desired driving force. The target CVT ratio was calculated by dividing the target engine speed and vehicle speed. In this way, the engine torque and CVT ratio that achieve the target driving force and trace the target engine operating line can be calculated.

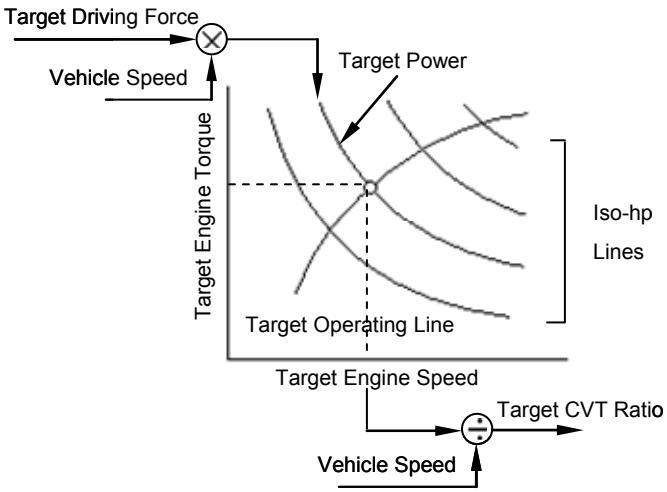

Figure 1-3 Method for generating operation point under steady state

Similar studies on engine and CVT integrated control can be found in [6-12]. In the way shown in Figure 1-3, a control map of engine torque and CVT ratio is developed so that the required power output can be obtained at the optimum fuel economy level.

The desired engine operating line may sometimes refer to an optimal emission line. For example, in [6], this line was generated by considering minimum emission of NOx. NOx emissions and BSFC reduction are not mutually compatible events and thus a trade-off between them must be considered to meet with legislative targets while achieving low fuel consumption.

Efficiency of CVT

The algorithm shown in Figure 1-3 can only be applied for a steady state driving condition without considering powertrain losses. However, in reality, substantial energy loss occurs in the powertrain, e.g. the transmission accessories. In fact, it was revealed in [7], that higher powertrain efficiency would probably ensure an improved overall fuel economy, even with a relatively high BSFC value and vice versa.

Unfortunately, CVTs do not hold a better mechanical efficiency compared with a manual transmission. When operated through a representative combined city/highway cycle, average efficiencies for typical manual, automatic and belt CVT transmissions would typically be 96.2 percent, 85.3 percent, and 84.6 percent respectively [13].

In [14], different sources of mechanical power loss inside a typical push belt CVT and their potential for reduction were described. It was pointed out that the main loss

occurs in the variator, pump and hydraulic actuation circuit. In the variator, power was lost in the form of friction, e.g. friction in the bearings of the shaft, friction between the belt and pulleys, and internal belt friction. The clamping force is the main initiator for the level of losses of these three phenomena. Normally, an excessive belt clamping force is applied based on a high safety factor because some parameters related to clamping force are not exactly known, and also the torque disturbances from engine or road are unknown. So accurately characterizing the friction and reducing the clamping force can lead to a reduction of power loss, which was investigated in a number of papers [15-19]. New control strategies were also designed to reduce the clamping force as in [14,20,21].

The actuation power for the variator is derived from a hydraulic pump and associated control circuit. The line pressure of the variator sub-circuit has an important influence on pumping losses. In [14], a smart independent pressure circuit was designed to optimise the line pressure. A high efficiency oil pump with a delivery switching mechanism was described in [22]. The concept of using electrically powered oil pump in addition to the main pump was also proposed in [14,23]. Furthermore, the conventional engine driven pump and control valves were replaced by a servo hydraulic control system, consisting of two servo pumps that control hydraulic circuit pressures. Since the hydraulic pressure was developed on demand, the losses were greatly reduced [24,25].

Moreover, to improve efficiency, a lock up clutch can be utilized to lock the torque converter above certain vehicle speeds. Optimization efforts were aimed at reducing losses by engaging the lock up clutch as soon as possible [14,22].

Driveability of CVT

Apart from the need to improve efficiency, another factor influencing the uptake of CVT technology is driveability. It is always difficult to obtain low fuel consumption and good vehicle driveability at the same time. Such a situation is a result of different courses of the dynamics (D-line) and economic (E-line) operating lines in the area of the engine torque speed map as shown in Figure 1-2. More specifically, the (quasi-stationary) operating points for minimal fuel consumption are located at high torque and low engine speed, whereas those for good driveability are located at low torque and high engine speed [26].

Generally, the efficiency is high if the power is delivered at low speed (large transmission ratio) and high torque (nearly wide open throttle). In this so called E-line strategy, only a small increase of the engine power will be obtained by completely opening the throttle. A further increase of this power is possible only if the engine is speeded up by down shifting the CVT. A fast downshift will result in a large engine acceleration. The engine then may not have enough power to accelerate its own inertia and thus power will be drawn from the vehicle, resulting in a vehicle deceleration. This is seen as a serious drawback of the E-line strategy, and as such it is hardly applied in practice [27]. The shifting characteristics of CVTs were presented in [28]. The same conclusion was drawn when down shifting the CVT. If the rate of ratio decrease is too great, a large negative inertia torque will be seen at the output shaft. If the rate of ratio decrease is too low, it will take more time to reach the desired engine power level. Therefore, an optimal choice of ratio changing rate is important.

A solution was suggested in [27,29] to overcome the discrepancy between driveability and fuel consumption by a power assist unit, embodied as a flywheel and a planetary gear set in parallel to a standard CVT driveline. If the CVT ratio was shifted down, the flywheel speed decrease at an increasing engine speed. The resulting decrease of the kinetic energy of the flywheel can be used to accelerate the engine. From a model point of view, it seems that the engine inertia was cancelled by the flywheel inertia. Therefore, the new driveline was called the Zero Inertia (ZI) driveline.

Further study on driveability issues like ratio schedule, pedal delay, shift speed, and torque converter lock up, etc. can be found in [30-34]. It was identified that these factors are likely to influence customer perception.

1.1.2 Testing of CVT

To further improve the efficiency and driveability of a CVT, experimental testing is an essential part of the powertrain development process. The automotive industry has long relied on vehicle testing to evaluate drivetrain components for new vehicle applications. Vehicle and engine based tests have many downfalls that could be avoided through the use of a laboratory based test system with electric prime movers and absorbers. Vehicle testing with human drivers is often subjectively controlled

and the exact test conditions are often unrepeatable. Vehicle tests are subject to weather changes and other environmental factors that can fluctuate tremendously during a test programme. Engine driven testing requires special facilities with exhaust removal systems and fuel storage capabilities.

The biggest downfall to vehicle and engine driven testing of drivetrain components for new vehicles is that powertrain engineers often wait months for prototype vehicles and engines to become available for their test programmes. This is especially frustrating to drivetrain engineers because in most cases they want to utilize existing transmission designs for new vehicle applications. They simply modify or recalibrate a transmission from their product line to work on a new vehicle with a new engine. The drivetrain development team has to wait months before they know if an existing component will work or if a new design is needed [35].

A solution to this problem is to develop a transmission test system that can simulate the characteristics of an engine and vehicle through the use of properly controlled electric motors. The reasoning behind this solution is that even if the new engine or vehicle does not yet exist, there will be initial computer-based models of the proposed engine and vehicle that can be run in real-time, together with electric motors to emulate a concept engine or loads of a vehicle.

1.2 Hardware in the Loop (HIL) Testing

Today's automotive development processes are characterised by increasing technical requirements within a competitive market and therefore by a growing complexity regarding mechanics and electronics. On the electronic side, comfort and safety requirements such as climate control or dynamic stability control systems will lead to an increasing number of on-vehicle embedded systems with more and more software solutions using several distributed Electronic Control Units (ECUs) [36]. On the mechanics side, more sophisticated devices such as double clutch or continuously variable transmissions (CVTs) are developed to improve vehicle performance or fuel economics, which also leads to an increasing number and complexity of ECUs. Both issues make testing a central task within the development process of automotive mechanics and electronics.

The automotive industry has long relied on vehicle testing for calibration of newly developed mechanics and electronics. Testing in real vehicles is time consuming and costly, and occurs very late in the automotive development process which can lead to costly mistakes when hardware iterations are required. It is therefore initiating technologies to replace the real vehicle by a laboratory environment. While new functions are still being developed or optimised, other functions are already undergoing certain tests, mostly on module level but also on system and integration level. To achieve the highest quality, testing must be done as early as possible within the development process.

Hardware in the loop (HIL) testing for ECUs is now a well established technology employed through the development process. Typical applications can be found in [37-40]. Instead of being connected to an actual vehicle, the prototype ECU is connected to a HIL simulation system. Software and hardware models simulate the behaviour of the vehicle and related sensors and actuators. The models are typically developed with a suitable modelling tool, such as Matlab/Simulink. C code is then generated automatically and downloaded to real-time processors for execution. I/O boards, together with signal conditioning for level adaptation to the automotive voltages required by the ECU, provide the interface to the ECU pins. Figure 1-4 shows a typical hardware-in-the-loop system architecture for an ECU testing [41].

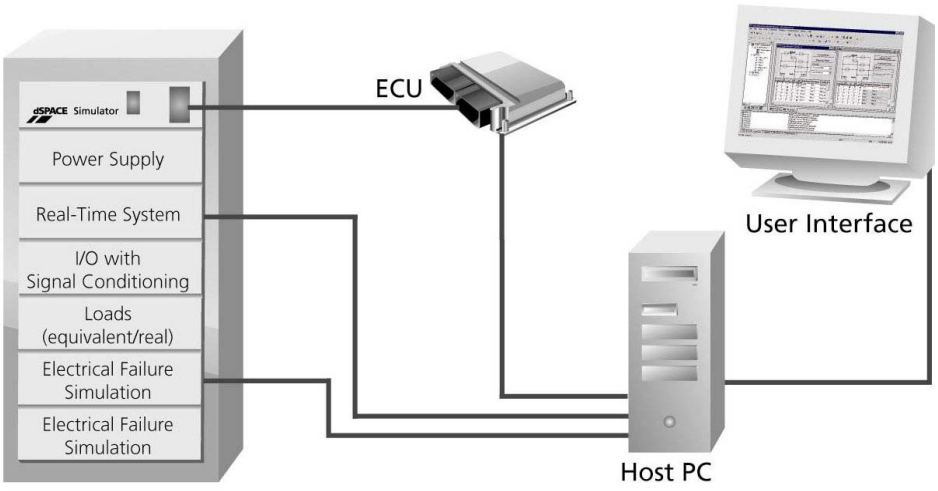

Figure 1-4 Typical hardware in the loop test system architecture

The extensive use of HIL technique includes introduction of transfer system, which is typically a set of actuators. The transfer system is used to provide an interaction between the software and hardware components of the system. It was called actuator-

based hardware in the loop (AbHWiL) testing in [42]. Such applications can be found in [43,44] and the references therein. An antilock braking system (ABS)/electronic stability program (ESP) HIL test bench was built in [43]. The whole brake system existed in hardware form, and integrated through specific interfaces, e.g. wheel pressures signals, with a vehicle model running in real-time on a dSPACE processor board. A hydraulic unit driven by an electric motor was included to actuate the booster input rod which was originally driven by the engine. In the vehicle model, a driver simulator performed the desired manoeuvres and computed the booster input rod reference signal. The four callipers pressure sensors sent their signals back to the vehicle model, permitting to estimate braking torque values. A HIL setup was developed in [44] for testing suspension units. An actuator was used to provide the compression and elongation for the suspension unit, while the resulted force was measured by a load cell. The mathematical simulation model of the vehicle dynamics was run on a computer with suitable inputs and outputs. One output of the model would be the displacement control signal for the actuator, while the measured force would be an input of the model.

The dynamics of the transfer system need to be compensated for when the HIL test is to be carried out in real time. PID controllers may be used if the actuator phase lag is seen to be acceptable within the operational frequency range [43,44]. For a lightly damped system with a small phase margin, the effect of heir dynamics may be significant, and advanced delay compensation techniques need to be developed. This will also apply to applications where electro-mechanical devices or complex circuitry are used as transfer systems, with the result that the effect of their dynamics may be significant within the operational range [42]. An emulator-based control strategy was presented in [42] to emulate the inverse of a transfer system in order to solve the problems of stability and fidelity caused by the unwanted transfer system dynamics.

Mitigating the effect of transfer system dynamics has been studied in detail in the context of the related testing technique of real time dynamic substructuring (RTDS). RTDS is an actuator-based HWiL technique (AbHWiL), which so far has primarily been considered for civil engineering systems [45,46].

1.3 HIL Test Facility for CVTs

In the research described in this thesis, a HIL test facility was developed for automotive powertrains, with a particular interest in continuously variable transmission (CVT) testing. In this case, the CVT, its ECU, and the engine ECU are proposed to exist in hardware form. Other parts of the vehicle powertrain will exist in software form, namely the engine and vehicle. Two electric machines are employed as actuators to be connected to the transmission to apply required duty cycles on the input and output shafts of the CVT.

1.3.1 Test Facility Architecture

Figure 1-5 shows a proposed schematic arrangement of the CVT HIL test facility. The real CVT to be tested is placed in between input and output dynamometers. The dynamometers are driven by a twin ABB regenerative drive system and controlled by a CP CADET V12 control and data acquisition system. The ECU of the CVT is connected to the real engine ECU and also to an ECU calibration and optimisation tool. Real-time engine and vehicle models are typically developed by Matlab/Simulink, and executed on a dSPACE DS1006 processor board. Execution results in the form of the engine brake torque are sent to CP CADET through a CAN bus as input dynamometer torque set points. The input dynamometer torque is usually controlled to exactly track these torque set points. Likewise, vehicle speed will be sent to CP CADET through a CAN bus as output dynamometer speed set points. The output dynamometer speed is usually controlled to exactly track these speed set points. Then perceived by CVT, the input dynamometer is a virtual engine while the output dynamometer is a virtual vehicle. Testing a CVT in this way would be similar to testing it with a real engine in a vehicle, and the real-time models of engine and vehicle can easily be updated for testing new engine and vehicle configurations in a short timeframe.

HIL testing of powertrains in this manner allows rapid calibration of the engine and transmission ECUs and the development of collaborative control strategies. It is also less costly and more flexible than testing of a complete developed powertrain, which is normally done on the vehicle. The software models of engine and vehicle can be

rapidly modified allowing investigations on a range of vehicle architectures within one test environment. The ECU calibration tool interfaces to the Matlab Model Based Calibration Toolbox, which enables advanced design of experiments and optimisation techniques to be applied to the powertrain calibration task.

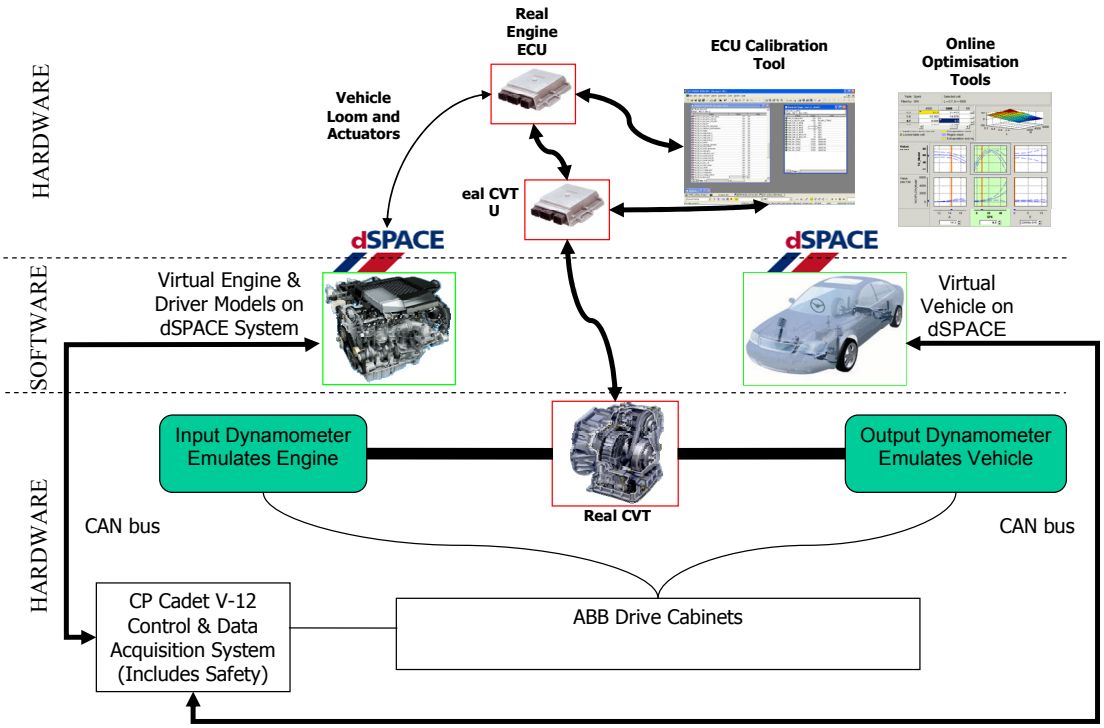

Figure 1-5 Architecture of CVT HIL test facility

1.3.2 Test Facility Components

The architecture of a HIL test facility for automotive transmissions was described in the previous section. Some details of the software and hardware components used in the test facility will be described in this section.

Electric Motor and Drive System

The test facility utilises a twin ABB regenerative drive system with a common DC bus to drive two electric motors as actuators to be connected to a CVT. The input electric motor is rated to 109 kW, 500 Nm and 4000 rev/min, while the output electric motor is rated to 200 kW, 1000 Nm, and 4000 rev/min for continuous operations. Transient overload potential of 100% is also available.

The torque from each motor is measured using HBM T10F torque flanges rated to +/-200% of the motor torque capacities, which allows safety margin for transient and

inertial loadings. The speed of each machine is measured using a 1024 pulse/rev encoder.

The electric motor and drive system is controlled by a CP Engineering CADET V12 control and data acquisition system, which is an advanced, integrated, Windows based engine and vehicle test system. It supports up to 256 physical input channels, such as speed encoders, and up to 64 digital input channels. It also supports 64 analogue output channels for control purposes, and up to 64 digital output channels. It is able to perform real-time direct digital control on 16 PID control loops at up to 320 Hz control frequency. Each of the PID loops supports linearization of input and output channels. Each motor is controlled by two PID control loops in either speed or torque mode.

CADET V12 supports both time based, and stage based testing methods. In stage based testing, the motor set points and modes are defined at each stage and 64 digital outputs may also be set on a per stage basis. The system includes data capture cards capable of sampling at rates of up to the control frequency at 16 bit resolution. Data can be logged in an optimised binary form at previous defined points in the test or as a result of events of any level of complexity. The system also offers safety interfaces to the electric motors, such as speed and torque overload protection. The electric motors and ABB drive cabinet is shown in Figure 1-6.

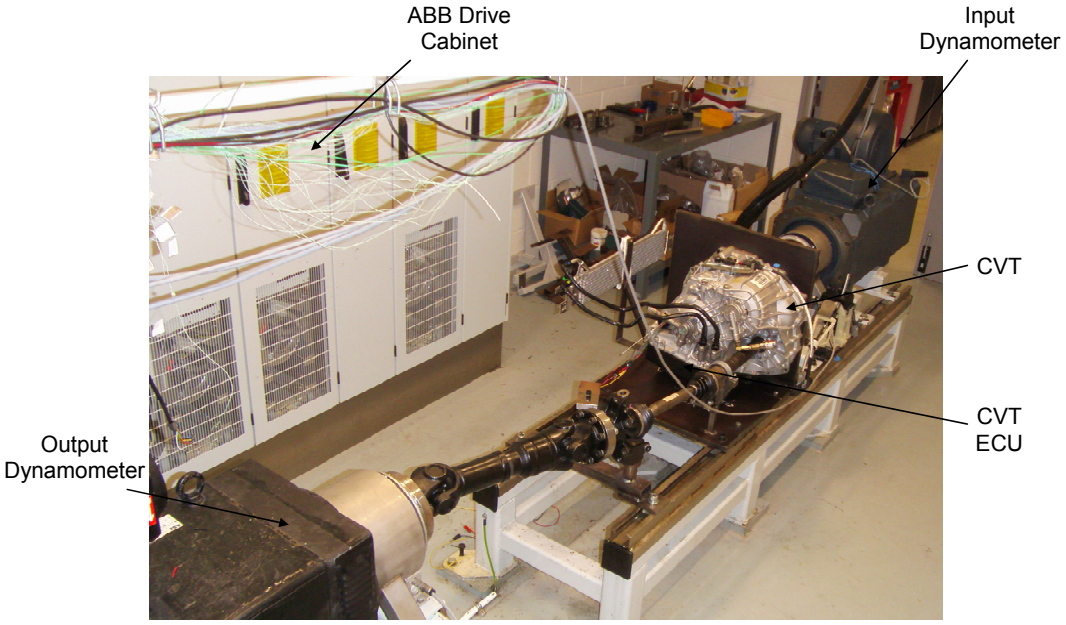

Figure 1-6 Electric motors and drive cabinet

Transmission

The transmission to be tested is a Ford ZF CFT23 CVT as shown in Figure 1-6, which is typically installed in Focus CMax vehicles. This is a pushing metal V-belt type CVT based on the Van Doorne metal V-belt design. The Transmission is an integrated transaxle design i.e. designed for use in transverse front wheel drive vehicles. The transmission incorporates a torque converter with lock up capability and may be operated in either a fully automatic mode or under manual control (with safety overrides) where clutchless shifting between a number of preset discrete ratios is achieved by sequential movement of the gear shift lever. The transmission control unit (TCU) is located in the sump of the CVT as a mechatronics unit incorporating ECU and hydraulic valving. Communication with the TCU for calibration and diagnostic purposes is achieved using INCA as described as follows.

INCA

Abbreviated from integrated calibration and acquisition system, INCA is a measuring, calibration, and diagnostic system that provides comprehensive measuring support, aids all essential tasks during control unit calibration, evaluates the measured data, and documents the calibration results. It communicates with CVT ECU through a K-line interface and allows calibrations to be carried out on-line. The calibration datasets can also be read from or written to the CVT control unit.

dSPACE

Both the engine and vehicle models are developed in Matlab/Simulink and executed utilising a dSPACE HIL platform. The main processing board is a DS1006, featuring an AMD Opteron processor of 2.6 GHz. There is also 256 Mb of local memory allocated to the processor board. The I/O capability is based on a DS2211 card designed specifically for automotive HIL applications. The primary task of the I/O is to undertake HIL interfacing with the production engine ECU, therefore the board features an angular processing unit to generate realistic cam shaft and crankshaft signals based on the predicted engine position of the real-time engine model. Additionally, the card enables capture of injection signals, and can simulate a wide range of transducers.

CAN Bus

A controller area network (CAN) bus interface to communicate between different systems was chosen due to its general adoption in the automotive industry. Both the production engine and transmission ECUs feature CAN bus communications to pass critical information between each other. The dSPACE hardware also features a CAN bus, so a CAN card was also installed into the CP CADET V12 system, with an add-on CAN interface component. A bespoke set of CAN messages were developed for passing measured values like speeds and torques, and set points between the dSPACE hardware and the CP CADET system.

1.3.3 Control of Dynamometers

A vital part of the proposed HIL testing scheme for automotive powertrains is that to emulate real engine and vehicle by using electric actuators, the torque and speed of the actuators need to be precisely controlled to track the simulation results of the real-time engine and vehicle model. The interaction between the two motors also needs to be considered when the two motors are coupled. Change in the measured input dynamometer torque will certainly result in the change in output dynamometer speed, and vice versa. Hence even if the two motors are controlled successfully on their own, the performance will be totally different when they are coupled.

There already exist certain controllers in the dynamometer drive system, like torque and flux hysteresis controllers, DC voltage and reactive power controllers. There are also PID controllers available for closed loop torque and speed control in CP CADET system. However, the control results are not satisfactory for tracking application. Large phase shift and gain error are observed for certain frequency range. Obviously, the control error can not be eliminated by tuning the PID controllers in CP CADET system. Other controllers existing in the drive system are not available to be modified by users.

In this project, feedforward controllers are developed for both dynamometers to further enhance the torque and speed control performance. Compensation is also made when the two motors are coupled and when there is a change in the gear ratio. The feedforward controllers are implemented on the dSPACE hardware along with the PID controllers. The CP CADET system is maintained in the test mainly for

processing signals, additional data acquisition capacity and the existence of robust safety protection of the dynamometers. Tracking controller design is the main effort of this project and will be presented in details in the following chapters.

1.4 Feedforward Control

Output tracking is a general control problem for dynamic systems. This problem can be dealt with a pure feedback strategy, but to achieve better performance, a combination of feedforward and feedback action can be utilized. An input-output inversion technique has been developed as an approach to design a feedforward action to perform exact output tracking. An inverse system is created by this technique according to the dynamics of the plant. The dynamics of the inverse system are designed to be opposite to the original system, thus the whole system will behave as a unit gain system without phase shift.

The inverse technique is in fact more complicated because of the stability and reliability concerning the inverse system. When the original system has unstable zeros, the inverse system will be unstable after direct inverse and perfect tracking of arbitrary reference is not possible. This motivated research into stable approximate inverse filters as a feedforward controller.

1.4.1 Control Scheme

A feedforward controller can be arranged in a system as shown in Figure 1-7, where the plant includes the original control system, which can be either open or closed loop.

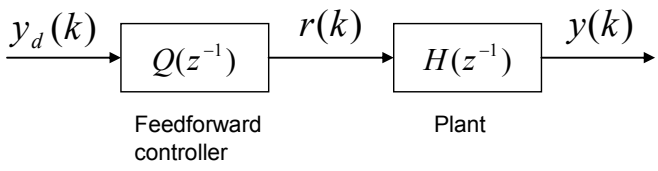

Figure 1-7 General feedforward control scheme

Two main types of feedforward control structures were found in the literature as shown in Figure 1-8. In both schemes, the main role of feedback controller is regulating the disturbance, while the main role of feedforward controller is

improving tracking performance. In structure (a) in Figure 1-8, the feedforward controller is designed in addition to a closed loop system, to compensate for the closed loop transfer function between $r(k)$ and $y(k)$. The feedback controller improves the system dynamics by rejecting disturbance and enhancing robustness. In structure (b), the feedforward controller is designed to compensate for the open-loop transfer function between $r(k)$ and $y(k)$. If the dynamics of the plant was changed because of external disturbance or additional load applied, the feedforward controller has to be modified accordingly. However, the feedback controller will assist to reduce the tracking errors.

Alternatively, an outer feedback loop controller can be added to structure (a), as shown in Figure 1-9 (a), and an inner feedback loop controller can be added to structure (b), as shown in Figure 1-9 (b). This will result in two control structures having exactly the same transfer function between $y_d(k)$ and $y(k)$.

It can be seen that after these modifications, the control structure would have an additional feedback loop. The inner feedback loop controller is mainly used to stabilize the dynamics of the plant, and the outer feedback loop controller is used to further reduce the tracking error.

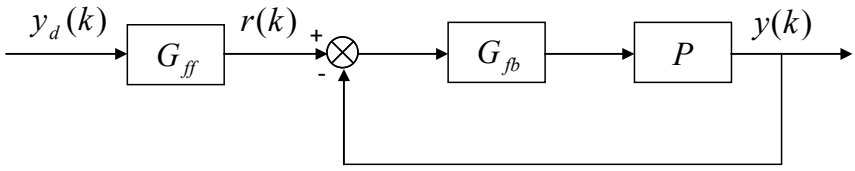

(a)

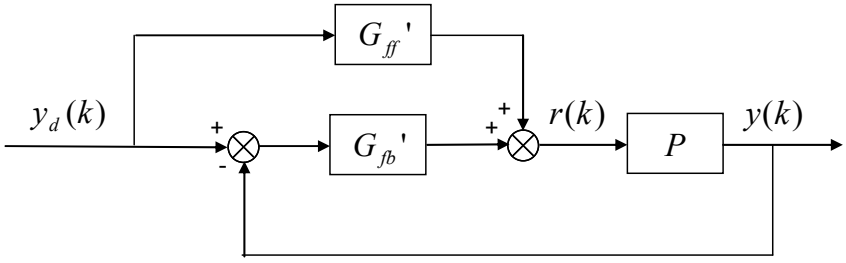

(b)

Figure 1-8 Feedforward control structures

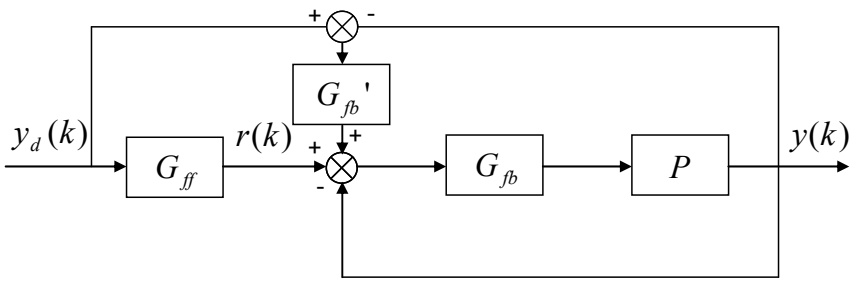

(a)

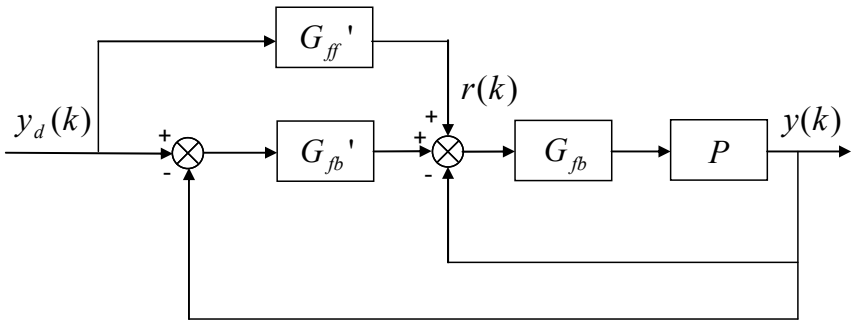

(b)

Figure 1-9 Modified feedforward control structures

1.4.2 Inverse Feedforward Control

To introduce minimum phase and non-minimum phase systems, consider a generic transfer function as follows:

$$G(s) = \frac{B(s)}{A(s)} \qquad \textbf{(1-1)}$$

If all the zeros of the transfer function are on the left side of the s plane, it is called a minimum phase system. It is characterised by the fact that for a given amplitude response, the phase response can be determined with the least phase shift.

If the transfer function (1-1) has zeros in the right side of s plane, it is called non-minimum phase system. The phase response is then always larger than that of a minimum phase system, with the same amplitude response.

To design a digital controller, an equivalent discrete time transfer function for the transfer function (1-1) can be written in the following form:

$$H(z^{-1}) = \frac{N(z^{-1})}{D(z^{-1})} \tag{1-2}$$

Then for a minimum phase system, all the zeros of the transfer function (1-2) lie within the unit circle in the z plane. If one or more zeros are outside of the unit circle, then the system is a non-minimum phase system.

A feedforward controller shown in Figure 1-7 can be formulated by inverting Equation (1-2):

$$Q(z^{-1}) = \frac{1}{H(z^{-1})} = \frac{D(z^{-1})}{N(z^{-1})} \tag{1-3}$$

Then the zeros and poles of the plant will be cancelled by the poles and zeros of the feedforward controller. The whole system will behave as a unit gain system without phase shift.

The inversion is more challenging for a non-minimum system. It will lead to an unbounded $r(k)$, and can not be implemented in practice. Therefore much research effort has been devoted to find a stable inversion method for non-minimum phase systems.

1.4.3 Stable Inversion of Non-minimum Phase Systems

The basic idea for inverse control is to carry out zero-pole cancellation. For a minimum phase system, this can be achieved by direct inversion. However, because of the existence of unstable zeros in a non-minimum phase system, the inverse system becomes unstable. Only the stable zeros can be inverted, so the dynamics of original system can not be totally cancelled. However, by applying certain stable inversion techniques to the unstable zeros, one of the following characteristics in frequency domain can be obtained:

- *C1* The phase shift is equal to zero for all frequencies
- *C2* The gain is equal to one for all frequencies
- *C3* The phase shift is equal to zero for all frequencies and the gain is equal to unity at a given frequency
- *C4* The phase shift is equal to zero for all frequencies and the gain is roughly equal to unity for a given frequency range

C5 The frequency response is close to one for all frequencies

A popular substitution scheme for the inverse of unstable zeros to achieve *C1* characteristics is zero phase error tracking controller (ZPETC). It was first proposed by Tomizuka in 1987 [47]. ZPETC has drawn much research interest in its achievement of a zero phase shift for all frequencies and a small amplitude error at low frequencies.

A cousin controller named zero magnitude error tracking controller (ZMETC), which was designed for *C2* characteristics, can achieve the gain of one for all frequencies. However, it is difficult to compensate the phase without changing the gain characteristics. Therefore, most researchers have used ZPETC as the initial design of an inverse controller for non-minimum phase systems, and then improve the magnitude response if the performance was not satisfactory. ZMETC was described and compared with ZPETC in [48].

The majority of the inverse controller design techniques for non-minimum phase systems are based on the structure of ZPETC. Research has mainly focused on three aspects: (a) further improvement of the gain characteristics, (b) the optimal design, and (c) enhancement of the robustness to parameter variations. These aspects will be reviewed and commented on in this section.

(A-1) Improvement of Gain Characteristics – Adding Zeros

ZPETC provides a zero phase error at any frequency and the gain approaches unity at low frequencies. At high frequencies, the gain falls for unstable zeros in the left half plane and rises for zeroes in the right half plane. This effect can be utilized by adding a filter with a zero to the right of the imaginary axis to cancel the gain error due to a plant zero in the left half plane. A typical application of this method can be found in [49], which was referred to as an ‘E filter’.

By adding one zero, the overall gain can be made equal to one at a specified frequency, providing *C3* characteristics. However, in general, this would result in a gain greater than unity at lower frequencies and would be of limited use. An approximation of the error term with ZPETC controller is given in [49], under the assumption of small normalized frequencies. Then, the location of additional zero

can be optimised to reduce the error to zero, resulting the gain being closer to unity at all frequencies within the limitation of approximation.

(A-2) Improvement of Gain Characteristics – Preview Filter

The concept of preview filter was first introduced in [50]. It can also be interpreted as adding more than one zero. Adding one zero to the feedforward controller, called the first order preview filter, requires one step preview of the command signal. An *N*th order preview filter was defined in [50]. The parameters of the preview filter were obtained by minimizing a penalty function. To add more zeros, increasing the bandwidth of the inversion increases the penalty function, which can be reduced significantly by increasing the order *N* of the preview filter.

Another preview filter was formulated in a different way in [51]. A minimal zero phase filter was defined as the zero phase kernel. The preview filter was formulated as a summation of zero phase kernels with increasing orders starting from zero. A penalty function with a frequency domain weighting function was given, and the parameters of the preview filter were derived by minimizing the penalty function.

It was also shown in [51], that the 'E filter' and the preview filter in [50] were special cases of the proposed preview filter when there were no complex unstable zeros.

In [52], a zero phase kernel was defined in a different way than that of [51]. The preview filter was also formulated as a summation of zero phase kernels with increasing orders starting from zero. The parameters of preview filter were obtained in the same way by minimizing a weighted penalty function. It provided similar results, but due to the novel design of the zero phase kernel, it is computationally more efficient in real-time applications. Digital preview filters provide stable inversion for unstable zeros to achieve *C4* characteristics, which will be realized for motor speed and torque control in this thesis.

(A-3) Improvement of Gain Characteristics – Series Expansion

The series expansion method can be used as an alternative to ZPETC when better gain characteristics are required for non-minimum phase systems. In [53,54], the inversion of unstable zeros was approximated by a truncated series expansion. It was

shown that for a known plant transfer function with no zeros on the unit circle, a frequency response close to one can be obtained.

This approximation was modified in [55], to give a better frequency response than that in [53,54] in the low frequency range, but with a worse response in the high frequency range. Both techniques can be categorized to achieve *C5* characteristics.

The series expansion method can also be used with ZPETC. In [56,57] , Taylor series expansion was applied to the overall transfer function after using ZPETC, and the convergence region was given. However, if the power series diverges, the gain became worse than that of ZPETC. In [58], Laurent series expansion was applied to the stable term of negative powers of z of the overall transfer function after using ZPETC.

In [59], a free parameter was introduced, and the overall transfer function with ZPETC was expanded in a power series in a different way than in [56,57], so that the power series can always converge. It was shown that the method in [56,57] is a special case when the free parameter was equal to one. Both applications can be categorized to achieve *C4* characteristics.

(A-4) Improvement of Gain Characteristics – Diophantine Equation

A Diophantine Equation is an indeterminate polynomial equation that allows the variables to be integers only. In [60], a Diophantine Equation was used to parameterize the class of all controllers satisfying the condition *C1* and *C3*. The general solution of ZPETC was given in an explicit form.

Another application of Diophantine Equation in the feedforward controller design can be found in [61,62], which was referred to as steering along zeros control (SAZC). It steered the state of the system along the unstable zero dynamics towards a suitable initial state, such that the corresponding free evolution of the plant generates an output response equal to that obtained by applying an unbounded control input.

(B-1) Optimisation - Least Square Method

In [60], after parameterization of ZPECT using the solution of a Diophantine Equation, a cost function was introduced in L_2 – norm. The optimal solution minimizing the cost function was obtained by an ordinary least square method.

(B-2) Optimisation - Lagrange Method

Typical application of this method can be found in [51] and [52]. A penalty function was also introduced in L_2 – norm. Additionally, a frequency domain weighting function was incorporated into the penalty function. The weighting function can be arbitrarily defined to emphasize good performance in an interested frequency range. The Lagrange function was formulated using the penalty function and Lagrange multipliers were introduced for steady state performance. Then the optimal solution was derived by Lagrange method. Details of this method are given in the following section.

(C) Robustness to Parameter Variation

Feedforward controllers are designed to invert the dynamics of the plant. So robustness of the controller performance needs to be considered when the dynamics of the plant changes or when there are variations of the plant parameters.

In [53], the robustness of the controller was examined when there was uncertainty in the location of one or more zeros. It was shown that the system tracking performance is much less robust to parameter variations for zeros near the unit circle. In [61], to preserve the asymptotic robustness to a step or ramp input, the feedforward controller was fed with the first difference of the reference input. Feedforward controllers can be designed to be adaptive to enhance the robustness. In [63], an adaptive ZPETC was implemented for slowly varying plant dynamics. The parameters of the plant were identified on line by using a normalized least squares algorithm, and the parameters of ZPETC were adjusted according to the estimated plant parameters. A similar adaptive inversion technique can be found in [52], where a preview filter was regulated on line by including a real-time estimation technique to cope with the external load perturbation and parameter variation. It is shown in [52], that the adaptive filter works better only when there is a load disturbance. When there is no load disturbance, the adaptive implementation of the preview filter has worse performance than the static one.

To handle the case where the gain can not be made unity for the desired frequency spectrum, a trajectory adaptive controller was proposed in [58]. This controller automatically retunes itself when the frequency components of the trajectory change.

1.4.4 Comments on Stable Inversion Techniques

Several stable inversion techniques for non-minimum phase system were reviewed above. Many of these techniques have the form of a Finite Impulse Response (FIR) filter. So the design of the feedforward controller can also be put into the framework of signal processing. Therefore, a typical adaptive signal processing technique such as Recursive Least Square (RLS) or a multirate signal processing technique can be employed in the design of feedforward controllers. As introduced in [64], the adaptive filter could be updated on line to be a best least squares inverse of the plant for a given input spectrum and for a given set of weights. Thus the adaptive filter can be deemed as an inverse model of the plant and can be used as a feedforward controller.

However, adaptive signal processing techniques have some weakness when used in control. They need time to converge, and require slow changes in the dynamics of the system. Due to these limitations, they are not used here. Applying multirate signal processing techniques to feedforward control can be found in [65]. However, the fastest sampling rates for the input control signal and the output measured signal, i.e. speed and torque, are the same in the CP CADET system, therefore this technique is not applicable in here.

Research on stable inversion techniques concluded three areas of improvements: the improvement of gain characteristics, the optimal design, and the enhancement of robustness to parameter variation respectively. However, it should be noted that non-minimum phase system inversions using the techniques above are all non-causal, so future information of input trajectory is required to implement the controller. This is not a problem if the input trajectory is known prior. In our case, speed and torque demands of the motors were calculated from the vehicle and engine models, and these models can not be executed ahead of time to provide future information because the models require current information, like current engine torque and speed, to carry out the calculations. Therefore, causality is taken as the forth aspect to be considered when implementing feedforward inverse control in the context of this work. A predictor to predict future information using past values could be developed, but the prediction can not be perfect, and the prediction error will significantly affect the control performance and stability.

1.5 Thesis Scope

In the next chapter, a system identification method in frequency domain is introduced. The characteristics of the dynamometers and their drive systems are identified experimentally, and also the characteristics of the loads, i.e. inertias and damping ratios. Signal transmission delays on the CAN bus system are determined. An overall transfer function is estimated for the output dynamometer speed control including the CAN bus delays. In Chapter 3, based on estimations, feedforward controllers are designed for the output dynamometer speed control and the input dynamometer torque control. Test results with multi frequency signals as speed and torque demands are presented in both time and frequency domains to verify the designed feedforward controllers. The robustness of the designed tracking controllers is discussed in Chapter 4, when the two motors are coupled and there is a change in the gear ratio. The coupled control method is also verified by the tests with multi frequency speed and torque demands. In Chapter 5, tests are carried out by using simulation results of the real-time whole vehicle model as speed and torque demands. HIL testing results are also presented. Finally, conclusions and future work are presented in Chapter 6.

Chapter 2 System Identification

To design a precise tracking controller, a model of the dynamometer is required. Quite often, a linear model is preferred in the preliminary control design, which can employ well established linear control techniques.

Due to the nonlinear character of mutual inductance within dynamometers, the overall system is nonlinear. There are two ways to obtain a linear model: the first way is to develop a nonlinear model and then linearize it by performing a small perturbation on all the machine variables of the full nonlinear model. The second way is to assume a linear model for the system and identify the model parameters experimentally. In either technique, the linear region, where the linear model can represent the system properly, needs to be indicated. If necessary, different linear models can be used for each region, to cover the whole operating range of the dynamometers.

For the first method, the operating principles of induction motors and the drive system needs to be thoroughly understood. Any assumptions and approximations used in the original modelling for the nonlinear system will introduce errors into the final linear model, but in this way, parameters of the system can be easily modified and examined. By contrast, the second method is based on the experimental results. Only the input and output signals are considered, but not what happens in between. It will lead to a more accurate model if there are uncertainties in the motor and drive system behaviour. Because the main purpose of the project is to design a feedforward compensator for the existing system, but not to examine the effect of parameters on the system behaviour, the second method is applied here.

In this chapter, a frequency domain identification method for a linearized model is introduced first. The transfer function for motor and its drive system is estimated using this method, and also the load of the system, in terms of inertias and damping ratios. To operate the system with the CAN bus, transmission delays on the CAN bus

were identified. Then these delays are included in the Simulink model of the closed loop speed control for the output dynamometer which is constructed from the estimated transfer functions. After that, an overall transfer function for the closed loop speed control for the output dynamometer is obtained by calculation and by estimation. Transfer functions developed from these two methods are compared with test results

2.1 Identification Method

A linearized system model identification method based on the experimental data is given in this section. The experimental data are obtained by operating the motors with a multi-frequency demand signal. An approach to generate a multi-frequency signal with low peak factor is explained. Statistical analysis of the estimation results is also provided.

2.1.1 Least Squares Estimation

In parametric statistics, the least-square estimator is often used to estimate the coefficients of a linear regression, which aims to minimize the sum of the square of the residuals. To apply the method, a parametric linear model for the system must be established.

A general linear transfer function was considered for the system to be estimated as follows:

$$G(s) = \frac{Y(s)}{R(s)} = \frac{b_n s^n + \cdots + b_2 s^2 + b_1 s + b_0}{s^m + a_{m-1} s^{m-1} + \cdots + a_2 s^2 + a_1 s + a_0} \quad (n \le m) \qquad \textbf{(2-1)}$$

where $a_0, a_1, \cdots a_{m-1}, b_0, b_1, \cdots b_n$ are the parameters to be estimated. $R(s)$ and $Y(s)$ denote the Laplace Transform of the reference and response signals respectively. This can be written as follows:

$$\begin{bmatrix} -Y(s)s^{m-1} & \cdots & -Y(s)s & -Y(s) & R(s)s^{n} & \ldots & R(s)s & R(s) \end{bmatrix} \times \begin{bmatrix} a_{m-1} \\ \vdots \\ a_1 \\ a_0 \\ b_n \\ \vdots \\ b_1 \\ b_0 \end{bmatrix} = Y(s)s^{m} \tag{2-2}$$

or

$$\mathbf{Z}(s)\mathbf{C} = F(s) \tag{2-3}$$

Replacing $s = j\omega$ at $\omega = k\omega_0$ for $k = 1 \cdots K$, where ω_0 is the fundamental frequency and K is the number of frequency components, and separating the real and imaginary components gives $2K$ real equations in terms of the discrete frequency responses of the input $R(j\omega)$ and output $Y(j\omega)$ of the system, as follows:

$$\begin{bmatrix} \mathrm{Re}\{\mathbf{Z}(j\omega_0)\} \\ \mathrm{Im}\{\mathbf{Z}(j\omega_0)\} \\ \vdots \\ \mathrm{Re}\{\mathbf{Z}(jK\omega_0)\} \\ \mathrm{Im}\{\mathbf{Z}(jK\omega_0)\} \end{bmatrix} \times \mathbf{C} = \begin{bmatrix} \mathrm{Re}\{F(j\omega_0)\} \\ \mathrm{Im}\{F(j\omega_0)\} \\ \vdots \\ \mathrm{Re}\{F(jK\omega_0)\} \\ \mathrm{Im}\{F(jK\omega_0)\} \end{bmatrix} \tag{2-4}$$

or

$$\mathbf{Z}_L\mathbf{C} = \mathbf{F}_L \tag{2-5}$$

A least squares estimation of the coefficient vector can then be obtained as follows [66]:

$$\hat{\mathbf{C}} = (\mathbf{Z}_L^T\mathbf{Z}_L)^{-1}\mathbf{Z}_L^T\mathbf{F}_L \tag{2-6}$$

The measurement matrices $\mathbf{Z}_L$ and $\mathbf{F}_L$ are functions of the frequency domain representation of the input and output signals, and can be obtained by a Fourier Transform.

In order to guarantee an arbitrary steady state gain k_s, the following model can be used:

$$G(s)=\frac{Y(s)}{R(s)}=\frac{b_n s^n+\cdots+b_2 s^2+b_1 s+k_s a_0}{s^m+a_{m-1}s^{m-1}+\cdots+a_2 s^2+a_1 s+a_0} \quad (n<m) \qquad \textbf{(2-7)}$$

Then Equation (2-2) becomes:

$$\begin{bmatrix}-Y(s)s^{m-1} & \cdots & -Y(s)s & k_s R(s)-Y(s) & R(s)s^n & \cdots & R(s)s\end{bmatrix}\times\begin{bmatrix}a_{m-1}\\ \vdots\\ a_1\\ a_0\\ b_n\\ \vdots\\ b_1\end{bmatrix}=Y(s)s^m \qquad \textbf{(2-8)}$$

Equations (2-3), (2-4), and (2-5) will be the same, and the least square estimator will also be given by Equation (2-6).

The orders of estimated transfer functions, i.e. *m* and *n*, should be selected to give the best fit into the experimental data and also satisfy the requirements of designing the feedforward controllers as will be discussed later.

2.1.2 Multi-Frequency Signal

The success of the estimator is heavily dependent on the selection of the test signal, which should cover all the frequencies of interest. Using a sinusoidal signal will require K groups of tests, one group for each frequency, and each group will require a number of single tests for the purpose of averaging the response to reduce the effects of noise. If a multi-frequency test signal is generated by adding all the frequencies with arbitrary phases, it may result in unacceptable peak in the torque or speed signal, which is not acceptable in real applications. Decreasing the excitation amplitudes of all the frequencies is not a good solution, because this will result in weak perturbations in the frequency domain and will consequently increase the estimation errors [67].

The method of adjusting the phase angles of a periodic signal with a given power spectrum to minimize its peak-to-peak amplitude was first proposed by Schroeder [68], and was described in [67] as follows:

A periodic signal $s(t)$ is considered to have any user specified power spectrum p_k, $k = 1, 2, \cdots, K$. Defining P_k is the ratio of the power at $\omega = k\omega_0$ to the total power. i.e.

$$P_k = \frac{p_k}{\sum_{k=1}^{K} p_k}, \quad \sum_{k=1}^{K} P_k = 1 \tag{2-9}$$

Selecting the phase of each frequency component in accordance with the Schroeder Phased Harmonic Sequence (SPHS) will require:

$$\phi_k = \phi_{k-1} - 2\pi \sum_{i=1}^{k-1} P_i, \quad (k = 1, 2, \cdots, K) \tag{2-10}$$

Then the signal can be constructed as:

$$s(t) = \sum_{k=1}^{K} A_k \cos(k\omega_0 t + \phi_k) \tag{2-11}$$

where A_k is the amplitude of the k^{th} harmonic and is given by:

$$A_k = \sqrt{\frac{p_k}{2}} \tag{2-12}$$

Uniform amplitude ratio was defined in the test, that is:

$$A_k = 1, \quad p_k = 2, \quad P_k = \frac{1}{K} \tag{2-13}$$

An example of a uniform amplitude SPHS test signal covering a frequency range from 0.1 Hz to 20Hz, with 0.1 Hz fundamental frequency is shown in Figure 2-1, in both time and frequency domains.

It can be seen in frequency domain that the multi frequency has the sub-harmonics with uniform amplitude up to 20 Hz, and there is no unacceptable peak in amplitude in time domain. Noise exists above 20 Hz, in both amplitude and phase.

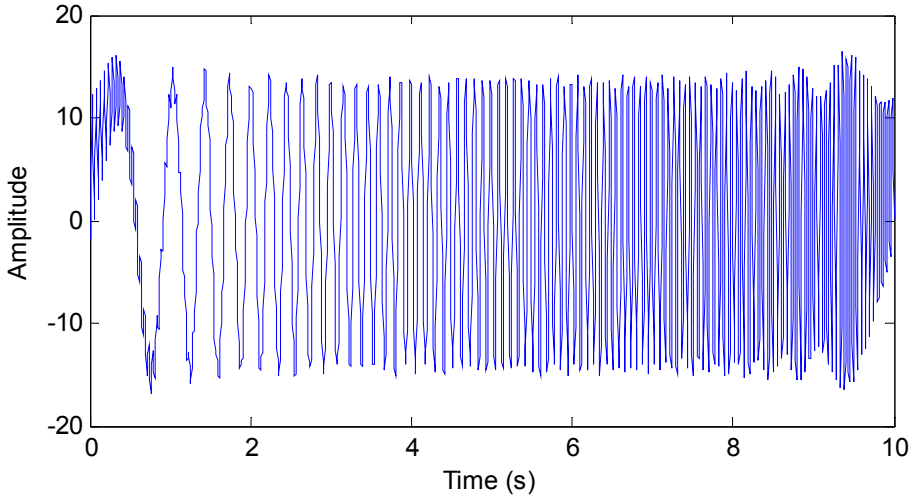

(a) Time domain

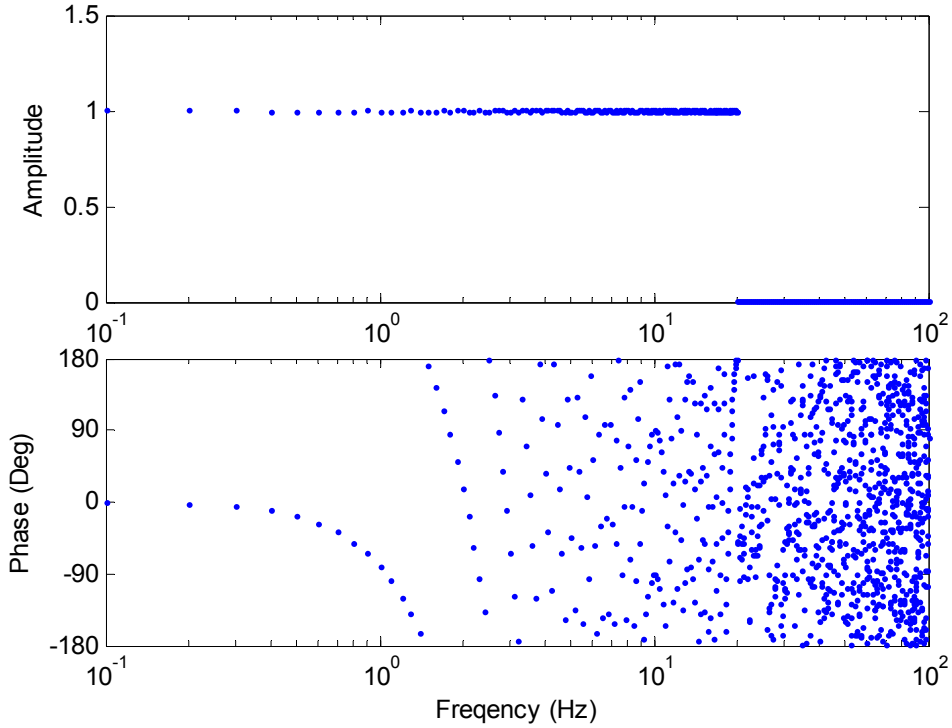

(b) Frequency domain

Figure 2-1 SPHS multi-frequency test signal

2.1.3 Statistical Analysis

Once the system model is estimated, basic statistical analysis can be employed to measure how well the estimated model represents the test results. Two statistics are used here, namely Goodness of Fit (GOF), and Standard Error (SE).

Goodness of Fit (GOF)

A standardized measure of Goodness of Fit is provided to indicate how well the estimation fits the observation. To give the definition of GOF, first of all, the residual for a specific predictor value is defined as the difference between the response value y and the predicted response value $\hat{y}$:

$$e = y - \hat{y} \tag{2-14}$$

Sum of Squares Error measures the total deviation of the response values from the fit to the response values. It is also called the summed square of residuals and is usually labelled as *SSE*:

$$SSE = \sum_{i=1}^{n} e^2 \tag{2-15}$$

A value closer to zero indicates a better fit.

The goodness of fit measure, R^2, quantifies how successful the fit is in explaining the variation of the data. It is defined as the ratio of the sum of squares of the regression (*SSR*) and the total sum of squares (*SST*). *SSR* is defined as:

$$SSR = \sum_{i=1}^{n} \left(\hat{y}_i - \bar{y}\right)^2 \tag{2-16}$$

SST is also called the sum of squares about the mean, and is defined as:

$$SST = \sum_{i=1}^{n} \left(y_i - \bar{y}\right)^2 \tag{2-17}$$

where $SST = SSR + SSE$. Given these definitions, R^2 is expressed as:

$$R^2 = \frac{SSR}{SST} = 1 - \frac{SSE}{SST} \tag{2-18}$$

R^2 can take any value between 0 and 1, with a value closer to 1 indicating a better fit.

If the number of fitted coefficients in the model is increased, R^2 might increase although the fit may not improve. To avoid this situation, the degree of freedom adjusted R^2 statistic is provided.

Degree of Freedom Adjusted R^2 uses the R^2 statistic defined in Equation (2-18), and adjusts it based on the residual degrees of freedom. The residual degrees of freedom is defined as the number of data points p minus the number of estimated coefficients q:

$$v = p - q \tag{2-19}$$

The adjusted R^2 statistic is generally the best indicator of the fit quality when additional coefficients are added to the model.

$$adjusted\ R^2 \quad = \quad 1 - \frac{SSE}{SST} \times \frac{p-1}{v} \tag{2-20}$$

The adjusted R^2 statistic can take any value less than or equal to 1, with a value closer to 1 indicating a better fit.

Standard Error (SE)

In order to determine how reliable the individual parameter estimates are, an estimation of the variability of the estimators is needed. Standard Error (SE) can be obtained by determining the covariance matrix of $\hat{\gamma}$ as:

$$\mathrm{cov}(\hat{\gamma}) = \hat{\sigma}^2 \left(\mathbf{W}^T \mathbf{W}\right)^{-1} \tag{2-21}$$

where $\hat{\sigma}^2$ is the variance of the error term in the simple linear regression model. The only assumption needed for Equation (2-1) to hold is that the errors are uncorrelated and all have the same variance.

The estimate of the error variance (or Mean Square Residual) is:

$$\hat{\sigma}^2 = \frac{\sum_{i=1}^{n} \left(y_i - \hat{y}_i\right)^2}{v-1} = \frac{SSE}{v-1} \tag{2-22}$$

The degree of freedom associated with the mean squared residual is $p - q - 1$. As a result, the Standard Error is defined as:

$$SE = \sqrt{\mathrm{diag}(\mathrm{cov}(\hat{\gamma}))} \tag{2-23}$$

From *SE*, the significance of estimated coefficients can be determined. The estimated coefficients can be divided by the corresponding standard error to get a *T* value. If

the absolute T value is greater than the value obtained from standard t distribution tables for a specified percent confidence interval, then the coefficient is designated as significant, i.e. nonzero.

For example, the 95 percent confidence interval values can be calculated as:

$$confidence\ interval = estimated\ coefficient \pm (t_{0.95})SE \quad \textbf{(2-24)}$$

where $t_{0.95}$ is the value obtained from the t distribution table for 95 percent confidence. A small confidence interval indicates a reliable estimate for the corresponding parameters. If the interval includes zero, then the parameter can be classified as in significant and be ignored in the model.

2.2 Identification Results

In this section, linear system models are identified using experimental data. The linear region, where the identified model can match the real system is also determined. To get experimental results, two motors were operated separately with closed loop speed control with the PID controller provided by the CP CADET system. The block diagram for a speed control system is shown in Figure 2-2.

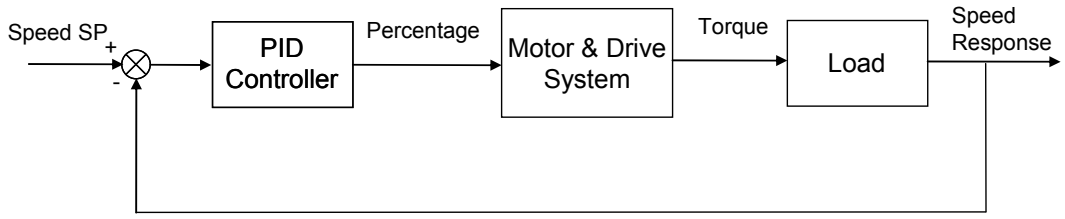

Figure 2-2 Closed loop speed control block diagram

The speed setpoint signal was constructed by using a DC plus SPHS signal covering a frequency range from 0.1Hz to 20 Hz. The percentage, torque and speed signals were recorded and used in identification. If the two motors were coupled, these signals would have to be measured and recorded separately for input and output dynamometers. As shown in Figure 2-2, the model for motor and drive system can be identified from the recorded torque and percentage signals. The model for load, in terms of inertia and damping can be identified from the recorded speed and torque

signals. The model for PID controller can easily be obtained as the parameters are known.

2.2.1 Estimation of Inertia and Damping

When there is no external disturbance, the inertia and damping ratio can be calculated from the measured torque and speed signals, e.g. by ramping the motor to a particular speed to calculate the inertia and by running the motor at a constant speed to calculate the damping ratio. This could also be achieved by exciting the motor with SPHS signal and carrying out estimation between measured torque and speed signals. The estimated transfer function will be forced to be first order, with inertia and damping ratio as denominator parameters. There are advantages to use SPHS signal, as the inertia and damping ratio can be estimated at the same time with a single test and the estimation process is optimised in a least-squares sense.

During the test, torque from each dynamometer was measured using HBM T10F torque flanges, while speed of each dynamometer was measured using 1024 pulse/rev encoder. Both signals were recorded at 160 Hz sampling frequency. As shown in Figure 2-3, the torque flanges were located on the shaft close to the dynamometers, so the measured torque was the torque acting on the shaft, rather than the total torque generated by the dynamometers. The difference between the generated torque and measured torque is the torque used to drive the motor rotor inertia and the damping inside the motor. This is the case for both input and output dynamometers. The difference between the two measured torques is the torque used to drive the input and output shafts and gear box inertias, and also the damping between gears and the damping at bearings inside the gear box.

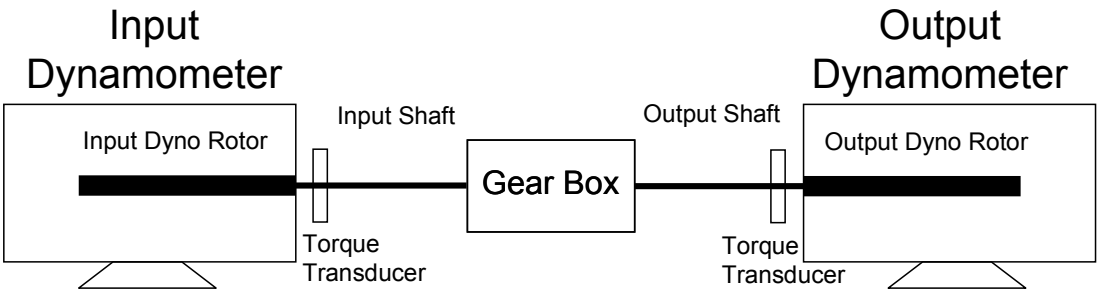

Figure 2-3 Location of torque transducers

As shown in Figure 2-3, inertias and damping ratios can be separated into four parts: input dynamometer rotor, input shaft, output shaft and output dynamometer rotor, among which, the gear box inertia and damping ratio was lumped into the input and output shafts. A number of tests were conducted to estimate the inertias and damping ratios for each part.

The output dynamometer was tested under closed loop speed control with input dynamometer switched off. The speed demand consisted of a DC and an SPHS signal with the frequency between 0.1 and 20 Hz. The constant speed component was set to 1000 rev/min, and the amplitude of SPHS signal was scaled to be 50 rev/min. Tests were carried out with a neutral gear and a 1:1 gear ratio. When testing with a neutral gear, the output dynamometer torque transducer measures the torque driving the output shaft. Therefore, the inertia and damping ratio of output shaft can be estimated using the recorded torque and speed signals of the output dynamometer. The estimation result is shown in Figure 2-4.

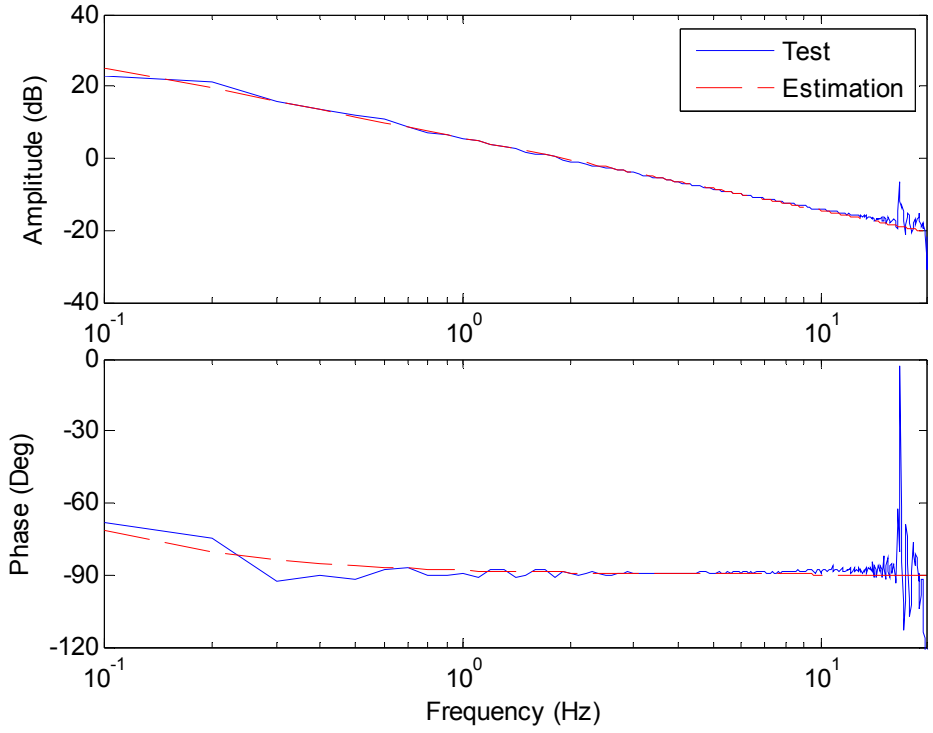

Figure 2-4 Experimental and estimated transfer functions between output dynamometer torque and speed with a neutral gear driven by output dynamometer

The estimated transfer function was:

$$L_{O\_Shaft}(s) = \frac{11.91}{s + 0.2143} \quad \textbf{(2-25)}$$

The inertia and damping ratio of the output shaft was calculated to be 0.084 kgm^2 and 0.018 Nm/rad/s.

The test result became noisy beyond 15 Hz, indicating the operational bandwidth of the motor and drive system, which means that the motor can only follow the demand signal up to 15 Hz. Hence the estimation was carried out using the experimental data up to 15 Hz. Because the torque was measured by a HBM T10F torque flange, which has an accuracy of +/-0.1% of full scale, i.e. +/-1 Nm, the error may be significant when the measurement was taken around 0 Nm. Since the SPHS signal was generated with a flat spectrum for all its sub harmonics, the acceleration would be smaller for lower frequency signals. Therefore the measured torque would be relatively small for low frequency signal and have a relatively large error, which was the reason for the fluctuation observed at low frequency range. These frequency points were carefully used, and some of them were not taken into account when carrying out estimation.

When testing with a 1:1 gear ratio, the input dynamometer torque transducer measures the torque driving the input dynamometer rotor. Therefore, the inertia and damping ratio of the input dynamometer can be estimated using the recorded torque and speed signal of the input dynamometer. The estimation result is shown in Figure 2-5.

The estimated transfer function was:

$$L_{I\_Dyno}(s) = \frac{2.275}{s + 0.0983} \quad \textbf{(2-26)}$$

The inertia and damping ratio of the input dynamometer was calculated to be 0.4396 kgm^2 and 0.0432 Nm/rad/s.

More noise in the data was observed than the previous test when the two motors were coupled with a 1:1 gear ratio, especially in the high frequency range. Oscillation in the low frequency range is thought to be mainly due to the measurement error of the torque transducer. In the high frequency range, the reason may be explained by the existence of backlash between the gears, which would result in nonlinearities.

Moreover, there was a rubber toroidal element connecting input dynamometer and input shaft to allow more compliance on the drive shaft for safety reasons. This may also influence the measured torque. Again, not all the frequency points were used in the estimation, especially for extremely low and high frequency points.

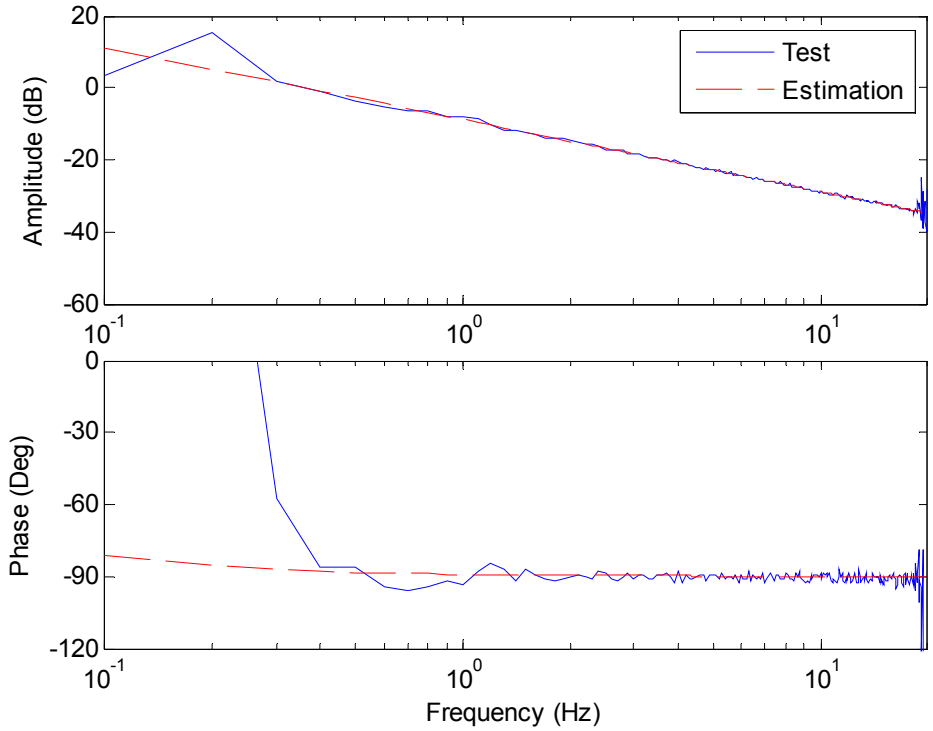

Figure 2-5 Experimental and estimated transfer functions between input dynamometer torque and speed with a 1:1 gear ratio driven by output dynamometer

Similar tests were carried out on the input dynamometer using closed loop speed control with the same speed demand as before. The output dynamometer was switched off in this case. Tests were also carried out with a neutral gear and a 1:1 gear ratio. When testing with a neutral gear, the input dynamometer torque transducer measures the torque driving the input shaft. Therefore, the inertia and damping ratio of input shaft can be estimated using the recorded torque and speed signal of the input dynamometer. The estimation result is shown in Figure 2-6.

The estimated transfer function was:

$$L_{I\_Shaft}(s) = \frac{24.65}{s + 0.8892} \qquad \textbf{(2-27)}$$

The inertia and damping ratio of the input shaft was calculated to be 0.0406 kgm^2 and 0.0361 Nm/rad/s.

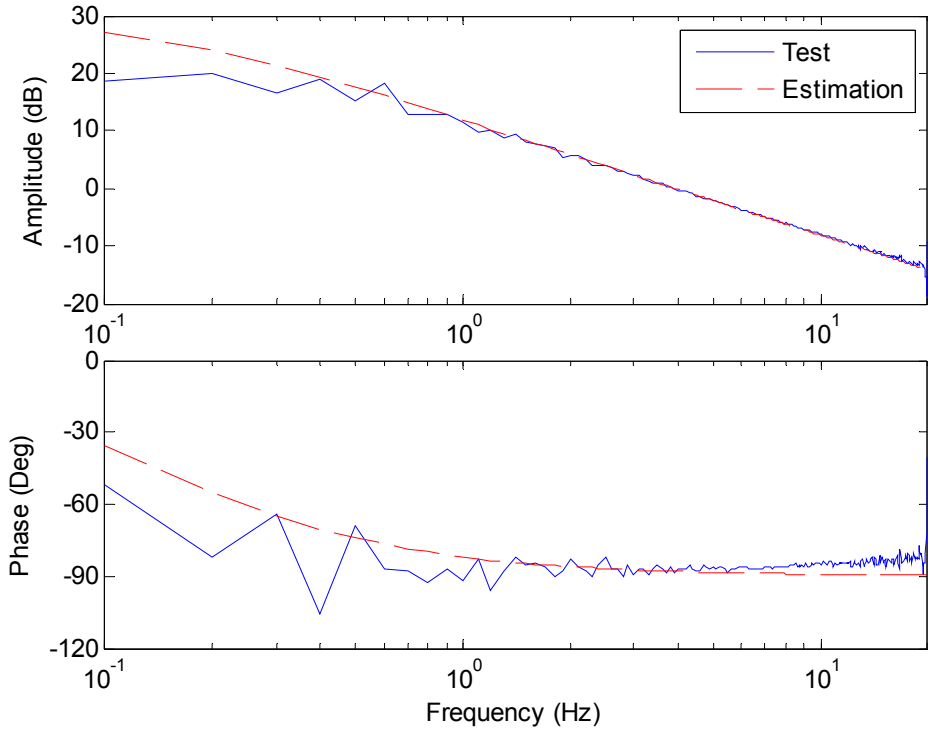

Figure 2-6 Experimental and estimated transfer functions between input dynamometer torque and speed with a neutral gear driven by input dynamometer

When testing with a 1:1 gear ratio, the output dynamometer torque transducer measures the torque driving the output dynamometer. Therefore, the inertia and damping ratio of the output dynamometer can be estimated using the recorded torque and speed signal of the output dynamometer. The estimation result is shown in Figure 2-7.

The estimated transfer function was:

$$L_{O\_Dyno}(s) = \frac{0.9581}{s + 0.0958} \qquad \textbf{(2-28)}$$

The inertia and damping ratio of the output dynamometer was calculated to be 1.0437 kgm^2 and 0.1 Nm/rad/s.

The inertias and damping ratios of input and output dynamometers, and input and output shafts were estimated by the previous 4 groups of test. The estimation results are concluded in Table 2-1.

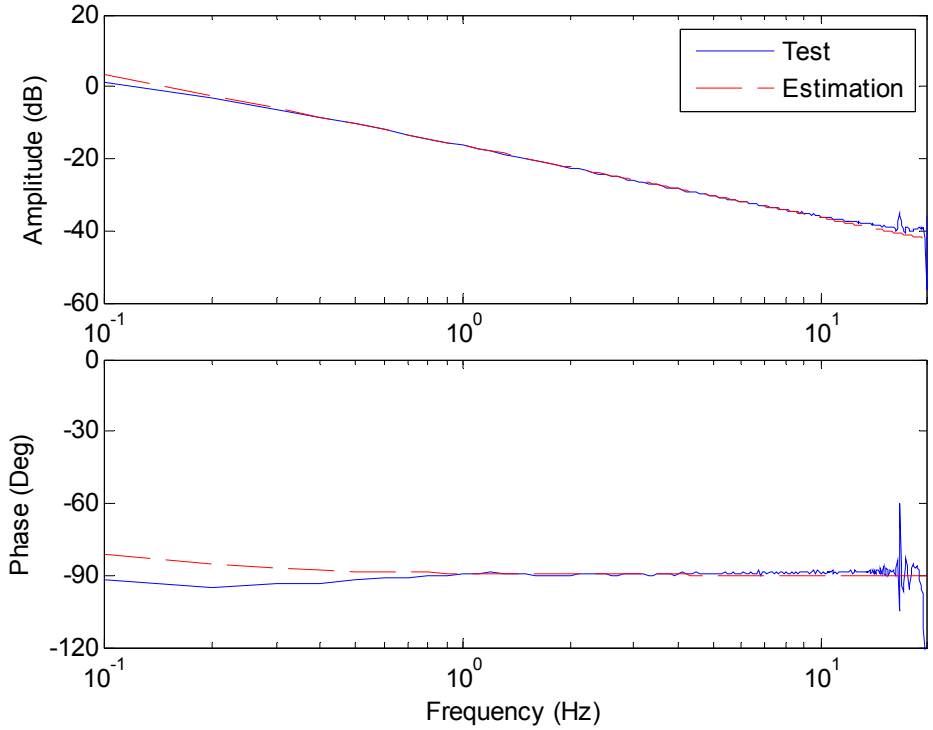

Figure 2-7 Experimental and estimated transfer functions between output dynamometer torque and speed with a 1:1 gear ratio driven by input dynamometer

Table 2-1 Estimation of system inertias and damping ratios

		I/P Dyno	I/P Shaft	O/P Shaft	O/P Dyno
Inertia	Estimation	0.4396	0.0406	0.084	1.0437
	Manufacture	0.43	N/A	N/A	0.9
	Total	0.5642			
Damping	Estimation	0.0432	0.0361	0.018	0.1
	Total	0.0973			

Furthermore, when testing on the output dynamometer with a 1:1 gear ratio, the output dynamometer torque transducer was measuring the torque driving the input and output shafts and input dynamometer. The total inertia and damping ratio of these three parts can be estimated using the recorded torque and speed signals of output dynamometer to verify the previous results. The estimation results for total inertia and damping ratio are shown in Figure 2-8.

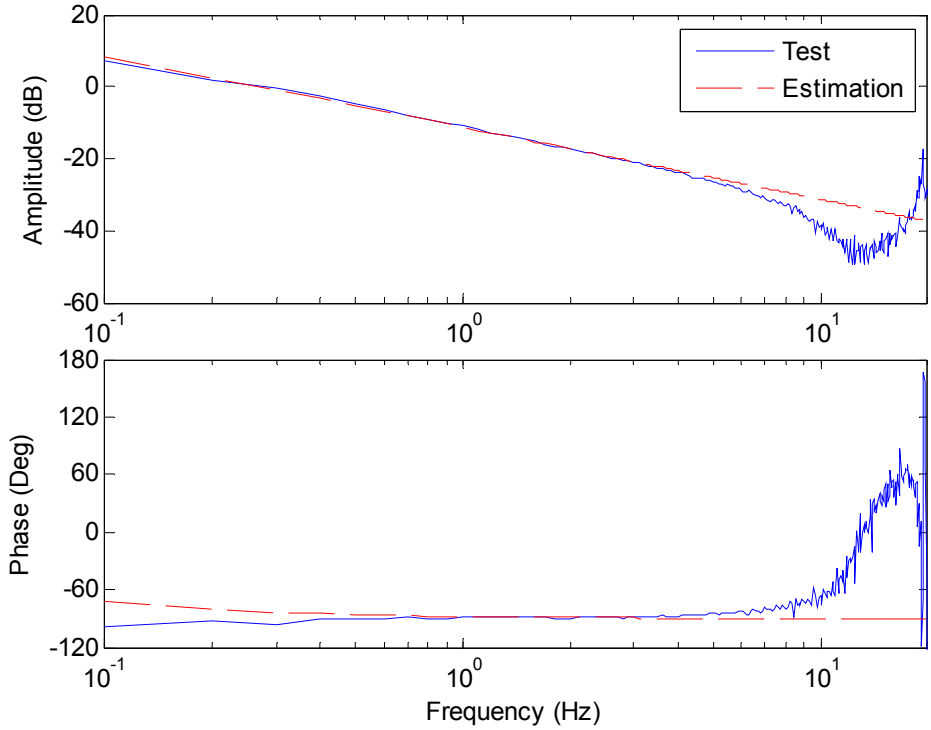

Figure 2-8 Experimental and estimated transfer functions between output dynamometer torque and speed with a 1:1 gear ratio driven by output dynamometer

Due to the backlash between the gears, the test result showed non-linear relationship between measured torque and speed at high frequencies. The estimation was carried out with a frequency range from 1 Hz to 3 Hz. It may represent the real system up to 6 Hz without obvious deviation from the test result. The estimated transfer function was:

$$L_{I\_D\&Shs}(s) = \frac{1.711}{s + 0.2076} \qquad \textbf{(2-29)}$$

The inertia and damping ratio of the input dynamometer and the whole shaft were calculated to be 0.5845 kgm^2 and 0.1213 Nm/rad/s. The values calculated from previous estimation were 0.5642 kgm^2 and 0.0973 Nm/rad/s. The values estimated for inertias are closer than the values estimated for damping ratios. From the estimation results, the values of the damping ratios were very small compared to the inertias, which will cause the cutoff frequency to be very low, e.g. 0.033 Hz in Equation (2-29), and the lack of data to estimate the damping ratios. Moreover, because the estimation of damping ratios relies on low frequency points, which are affected by measurement errors, the damping estimation results were not as accurate

as the inertias. Hence, the dynamics of the system load are mainly determined by the inertias of the system, especially in middle and high frequency range. Since the damping ratios are very small, the damping effect can actually be neglected.

Although the experimental results shown in Figures 2-5 and 2-8 were obtained from the same test on the output dynamometer speed control with a 1:1 gear ratio, the backlash effects are major in the latter case. The result shown in Figure 2-5 was obtained from the input dynamometer torque and speed signals, while the result shown in Figure 2-8 was obtained from the output dynamometer torque and speed signals. The load on the input dynamometer is the input dynamometer rotor, whereas the load on the output dynamometer is the combination of the input and output shafts, gear box, and the input dynamometer rotor. Therefore, the nonlinearity due to the backlash in the gear box has more effects on the results in Figure 2-8. The effect is significant above 10 Hz and would affect the performance of the feedforward controller as will be discussed later.

2.2.2 Estimation of Motor and Drive System

The next component to be estimated in the block diagram shown in Figure 2-2 is the motor and drive system. The motor and drive system takes a digital percentage control signal as input, converts it into analogue voltage signal in the drive system, and generates equivalent motor torque. There will be some dynamics between the percentage control signal and motor torque, which can be identified from the percentage and torque signals recorded in the test.

As mentioned above, the measured torque is the combined torque on the shaft. It is different from the torque generated by the motor. For a single motor without any external torque, the measured torque is the torque which is used to drive the connected shaft. When the inertia or damping of the shaft changes, the measured torque will change, even with the same control signal. Figure 2-9 shows the frequency responses between measured torque and percentage control signal of output dynamometer when running the motor with and without the output shaft attached.

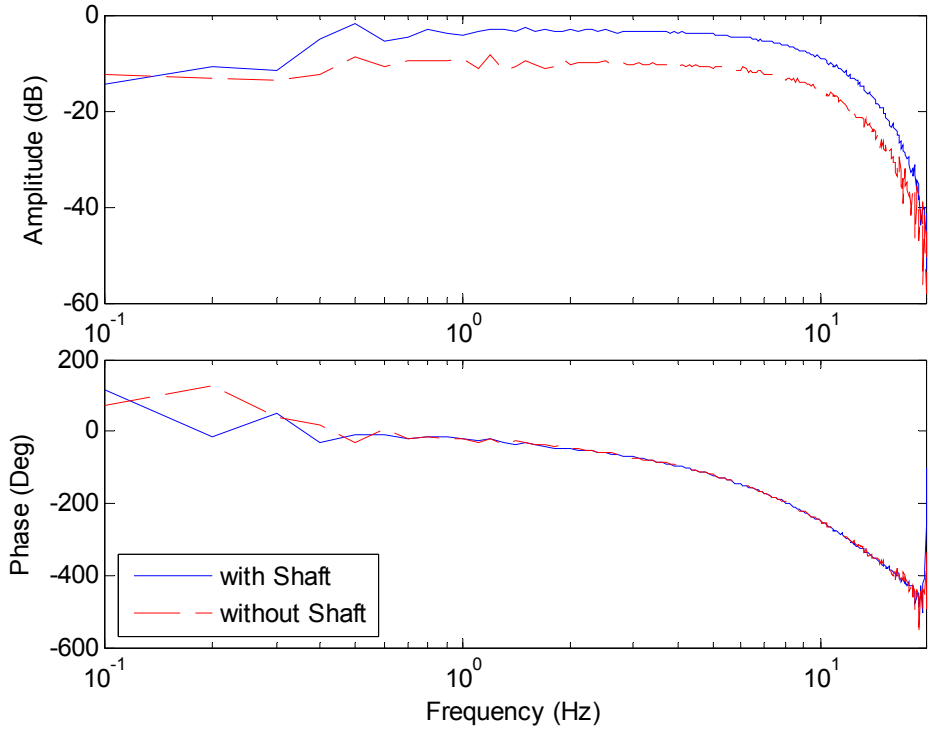

Figure 2-9 Frequency responses between measured torque and control signal of output dynamometer with and without output shaft attached

The low frequency range was still affected by torque measurement errors. Since the cutoff frequency can be very low, the damping effect can actually be neglected for middle and high frequency ranges. If only inertia effects were considered, then the measured torque would be proportional to the inertia attached to output dynamometer, as the motor inertia was constant. The relationship can be expressed as:

$$\frac{T_m}{T_g} = \frac{J_{Sh}}{J_{Sh} + J_M} \tag{2-30}$$

where T_g is the generated motor torque, T_m is the measured motor torque, J_M and J_{Sh} are the inertias of motor and attached shaft. Equation (2-30) implies that measured torque and generated torque are in phase, with a constant amplitude ratio. If the dynamics between the generated torque and the percentage control signal will not vary with the inertia attached to the motor, the measured torques will be in phase with a constant amplitude ratio, as observed in Figure 2-9. Therefore, to identify a relationship between the torque and percentage control signal, using generated torque will be a better solution. Moreover, when the two motors are coupled, torque generated by one motor will act as a disturbance torque to the other motor, which

will also have effects on the measured motor torque, but not on the generated motor torque.

Therefore, the model for motor and drive system was identified through a transfer function between generated motor toque and percentage control signal, rather than the measured torque. The generated motor torque can be calculated from the measured motor torque and motor speed as follows:

$$T_g = T_m + J_M \dot{\omega}_M + B_M \omega_M \quad \textbf{(2-31)}$$

where T_g is the generated motor torque, T_m is the measured motor torque, J_M and B_M are the inertia and damping ratio of the motor, and ω_M and $\dot{\omega}_M$ are the speed and acceleration of the motor. J_M and B_M were identified in previous section. T_m and ω_M were recorded. $\dot{\omega}_M$ was calculated from ω_M, by fitting a second order polynomial to three speed samples and calculating derivatives at each sample point. Since every speed sample was fitted a curve three times at the first, middle and last point, the acceleration was also calculated three times for each sampling instance. $\dot{\omega}_M$ used in Equation (2-31) was an average of these three values. The measured relationship between generated motor torque and percentage control signal for output dynamometer is shown in Figure 2-10, where there is no significant difference between the results with and without the output shaft attached.

The test result shown in Figure 2-10 further established that the relationship between generated motor torque and percentage control signal will not vary with the load inertia. Therefore, the dynamics of the motor and drive system is better to be interpreted using the generated motor torque instead of the measured motor torque. Referring back to the control diagram in Figure 2-2, the torque would be the torque generated by the motor and the load would be the external load plus the motor rotor inertia.

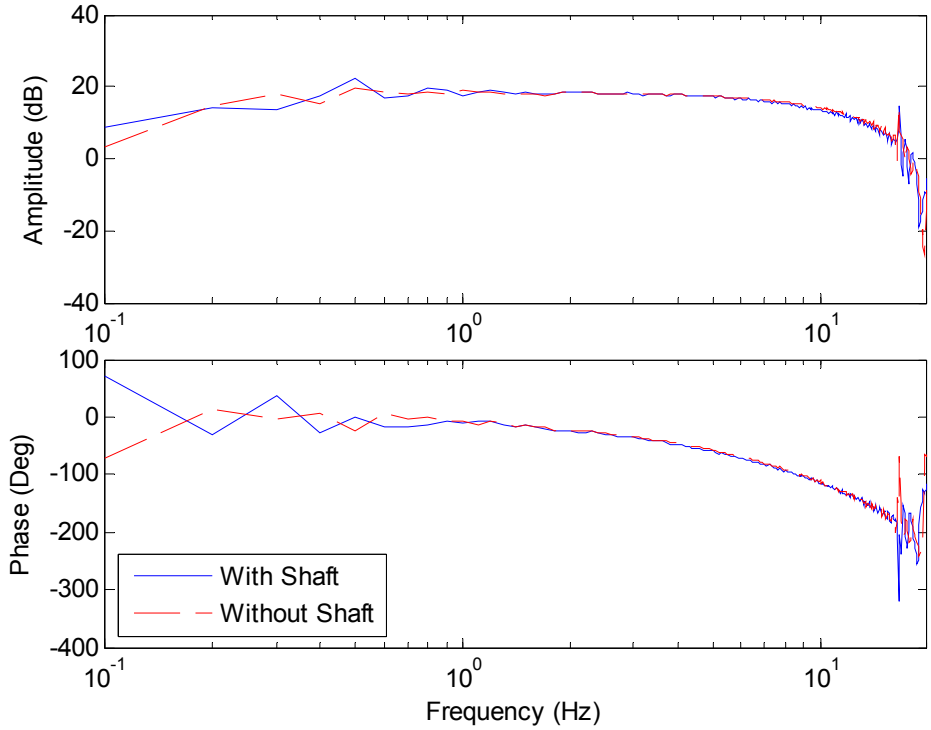

Figure 2-10 Frequency responses between generated torque and control signal of output dynamometer with and without output shaft attached

The test results become noisy beyond 15 Hz, as observed from the previous test results, which indicates the operation bandwidth of the motor. The smooth response indicates linear characteristics of the motor. Since the frequency range of up to 15 Hz was sufficient for testing CVTs, the estimation of motor and drive system model was carried out within the smooth range between 1 Hz and 15 Hz using averaged values from 5 tests. The estimated transfer function between generated torque and percentage control signals for output dynamometer is as follows:

$$G_{O\_Dyno}(s) = \frac{1.243s^3 - 121.7s^2 + 2.468e4s + 6.592e5}{s^3 + 97.29s^2 + 5660s + 7.184e4} \quad \textbf{(2-32)}$$

The frequency response of the estimated transfer function is shown in Figure 2-11, compared with the averaged test results.

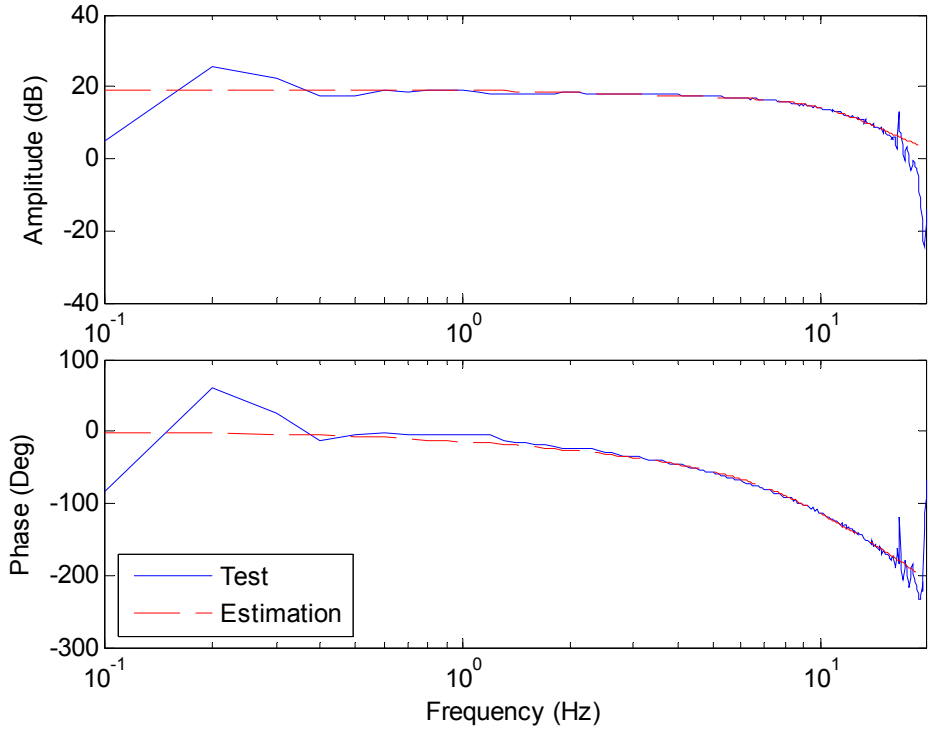

Figure 2-11 Experimental and estimated transfer functions between generated torque and control signal of output dynamometer

A similar identification procedure was carried out for the input dynamometer, also within the frequency range of 1 Hz to 15 Hz. The estimated transfer function between generated motor torque and percentage control signals was found to be:

$$G_{I\_Dyno}(s) = \frac{0.7651s^3 - 66.06s^2 + 1.478e4s + 5.141e5}{s^3 + 98.34s^2 + 6134s + 9.429e4} \qquad \textbf{(2-33)}$$

The frequency responses of the estimated transfer function and averaged test results are shown in Figure 2-12.

The transfer functions have been estimated for the motor and drive system for both input and output dynamometers at a certain motor speed. The linear regions i.e. different motor torques and speeds where the estimated transfer functions can represent the motor behaviour need to be further established.

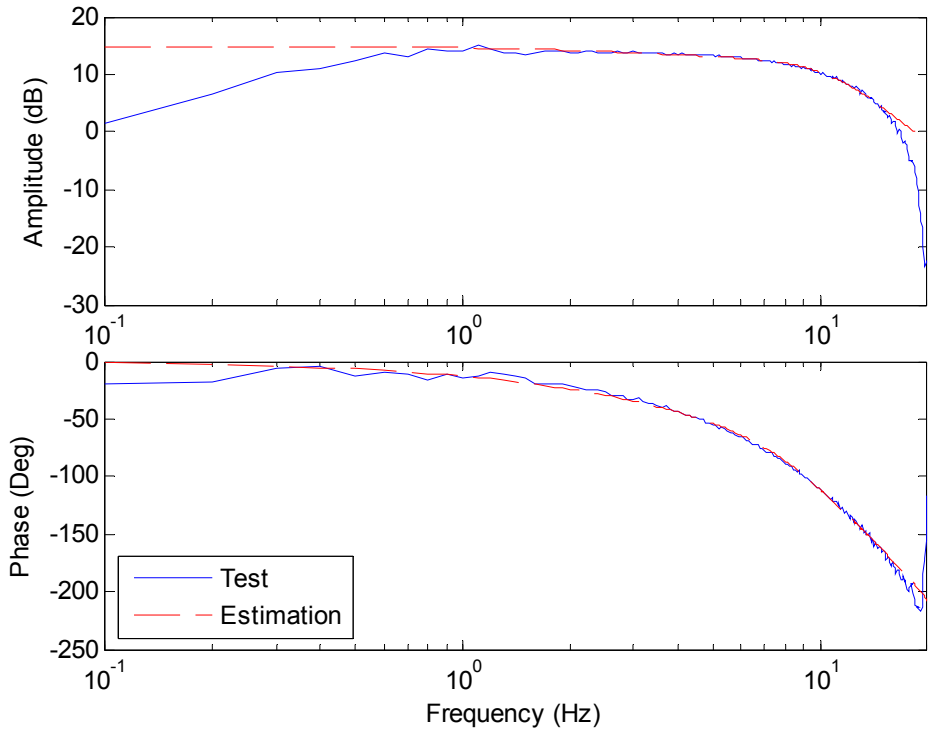

Figure 2-12 Experimental and estimated transfer functions between generated torque and control signal of input dynamometer

Further tests were carried out with different levels of speed demands, each demand consisting of a DC speed signal and an SPHS speed signal with an amplitude scaled to 5% of the DC speed. For the output dynamometer, the steady state speed was increased from 250 rev/min to 1500 rev/min, by 250 rev/min intervals. The torque generated by the motor was increased relatively due to the larger acceleration of the motor. The frequency response between generated torque and percentage control was obtained by Fourier Transform as in previous tests, and are shown in Figure 2-13 with three different speeds, where the frequency responses were very similar to each other. It can be concluded that the characteristics of output dynamometer and its drive system is linear. The generated motor torque depended only on the percentage control signal, but not on the motor torque or speed. The behaviour may be due to the control strategy that exists in the drive system.

The dynamic response of the motor and drive system was also examined for the input dynamometer in a similar way. Considering its application of emulating an IC engine, the steady state speed demand for the input dynamometer was increased from 500 rev/min to 4000 rev/min in 500 rev/min interval, plus an SPHS speed signal with

scaled amplitude of 5% of the steady state speed. The results are shown in Figure 2-14 with three different steady state speeds.

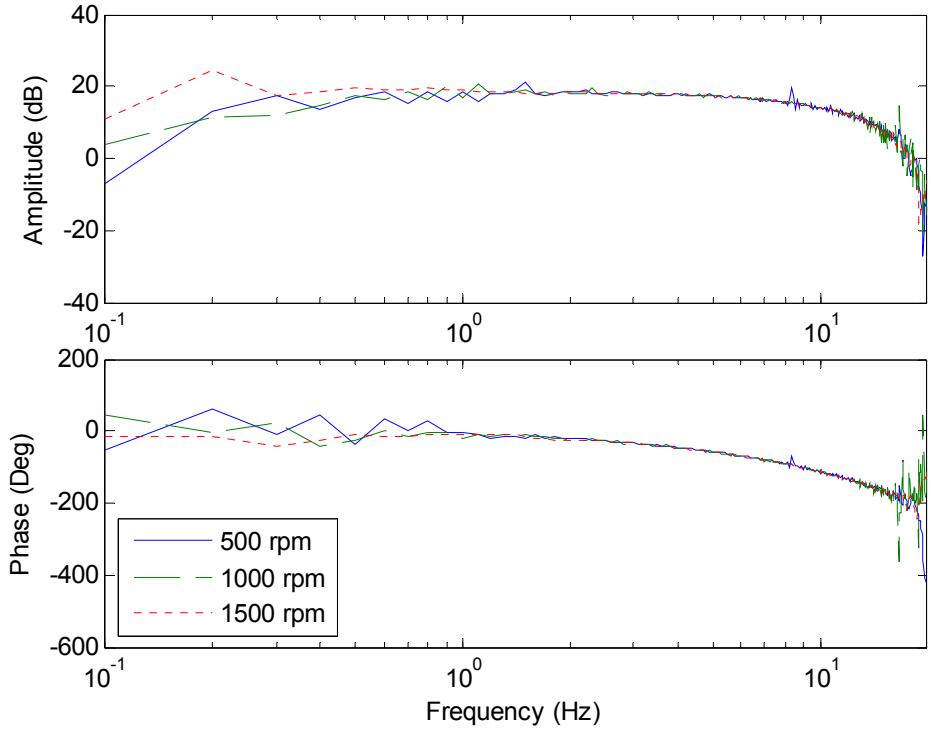

Figure 2-13 Frequency responses between generated torque and control signal of output dynamometer with different speeds

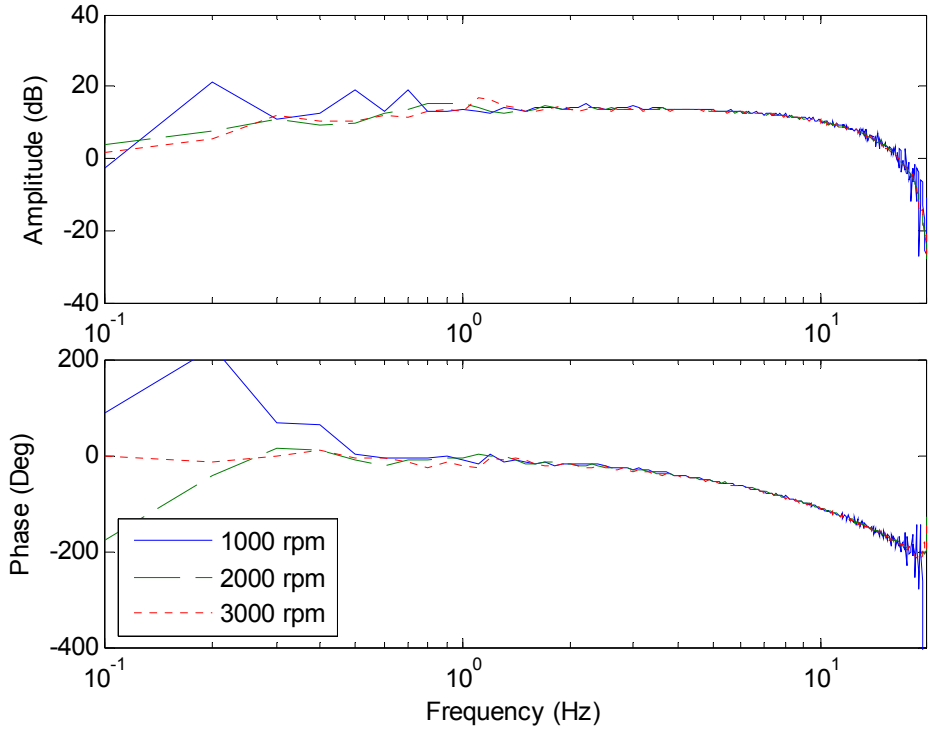

Figure 2-14 Frequency responses between generated torque and control signal of input dynamometer with different speeds

Similar conclusions can be drawn that the generated motor torque of the input dynamometer depends only on the drive signal, but not on motor torque or motor speed. Hence, the motor and drive system was linear for both the input dynamometer and the output dynamometers within the frequency range of up to 15 Hz. Therefore, the transfer functions (2-32) and (2-33) for output and input dynamometers can also be used for other motor torques and speeds.

It can also be seen from Figures 2-13 and 2-14 that there were fewer fluctuations in the low frequency range at higher speed as the increasing measured torque levels minimized the effects of measurement error.

2.3 Transmission Delay in CAN Bus

Previous identification tests were carried out with closed loop speed control, as shown in Figure 2-2, with a PID controller in the CP CADET system. When the PID controller was implemented in dSPACE, the two systems were communicating with each other through a CAN bus system. In other words, the CAN bus system was used to send the percentage control signal calculated from PID controller in dSPACE to CP CADET, and also the torque and speed measured by CP CADET back to the PID controller in dSPACE. There will be a time delay associated with transmitting and receiving signals between dSPACE and CP CADET systems. These delays need to be identified as they may affect the stability of the overall system.

The signals in the system were recorded at multiple locations. For example, the percentage control signal was recorded at five points on the signal transmission path. Figure 2-15 shows the locations where the control signal was recorded. Firstly, it was calculated from Simulink model of the PID controller (1). This signal was recorded by dSPACE control desk under the model root. Then it was sent to CP CADET through CAN bus as a transmitted (TX) message of the setpoint (2), which was recorded by dSPACE control desk under CAN bus configuration. After receiving this message by CP CADET, it was recorded in CP as a loopback signal (3) to drive the dynamometer. Although it was not used by the Simulink real-time model anymore, this signal was still sent back to dSPACE as a received (RX) message of loopback_CAN (4), which was recorded by dSPACE control desk under CAN bus

configuration. After receiving this signal by the real-time model, this signal was recorded again as loopback_Sim (5) by dSPACE control desk under the model root.

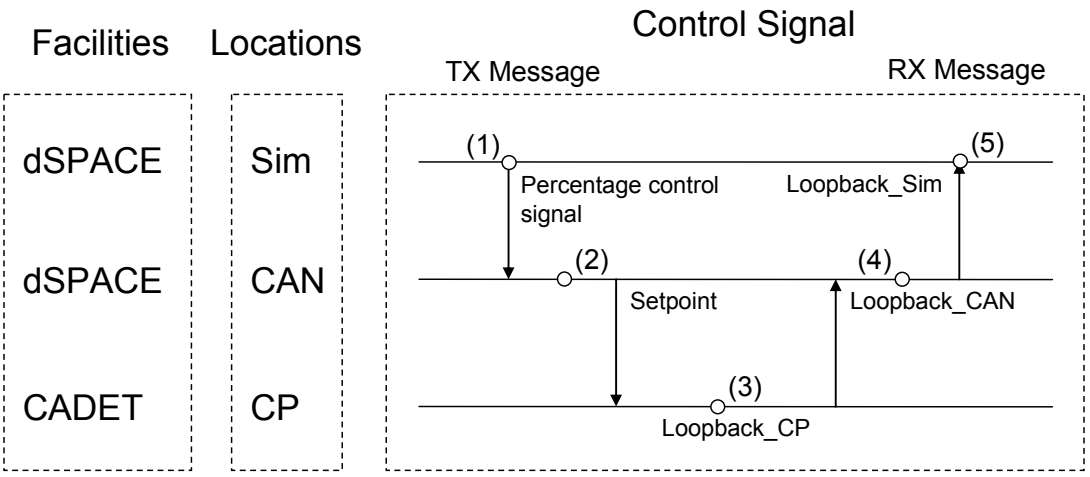

Figure 2-15 Recording locations for the percentage control signal

By comparing the same signal recorded from different locations in the system, the delay in transmitting and receiving messages can be identified. Figure 2-16 shows the control signal recorded by dSPACE control desk in Simulink model and CAN bus configuration, which were synchronized by dSPACE. The control signal recorded by CP CADET is not shown, because it was not synchronized with dSPACE.

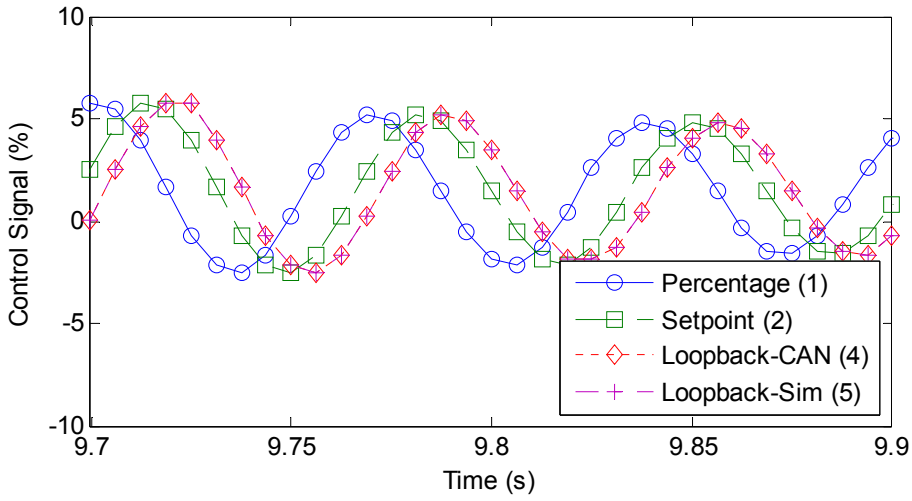

Figure 2-16 Percentage control signal recorded in different locations

Together with Figure 2-15, it can be observed that there are two samples delay from percentage signal (1) to setpoint signal (2), and no delay from loopback_CAN (4) to loopback_Sim (5). From setpoint (2) to loopback_CAN (4), there was one sample

delay. This one sample delay could exist either between setpoint (2) and loopback_CP (3), or between loopback_CP (3) and loopback_CAN (4). To examine this, different sampling frequencies were used for the CAN bus and CP control system. It was observed that the length of this delay varied with the CP control frequency, but not with the CAN bus sampling frequency. It was always one sample delay of CP control rate, which meant the delay existed between loopback_CP (3) and loopback_CAN (4). Different sampling frequencies were also applied to the Simulink model and the CAN bus. It was observed that the two samples delay between percentage (1) and setpoint (2) was depended on the Simulink model sampling rate. The delays on signal transmitting path in the system were concluded as in Figure 2-17.

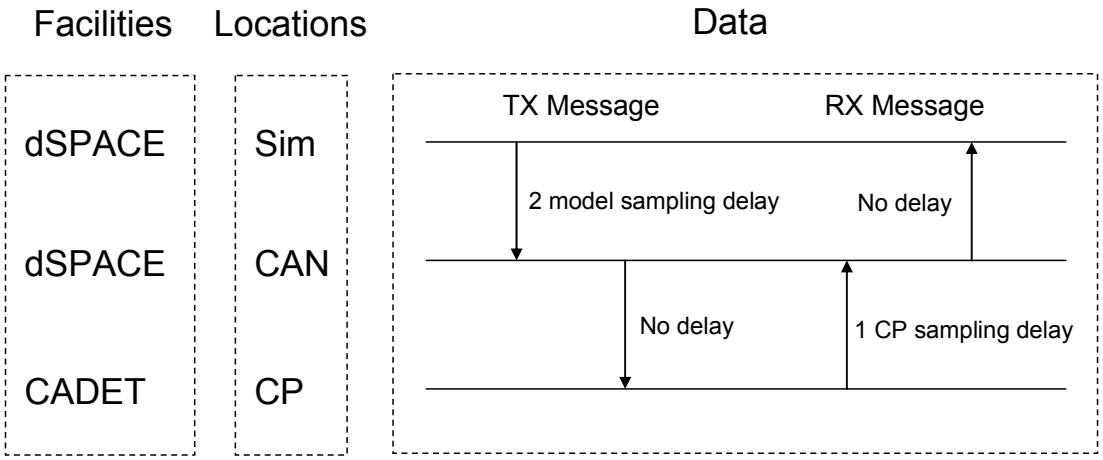

Figure 2-17 Delays on signal transmitting path

Normally, the sampling rate on the CAN bus system is slower than the simulation sampling rate by an integer divider. Delay in the TX message was dependent on the simulation sampling rate, while delay in the RX message was dependent on the control frequency in the CP CADET system. In the tests with the CAN bus, the percentage control signal calculated from the real-time model was sent to CP CADET as a TX message to drive the dynamometer, the delay can be reduced by increasing sampling rate in Simulink model to be as small as required. Measured torque and speed signals were sent back to the real-time Simulink model as RX message to calculate next control signal sample. The delay was restricted to be at least 6.25 ms, as the fastest control rate available on the CP CADET system is 160 Hz.

2.4 Model for Speed Control with CAN Bus Delay

When the CAN bus is implemented in the system to forward messages, the effects of the delays identified in previous section have to be considered. This was first examined for the output dynamometer speed control system. A Simulink model was constructed based on the identified models for the system components, and the effects of CAN bus delay on the system was investigated in simulation in order to retune the PID controller parameters. Then a transfer function for the whole closed loop system was derived to design the feedforward controller in the next chapter. Alternatively, the transfer function can be estimated directly from the test results between the speed demand signal and the measured speed signal. Both methods are described here and compared with test results.

2.4.1 Simulink Model

Based on the speed control diagram shown in Figure 2-2, a CAN bus system can be incorporated into the model. The PID controller is placed in dSPACE instead of in the CP CADET system. The output of PID controller, the percentage control signal, is sent to CP console through the CAN bus. The measured speed is then sent back to dSPACE through CAN bus. The block diagram is shown in Figure 2-18.

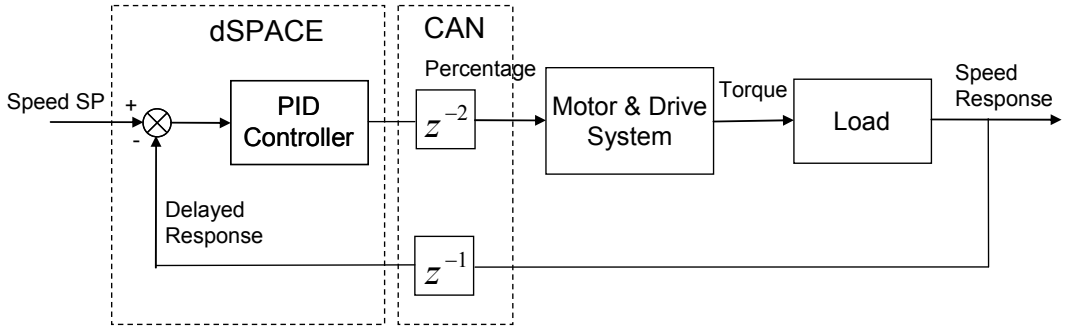

Figure 2-18 Speed control block diagram with CAN bus delay

After including the delays in the model, if the same PID parameters as in the CP CADET system are used, the simulation results in Figure 2-19 show oscillations in the speed response. The speed demand consisted of a DC speed of 1000 rev/min plus an SPHS signal with frequency up to 15 Hz and an amplitude of 40 rev/min.

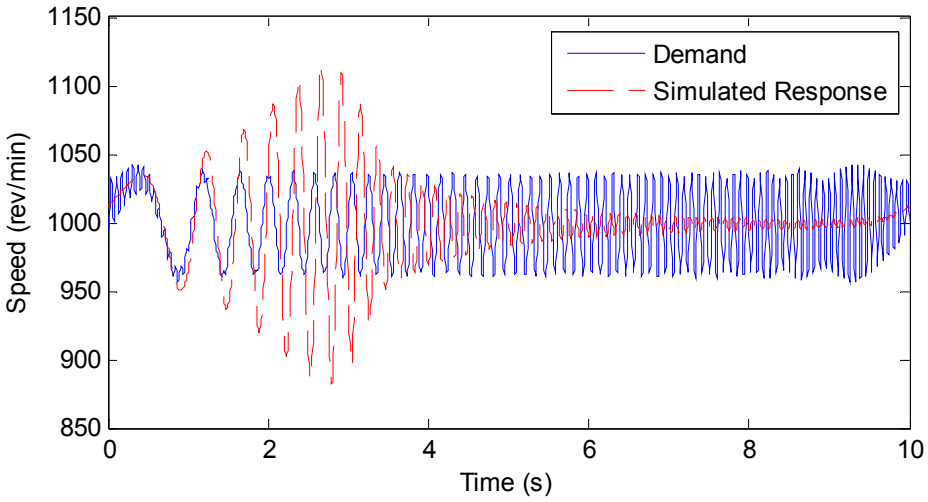

Figure 2-19 Simulated speed response with CAN bus and original PID parameters

The performance can be improved by retuning the PID parameters. This was first performed in simulation. Improved PID parameters were found to be 0.13 for proportional gain, 0.25 for integral gain, and 0 for derivative gain, which yields a new transfer function for the PID controller as follows:

$$G_{PID}(s) = \frac{0.13s + 0.25}{s} \qquad \textbf{(2-34)}$$

Simulations were run with these new PID parameters, with the same speed demand as before. The test results are shown in Figure 2-20.

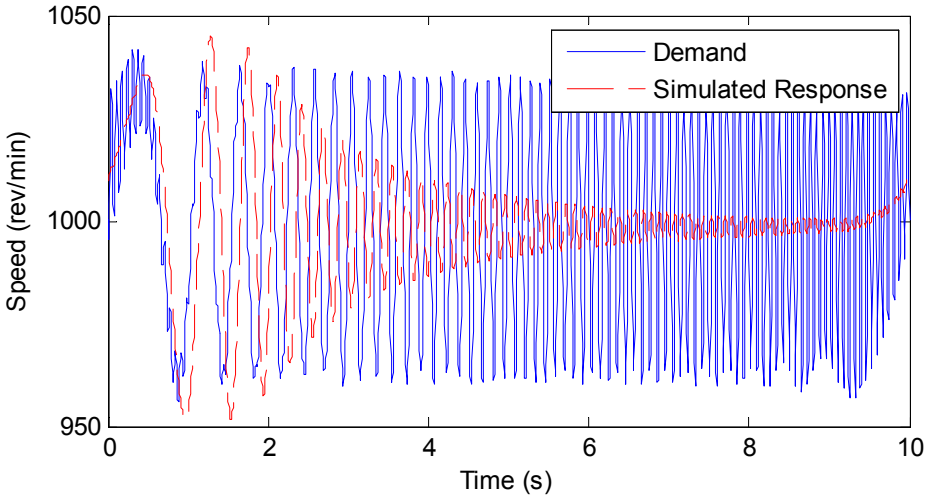

Figure 2-20 Simulated speed response with CAN bus and new PID parameters

Actual tests were carried out with the same speed demand to validate the Simulink model. The simulation results and test results are compared in Figure 2-21. Magnified views are shown in Figure 2-22.

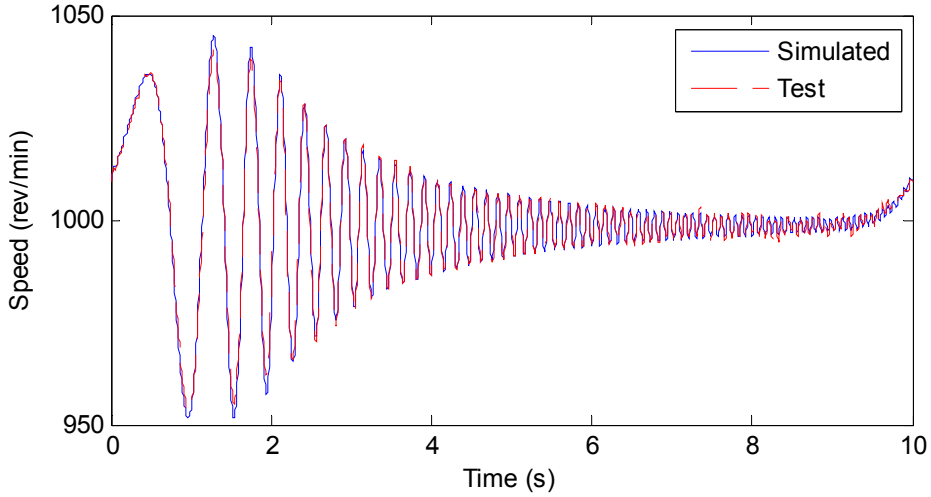

Figure 2-21 Comparison of simulation and test results of output dynamometer speed control with new PID parameters

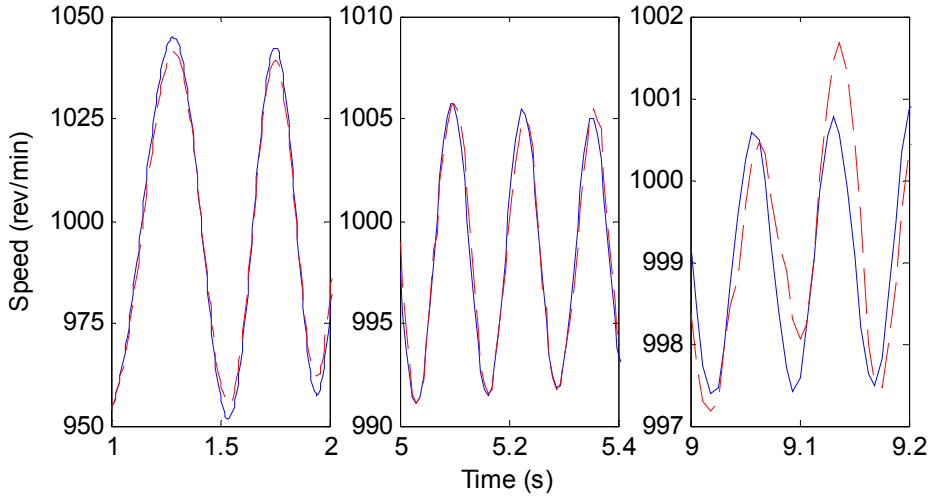

Figure 2-22 Magnified view of Figure 2-21

It can be seen that the simulation results offered a good fit to the test results, but there are some fluctuations for high frequency components, due to the small amplitude, hence high noise to signal ratio, of the signal. Comparison was also performed in the frequency domain in Figure 2-23. The frequency response was calculated by taking the Fourier Transform of the speed demand and speed response in both simulation and test results.

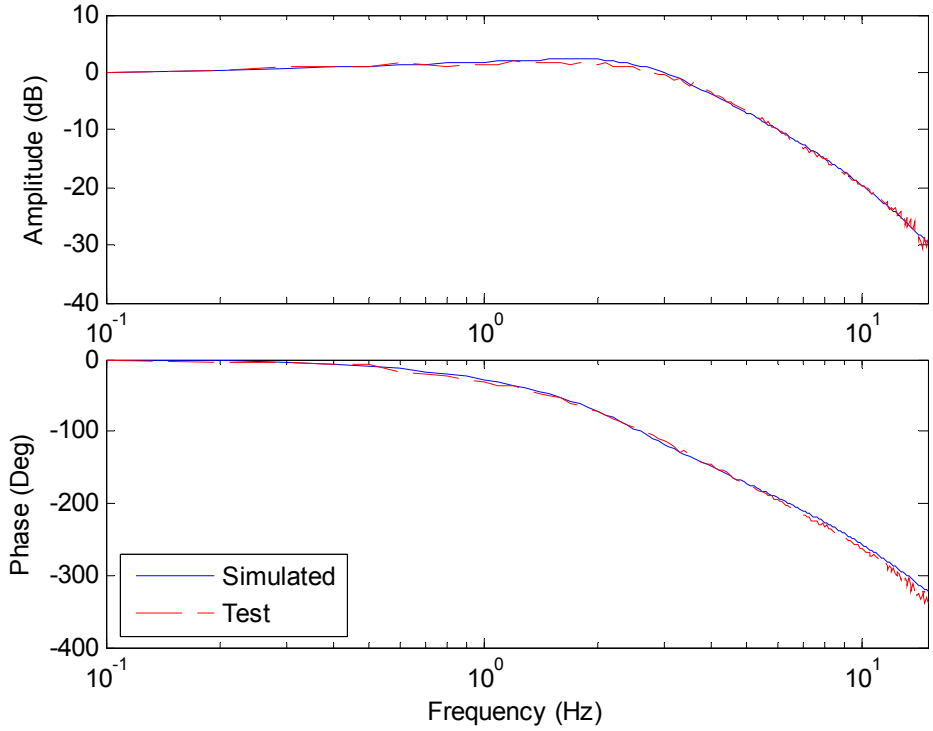

Figure 2-23 Frequency response of Figure 2-21

It can be seen that the simulated frequency response is close to the test results at most frequencies. Although they were slightly different in the range between 2 Hz and 4 Hz, it is acceptable for the application of using the model to examine the stability of the system and also to tune the PID parameters.

To design the feedforward controller, a transfer function for the whole speed control system between the speed demand and speed response is required. The transfer functions for load, motor and drive system were estimated in Section 2.2, and the PID parameters were also given in the previous section. Hence, the overall transfer function for speed control can be calculated.

The discrete time counterpart for motor and load with zero order hold on the input can be calculated as:

$$H_{M\&L}(z^{-1}) = \frac{0.04759z^{-1} - 0.1259z^{-2} + 0.167z^{-3} - 0.08104z^{-4}}{1 - 3.373z^{-1} + 4.302z^{-2} - 2.473z^{-3} + 0.5435z^{-4}} \quad \textbf{(2-35)}$$

and the discrete time counterpart for PID controller with zero order hold on the input can be calculated as:

$$H_{PID}(z^{-1}) = \frac{0.13 - 0.1284z^{-1}}{1 - z^{-1}} \quad \textbf{(2-36)}$$

According to the control diagram shown in Figure 2-18, including the delays in the system, the closed loop discrete time transfer function between the speed demand and speed response can be obtained as follows:

$$H_{Close}(z^{-1}) = \frac{\begin{array}{c} 0.006186z^{-4} - 0.02248z^{-5} + 0.03788z^{-6} \\ -0.03199z^{-7} + 0.01041z^{-8} \end{array}}{\begin{array}{c} 1 - 4.373z^{-1} + 7.675z^{-2} - 6.775z^{-3} + 3.023z^{-4} \\ -0.5659z^{-5} + 0.03788z^{-6} - 0.03199z^{-7} + 0.01041z^{-8} \end{array}} \quad \textbf{(2-37)}$$

The frequency response of the calculated closed loop transfer function is shown in Figure 2-24, compared with the experimental transfer function between derived and demanded speed signals.

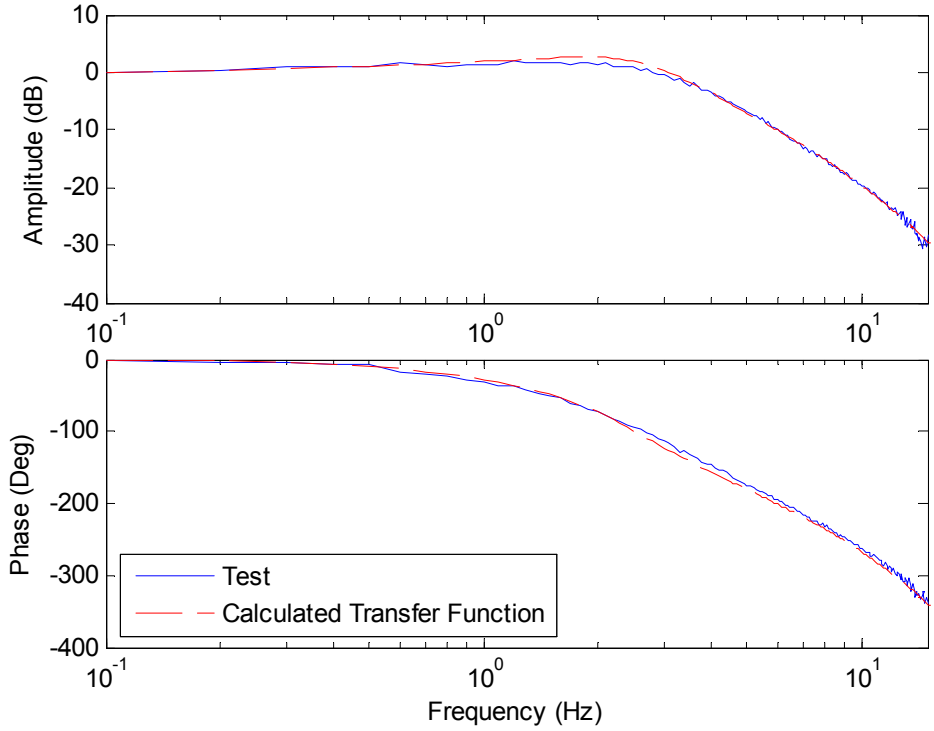

Figure 2-24 Experimental and calculated transfer function of output dynamometer speed control

The overall transfer function in Equation (2-37) was calculated from separate transfer functions, which were estimated within the frequency range of 1 Hz to 15 Hz, and therefore it represents the system within this frequency range.

2.4.2 Estimated Transfer Function

The overall transfer function could also be estimated directly by taking speed demand as input signal and speed response as output signal. The estimation was carried out within the frequency range of 1 Hz and 15 Hz. Different orders were specified for numerator and denominator of the estimated transfer function. The statistical analysis results showed that a third order for numerator and fourth order for denominator provided the best fit. The estimation result is as follows:

$$G_{Close}(s) = \frac{1.096s^3 - 47.86s^2 - 2043s + 1.336e6}{s^4 + 77.91s^3 + 5598s^2 + 9.494e4s + 1.336e6} \quad \textbf{(2-38)}$$

The equivalent discrete time transfer function with 160 Hz sampling frequency and zero order hold on the input is:

$$H_{Close}(z^{-1}) = \frac{0.004442z^{-1} - 0.0142z^{-2} + 0.01713z^{-3} - 0.005788z^{-4}}{1 - 3.434z^{-1} + 4.503z^{-2} - 2.682z^{-3} + 0.6145z^{-4}} \quad \textbf{(2-39)}$$

The frequency response of estimated transfer function is shown in Figure 2-25, and compared with test results.

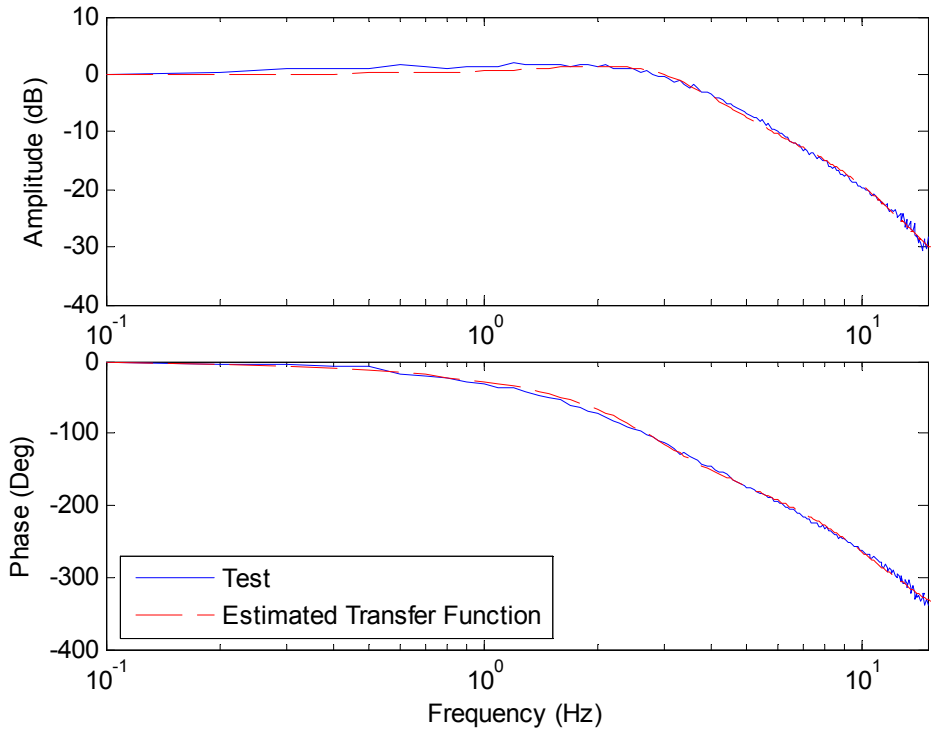

Figure 2-25 Experimental and estimated transfer functions of output dynamometer speed control

The estimated transfer function offered a better fit than the calculated transfer function in the middle frequency range, but a slightly worse fit in the low frequency range. Both calculated and estimated transfer functions can be considered as a good fit to the test results.

Frequency responses of the calculated transfer function and estimated transfer function are compared in Figure 2-26. The frequency range to be shown was extended to 50 Hz.

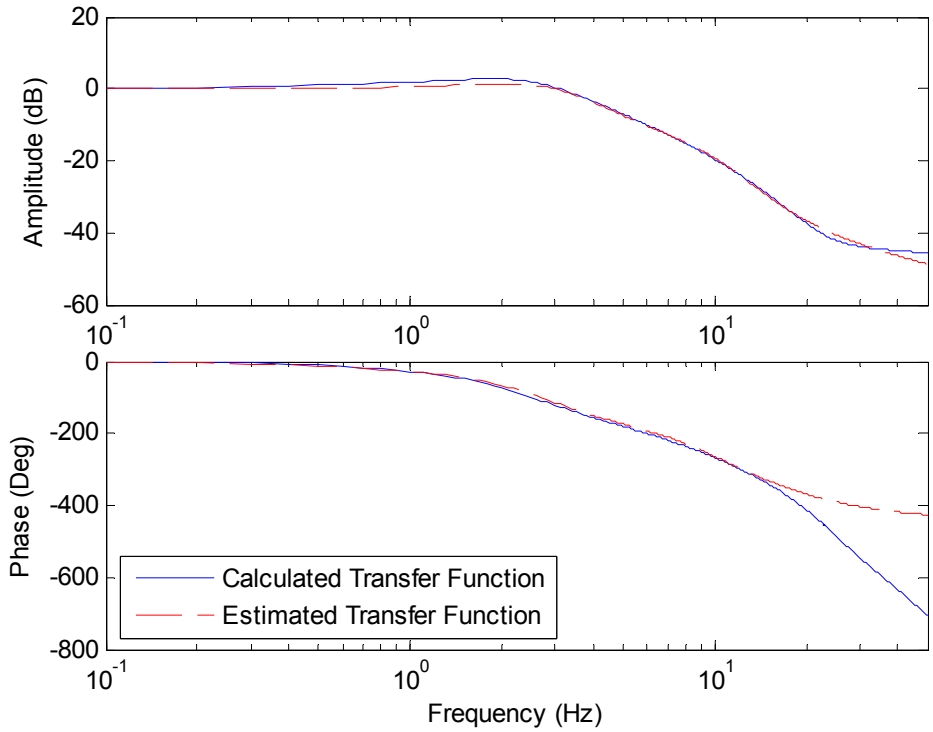

Figure 2-26 Calculated and estimated transfer functions of output dynamometer speed control

It can be seen that the calculated and estimated transfer functions possess different characteristics, but within the frequency range, where the estimation was carried out, they produced similar results.

Comparing the calculated transfer function in Equation (2-37) and estimated transfer function in Equation (2-39), the orders of the numerator and denominator are different. In Equation (2-37) the relative order, i.e. order of the denominator minus numerator, is four, while in Equation (2-39) the relative order is only one. When the overall transfer function is estimated, the relative order is specified to achieve a good fit for only the interested frequency range, rather than the whole frequency range. Moreover, in Equation (2-38), all the poles and zeros have break efficiencies within

20 Hz. They are considered to be significant to the system within the interested frequency range so that the estimated transfer function can not be simplified anymore. This characteristic is very useful and will be utilized in the design of a feedforward controller. It is beneficial to have a smaller relative order when inverting the transfer function, because smaller relative order means that less future sampling values are needed to implement the controller. This will be discussed in detail in the next chapter.

Chapter 3

Feedforward Tracking Controller

In the previous chapter, a methodology was presented to identify the dynamics of a linearized system in the desired frequency range, leading to a continuous time transfer function, and its counterpart in discrete time was obtained by placing a zero order hold on the input signal. The discrete time transfer function is now used to create an inverse system to be used as a feedforward controller.

The concepts of minimum and non-minimum phase system are introduced first. Direct inverse for minimum phase systems is stable and straightforward. For non-minimum phase systems, the technique of developing a digital preview filter (DPF) is employed here to approximate the inverse of unstable zeros using Lagrange method as part of the feedforward controller. To apply DPFs, future information of the input trajectory was required. Normally, the future values can be predicted in some way, but the prediction can never be perfect, and will certainly affect the control performance. In this chapter, DPFs will be designed for the output dynamometer speed control and input dynamometer torque control in a novel way, so that no future information of input trajectories is required, which allows a non-causal controller to be causal.

3.1 Digital Preview Filter

On an approximate inversion of a non-minimum system, the zero phase error tracking control (ZPETC) has drawn interest among researchers, because zero phase shift is obtain at all frequencies, with a small gain error at low frequencies. Based on ZPETC, a precision tracking control scheme was proposed in [51] to further improve gain characteristics at higher frequencies. The optimal design was also obtained by Lagrange method.

One of the merits of this scheme was that a weighting function can be incorporated into the penalty function. This will ensure the gain error is better compensated in the desired frequency range. The parameterization of the digital preview filter was presented in an explicit form. Given a discrete time transfer function, the filter could easily be parameterized to minimize the penalty function with a fixed number of preview steps. The preview steps can be chosen arbitrarily. Generally, a greater number of available preview steps renders better tracking performance.

3.1.1 Design of DPF

The feedforward control scheme as shown in Figure 1-7, $Q(z^{-1})$ is the feedforward controller transfer function, and $H(z^{-1})$ is the original system transfer function, which can be either closed or open-loop. When the system is a non-minimum phase system, the transfer function can normally be separated into two parts:

$$H(z^{-1}) = H_a(z^{-1})H_u(z^{-1}) \quad \textbf{(3-1)}$$

in which $H_u(z^{-1})$ includes all the unstable zeros.

$$H_u(z^{-1}) = \prod_{i=1}^{P}(1 - z_i z^{-1}) \quad \textbf{(3-2)}$$

$H_a(z^{-1})$ can be directly inverted to be $H_a^{-1}(z^{-1})$ as part of feedforward controller. A digital preview filter $DPF(z^{-1})$ can be designed to approximate $H_u^{-1}(z^{-1})$ as another part of feedforward controller. Hence, the feedforward controller can be expressed as:

$$Q(z^{-1}) = H_a^{-1}(z^{-1})H_u^{-1}(z^{-1}) \approx H_a^{-1}(z^{-1})DPF(z^{-1}) \quad \textbf{(3-3)}$$

The ratio $R(z^{-1})$ is defined as follows to measure the tracking performance:

$$R(z^{-1}) = DPF(z^{-1})\prod_{i=1}^{P}(1 - z_i z^{-1}) \quad \textbf{(3-4)}$$

To achieve perfect tracking, the ratio function $R(z^{-1})$ should have a unity gain and zero phase shift within the desired frequency range. To achieve this objective, the digital preview filter $DPF(z^{-1})$ is divided into two parts as follows:

$$DPF(z^{-1}) = DPF_A(z^{-1})DPF_\Phi(z^{-1}) \tag{3-5}$$

where $DPF_\Phi(z^{-1})$ is to make the digital preview filter have the same phase as that of $H_u^{-1}(z^{-1})$, and $DPF_A(z^{-1})$ is to make the gain of the digital preview filter to be as close to that of $H_u^{-1}(z^{-1})$ as possible.

The design of $DPF_\Phi(z^{-1})$ was initially presented in [47] as ZPETC controller.

$$DPF_\Phi(z^{-1}) = \prod_{i=1}^{P} \frac{(1-\bar{z}_i z)}{(1-z_i)(1-\bar{z}_i)} \tag{3-6}$$

where $\bar{z}_i$ is the complex conjugate of the unstable zero z_i. The denominator in Equation (3-6) ensures a unity DC gain. Substituting Equations (3-5) and (3-6) into Equation (3-4), the ratio function $R(z^{-1})$ becomes:

$$R(z^{-1}) = DPF_A(z^{-1}) \prod_{i=1}^{P} \frac{(1-\bar{z}_i z)(1-z_i z^{-1})}{(1-z_i)(1-\bar{z}_i)} \tag{3-7}$$

If, among P unstable zeros, there are P_1 real unstable zeros, and P_2 pairs of the complex unstable zeros, Equation (3-7) can be rewritten as:

$$\begin{aligned} R(z^{-1}) &= DPF_A(z^{-1}) \prod_{k=1}^{P_1} \left[\eta_k^0 + \eta_k^1 (z+z^{-1})\right] \prod_{j=1}^{P_2} \left[\xi_j^0 + \xi_j^1 (z+z^{-1}) + \xi_j^2 (z+z^{-1})^2\right] \\ &= DPF_A(z^{-1}) \sum_{i=0}^{P} \gamma_i (z+z^{-1})^i \end{aligned} \tag{3-8}$$

where

$$\eta_k^0 = \frac{1+z_k^2}{(1-z_k)^2} \quad \eta_k^1 = \frac{-z_k}{(1-z_k)^2}$$

$$\xi_j^0 = \frac{1+2(2\cos^2\theta_j - 1)r_j^2 + r_j^4}{(1-2r_j\cos\theta_j + r_j^2)^2} \quad \xi_j^1 = \frac{-2r_j\cos\theta_j(1+r_j^2)}{(1-2r_j\cos\theta_j + r_j^2)^2} \quad \xi_j^2 = \frac{r_j^2}{(1-2r_j\cos\theta_j + r_j^2)^2} \tag{3-9}$$

In which r_j and θ_j are the magnitude and argument of the complex unstable zeros. It can be seen from Equation (3-8) that $DPF_{\Phi}(z^{-1})H_u(z^{-1})$ can be expressed as a function of $z+z^{-1}$ and has zero phase shift. In fact, $z+z^{-1}$ is a minimal zero phase filter and it is defined as the zero phase kernel in [51]. To make $R(z^{-1})$ to have a zero phase shift, $DPF_A(z^{-1})$ must also have zero phase shift. Therefore, it can be also formulated as a function of the zero phase kernel as:

$$DPF_A(z^{-1}) = \sum_{k=0}^{N-P} \alpha_k (z+z^{-1})^k \tag{3-10}$$

where N is the required preview steps of the digital preview filter. Now the ratio function can be expressed as:

$$R(z^{-1}) = \left[\sum_{i=0}^{P} \gamma_i (z+z^{-1})^i\right]\left[\sum_{k=0}^{N-P} \alpha_k (z+z^{-1})^k\right] \tag{3-11}$$

3.1.2 Norm Optimization for DPF

The coefficients α_k can be determined by minimizing the following penalty function J, formulated by L_2-norm:

$$J = \int_0^{\pi} w(\theta)\left[R(e^{j\theta})-1\right]^2 d\theta \tag{3-12}$$

with the constraint:

$$R(e^{j\theta})\big|_{\theta=0} = 1 \tag{3-13}$$

where θ is the normalized frequency, $\theta = \omega T_s$, ω is the frequency, T_s is the sampling time, and $w(\theta)$ is the weighting function, which can be chosen according to particular applications and the available information. The constraint in Equation (3-13) is to ensure that both the digital preview filter $DPF(z^{-1})$ and the unstable inverse model $H_u^{-1}(z^{-1})$ have the same DC gain. In order to obtain the L_2-norm optimal solution for the polynomial parameters, α_k , Lagrange method is employed here. The Lagrange function $\Gamma(\alpha,\lambda)$ is defined as:

$$\Gamma(\alpha,\lambda)=\int_0^{\pi} w(\theta)\left[R(e^{j\theta})-1\right]^2 d\theta+\lambda\left[R(e^{j\theta})\big|_{\theta=0}-1\right] \tag{3-14}$$

where λ is the Lagrange multiplier. From (3-11), $R(e^{j\theta})$ can be expressed as:

$$\begin{aligned} R(e^{j\theta}) &= \left[\sum_{i=0}^{p}\gamma_i(2\cos\theta)^i\right]\left[\sum_{k=0}^{N-p}\alpha_k(2\cos\theta)^k\right] \\ &= \boldsymbol{\gamma}^T\begin{bmatrix}1\\ 2\cos\theta\\ \vdots\\ (2\cos\theta)^p\end{bmatrix}\begin{bmatrix}1 & 2\cos\theta & \cdots & (2\cos\theta)^{N-p}\end{bmatrix}\boldsymbol{\alpha} \\ &= \boldsymbol{\gamma}^T\begin{bmatrix}1 & 2\cos\theta & \cdots & (2\cos\theta)^{N-p}\\ 2\cos\theta & (2\cos\theta)^2 & \cdots & (2\cos\theta)^{N-p+1}\\ \vdots & \vdots & \ddots & \vdots\\ (2\cos\theta)^p & (2\cos\theta)^{p+1} & \cdots & (2\cos\theta)^N\end{bmatrix}\boldsymbol{\alpha} \\ &= \boldsymbol{\gamma}^T\mathbf{A}\boldsymbol{\alpha} \end{aligned} \tag{3-15}$$

where

$$\begin{aligned} \boldsymbol{\gamma} &= \begin{bmatrix}\gamma_0 & \gamma_1 & \cdots & \gamma_p\end{bmatrix}^T \\ \boldsymbol{\alpha} &= \begin{bmatrix}\alpha_0 & \alpha_1 & \cdots & \alpha_{N-p}\end{bmatrix}^T \\ \mathbf{A} &= \begin{bmatrix}1 & 2\cos\theta & \cdots & (2\cos\theta)^{N-p}\\ 2\cos\theta & (2\cos\theta)^2 & \cdots & (2\cos\theta)^{N-p+1}\\ \vdots & \vdots & \ddots & \vdots\\ (2\cos\theta)^p & (2\cos\theta)^{p+1} & \cdots & (2\cos\theta)^N\end{bmatrix} \end{aligned} \tag{3-16}$$

Therefore,

$$\begin{aligned} \left[R(e^{j\theta})-1\right]^2 &= \left[R(e^{j\theta})\right]^2-2R(e^{j\theta})+1 \\ &= \boldsymbol{\alpha}^T\mathbf{A}^T\boldsymbol{\gamma}\boldsymbol{\gamma}^T\mathbf{A}\boldsymbol{\alpha}-2\boldsymbol{\gamma}^T\mathbf{A}\boldsymbol{\alpha}+1 \end{aligned} \tag{3-17}$$

and

$$R(e^{j\theta})\big|_{\theta=0}=\begin{bmatrix}1 & 2 & \cdots & 2^{N-p}\end{bmatrix}\begin{bmatrix}\alpha_0\\ \alpha_1\\ \vdots\\ \alpha_{N-p}\end{bmatrix}=\boldsymbol{\beta}^T\boldsymbol{\alpha} \tag{3-18}$$

where

$$\boldsymbol{\beta} = \begin{bmatrix} 1 & 2 & \cdots & 2^{N-p} \end{bmatrix}^T \tag{3-19}$$

By substituting Equations (3-17) and (3-18) into Equation (3-14), it is obtained that:

$$\Gamma = \boldsymbol{\alpha}^T \mathbf{A}_1 \boldsymbol{\alpha} - 2\boldsymbol{\gamma}^T \mathbf{A}_2 \boldsymbol{\alpha} + \int_0^{\pi} w(\theta) d\theta + \lambda(\boldsymbol{\beta}^T \boldsymbol{\alpha} - 1) \tag{3-20}$$

where

$$\mathbf{A}_1 = \int_0^{\pi} w(\theta) \mathbf{A}^T \boldsymbol{\gamma} \boldsymbol{\gamma}^T \mathbf{A} d\theta \quad \mathbf{A}_2 = \int_0^{\pi} w(\theta) \mathbf{A} d\theta \tag{3-21}$$

Let

$$\frac{\partial \Gamma}{\partial \boldsymbol{\alpha}} = 2\mathbf{A}_1 \boldsymbol{\alpha} - 2\mathbf{A}_2^T \boldsymbol{\gamma} + \lambda \boldsymbol{\beta} = 0 \tag{3-22}$$

$$\frac{\partial \Gamma}{\partial \lambda} = \boldsymbol{\beta}^T \boldsymbol{\alpha} - 1 = 0 \tag{3-23}$$

Multiplying both sides of Equation (3-22) by the matrix $\boldsymbol{\beta}^T \mathbf{A}_1^{-1}$:

$$2\boldsymbol{\beta}^T \boldsymbol{\alpha} - 2\boldsymbol{\beta}^T \mathbf{A}_1^{-1} \mathbf{A}_2^T \boldsymbol{\gamma} + \lambda \boldsymbol{\beta}^T \mathbf{A}_1^{-1} \boldsymbol{\beta} = 0 \tag{3-24}$$

From Equation (3-23):

$$\boldsymbol{\beta}^T \boldsymbol{\alpha} = 1 \tag{3-25}$$

By substituting Equation (3-25) into Equation (3-24), the Lagrange multiplier can be obtained as:

$$\lambda = 2 \frac{\boldsymbol{\beta}^T \mathbf{A}_1^{-1} \mathbf{A}_2^T \boldsymbol{\gamma} - 1}{\boldsymbol{\beta}^T \mathbf{A}_1^{-1} \boldsymbol{\beta}} \tag{3-26}$$

Again by substituting Equation (3-26) into Equation (3-22), optimal parameters α of $DPF_A(z^{-1})$ can be obtained as:

$$\boldsymbol{\alpha} = \mathbf{A}_1^{-1} \left(\mathbf{A}_2^T \boldsymbol{\gamma} + \frac{1 - \boldsymbol{\beta}^T \mathbf{A}_1^{-1} \mathbf{A}_2^T \boldsymbol{\gamma}}{\boldsymbol{\beta}^T \mathbf{A}_1^{-1} \boldsymbol{\beta}} \boldsymbol{\beta} \right) \tag{3-27}$$

where the definition of the notations is given in Equations (3-16), (3-19) and (3-21).

It can be seen from Equations (3-6) and (3-10), that the DPF is non-causal. To implement it, *N* future values are required, among which, *P* steps are required to

compensate the phases shift, and *N-P* steps are required to further compensate the amplitude at the frequency range of interest. Additional preview steps may also be required due to the relative order *R* of the transfer function when taking the inverse of the stable part. Therefore the total number of preview steps required for the feedforward controller is as follows:

$$D = N + R \tag{3-28}$$

3.2 Causal Design of DPF

The digital preview filter described in the previous section solved two problems in the design of feedforward controller: (a) improved the gain characteristics and (b) provided an optimal solution. The problem of causality will be dealt with in this section. Because the DPF is non-causal, *N* steps of future value of input trajectory are needed to implement it. Otherwise, the tracking will be delayed by *N* steps. Generally speaking, a larger *N* will render better tracking performance if the desired trajectory is known prior. In the case that the desired trajectory is not known in advance, a prediction method is needed for the feedforward controller. However, a larger *N* will make the future values harder to predict. Several examples of predictor can be found in literature, e.g. [58,69,70]. But there are no perfect prediction technique, errors in the prediction may jeopardise control performance.

It is proposed in this section to make the application of DPF causal within a desired frequency range by employing system identification techniques. Additional time delays will be manually added after the measured response. The stability of the closed loop system will be ensured by retuning the PID parameters after adding manual delays. Then the feedforward controller will be designed according to this delayed signal rather than the actual response signal. If the overall delay from the delayed response to the actual response is made equal to the prediction length, then the actual response will be tracking the demand without any preview action.

The following process was developed to eliminate the need to provide future values of the reference signal in the design of feedforward controller:

(a) Guess the D value, i.e. the total number of preview steps required for the feedforward controller.

(b) Add manual delays after actual response, equal to D minus the delay that already exists in the CAN bus. Retune the feedback controller parameters for closed loop system if necessary.

(c) Identify the transfer function of the new system with the added delay between the demand signal and delayed response signal by seeking as low a relative order R.

(d) Check if the selected number of preview steps D is appropriate by taking into account of the relative order R and the number of unstable zeros P of the estimated transfer function.

  (d1) if (d) is satisfied, design the non-causal digital preview filter as described in Section 3.1.

  (d2) if (d) is not satisfied, select a different D, and repeat the process

There is one premise that after adding the manual delay, the total delay D from the actual response to the delayed response must be much greater than the relative order of estimated transfer function R.

Normally, after adding the manual delays, the relative order of the transfer function between the demanded and delayed responses should be increased by D. The relative order can be significantly reduced by seeking a lower R when identifying the delayed system transfer function within a desired frequency range. So using the estimated transfer function with a smaller relative order R for the feedforward controller design can allocate more preview steps N for the inverse of the unstable zeros, among which, P delays are used to compensate the phase, and N-P delays are used to further compensate the amplitude. Generally speaking, better performance in compensating amplitude error can be expected if more preview steps are available.

The selection of the D value is very flexible. Larger D may allow larger N (assuming the same R) and larger N-P (assuming the same P) to compensate the amplitude error, which will render a better compensation performance. But adding more delays to the system will probably result in a higher relative order R in the estimated transfer function to provide a good fit into test results. Even though the relative order can be arbitrarily specified, adding more delays may cause the number of unstable zeros, P,

to increase. So, *D-R-P* may not increase as *D* increases, which will not help to improve the performance of DPF. On the contrary, smaller *D* may result in smaller *R* or *P*, which may provide better performance than larger *D* value. Therefore, it is hard to say that larger or smaller *D* value is better. It needs to be evaluated for the specific application.

Examples of the application of the proposed process in the design of the feedforward controller for both closed loop and open-loop systems are given in the following sections. Feedforward controllers are designed and implemented for the closed loop speed control of the output dynamometer and the open-loop torque control of the input dynamometer.

3.3 Causal Application of DPF to a Single Motor

The proposed causal design of digital preview filters is applied to a single motor in this section. Feedforward controllers are designed for the output dynamometer speed and the input dynamometer torque control.

3.3.1 Output Dynamometer Speed Tracking Control

The speed control diagram including sampling delay on the CAN bus is shown in Figure 2-18, and the response to an SPHS demand signal with a frequency range up to 15 Hz is shown in Figure 2-20. To carry out the process proposed in the previous section, another 7 delays are added to the feedback loop in dSPACE as shown in Figure 3-1.

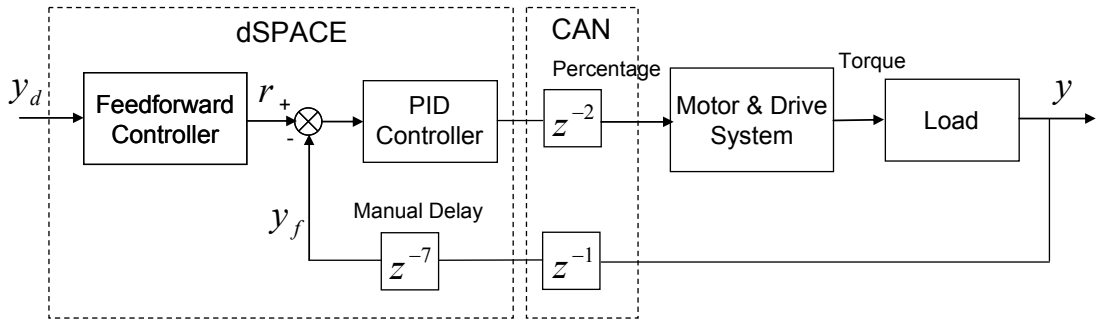

Figure 3-1 Speed control block diagram with manual delay

The PID controller was retuned in simulation without the feedforward controller to ensure the stability of the closed loop system. New PID parameters were selected as 0.15 for proportional control, 0.25 for integral control and 0.003 for derivative control. Tests were carried out with a speed demand signal, *r*, consisting of a SPHS signal superposed on a 1000 rev/min constant value. The delayed response of the system, y_f, is shown in Figure 3-2. The test result shown here is the average over three tests.

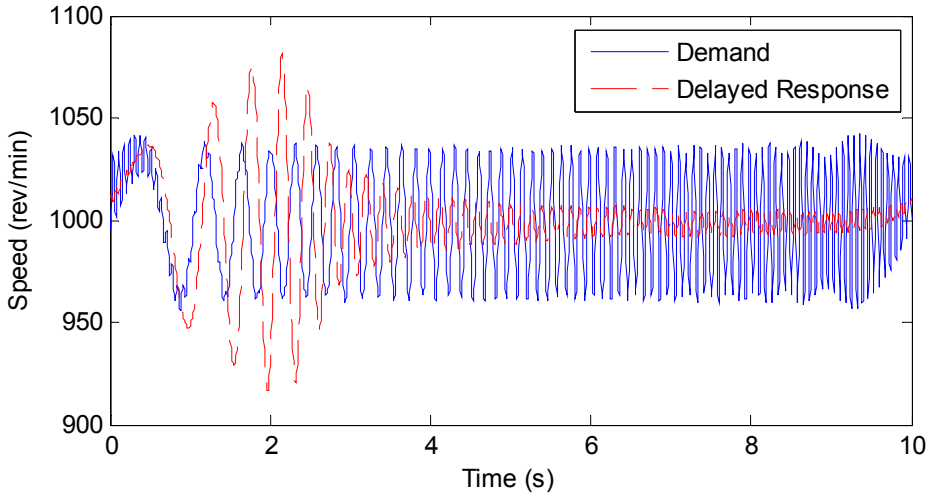

Figure 3-2 Delayed system response of output dynamometer speed control with 7 manual delays

By using the FFT of the recorded signals, and setting the relative order to one, the transfer function between the delayed speed response y_f and speed demand *r*, was estimated as follows:

$$G_{Speed}(s) = \frac{\begin{array}{r} 4.979s^5 - 761.8s^4 + 8.979e4s^3 - 4.705e6s^2 \\ + 9.175e7s + 2.303e9 \end{array}}{\begin{array}{r} s^6 + 116s^5 + 1.23e4s^4 + 6.978e5s^3 + 1.628e7s^2 \\ + 2.321e8s + 2.303e9 \end{array}} \qquad \textbf{(3-29)}$$

This gives four unstable zeros. The frequency response of the estimated and experimental transfer functions are shown in Figure 3-3. Because of the added delays, the phase shift of the speed response was increased, especially at high frequencies. The phase shift is approximately 550 degrees at 15 Hz.

In order to design the digital preview filter, a discrete time equivalent of the estimated transfer function between delayed speed response y_f and speed demand *r*

can be derived with zero order hold on the input at a sampling rate of 160 Hz as follows:

$$H_{Speed}(z^{-1}) = \frac{\begin{array}{r} 0.01163z^{-1} - 0.06594z^{-2} + 0.1556z^{-3} - 0.1909z^{-4} \\ + 0.1215z^{-5} - 0.03178z^{-6} \end{array}}{\begin{array}{r} 1 - 5.087z^{-1} + 10.97z^{-2} - 12.85z^{-3} + 8.625z^{-4} \\ - 3.143z^{-5} + 0.4844z^{-6} \end{array}} \quad \textbf{(3-30)}$$

with four zeros outside the unit circle.

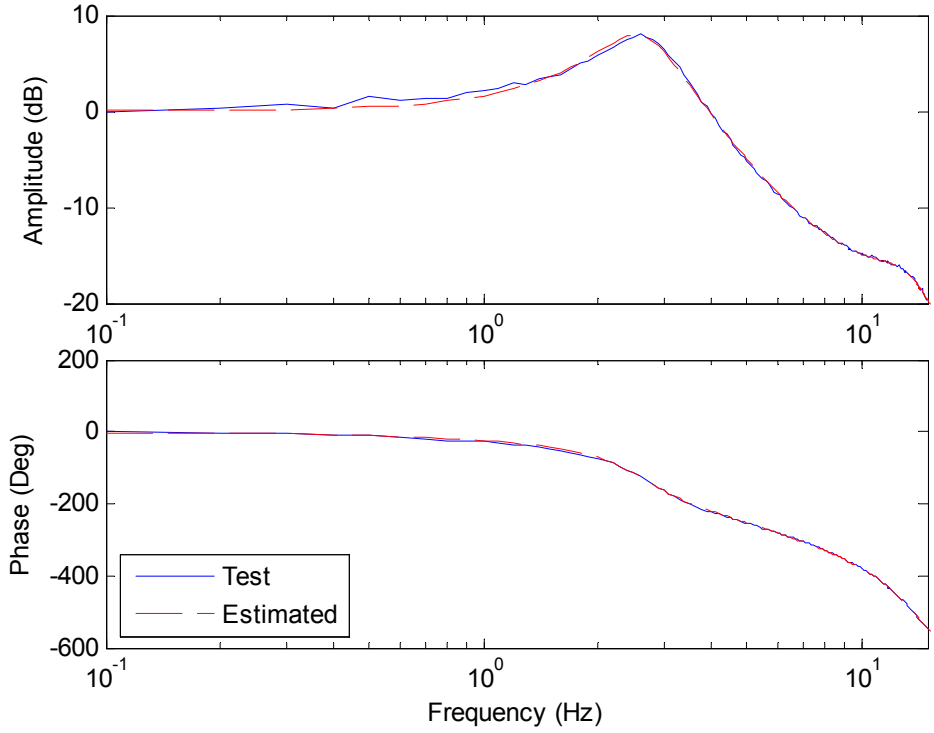

Figure 3-3 Delayed frequency response of output dynamometer speed control with 7 manual delays

A feedforward controller can be formulated as:

$$Q(z^{-1}) = H_a^{-1}(z^{-1}) DPF_{\Phi}(z^{-1}) DPF_A(z^{-1}) \quad \textbf{(3-31)}$$

where $H_a^{-1}(z^{-1})$ is the inverse of the stable part of Equation (3-29), and can be calculated as:

$$H_a^{-1}(z^{-1}) = \frac{\begin{array}{r} 85.96 - 437.3z^{-1} + 942.9z^{-2} - 1104z^{-3} + 741.4z^{-4} \\ - 270.1z^{-5} + 41.64z^{-6} \end{array}}{z^{-1} - 0.92z^{-2}} \quad \textbf{(3-32)}$$

$DPF_{\Phi}(z^{-1})$ can be calculated from Equation (3-6):

$$DPF_{\Phi}(z^{-1}) = \frac{2.969 - 8.127z^{-1} + 9.007z^{-2} - 4.749z^{-3} + z^{-4}}{0.01015z^{-4}} \qquad \textbf{(3-33)}$$

Then γ was obtained from Equations (3-8) and (3-9) to be:

$$\gamma = 10^3 \times [3.6252 \quad -7.7021 \quad 6.1548 \quad -2.1900 \quad 0.2926]^T$$

Because the total delay D is 8 and the relative order of estimated transfer function R is 1, the preview steps for digital preview filter N can be chosen to be D-R=7, and the number of unstable zeros P=4. The weighting function $w(\theta)$ was specified to be uniform within the frequency range of up to 15 Hz, That is:

$$w(\theta) = \begin{cases} 1 & \theta \le \frac{3}{16}\pi \\ 0 & \frac{3}{16}\pi < \theta \le \pi \end{cases} \qquad \textbf{(3-34)}$$

The penalty function J becomes:

$$J = \int_0^{\frac{3}{16}\pi} \left[R(e^{j\theta}) - 1 \right]^2 d\theta \qquad \textbf{(3-35)}$$

The matrices $\mathbf{A}_1$ and $\mathbf{A}_2$ are defined as:

$$\mathbf{A}_1 = \int_0^{\frac{3}{16}\pi} \mathbf{A}^T \boldsymbol{\gamma}\boldsymbol{\gamma}^T \mathbf{A} d\theta \qquad \mathbf{A}_2 = \int_0^{\frac{3}{16}\pi} \mathbf{A} d\theta \qquad \textbf{(3-36)}$$

Then the polynomial parameter vector α for $DPF_A(z^{-1})$ can be calculated from Equation (3-27) as:

$$\alpha = [19.2762 \quad -31.0421 \quad 15.9952 \quad -2.5216]^T$$

This gives the following digital preview filter to compensate for the amplitude using Equation (3-10):

$$DPF_A(z^{-1}) = \frac{-2.522 + 16z^{-1} - 38.61z^{-2} + 51.27z^{-3} - 38.61z^{-4} + 16z^{-5} - 2.522z^{-6}}{z^{-3}} \qquad \textbf{(3-37)}$$

One preview step is needed in Equation (3-32) because the relative order is one (R=1). This leaves a total of 7 preview steps for the DPF design (N=7). Four preview steps are needed in Equation (3-33) for the design of ZPETC, because the number of

unstable zeros is four (P=4). Three preview steps are used in Equation (3-37) to further compensate for the gain characteristics within the interested frequency range (N-P=3). Generally speaking, increasing the preview steps allowed for DPF would improve the compensation results, but would also increase the total delay required, D.

Estimated frequency responses between delayed speed response y_f and speed demand r, with and without the feedforward controller are shown in Figure 3-4. Simulation shows that system dynamics is compensated with a unit gain and zero phase shift up to 15 Hz.

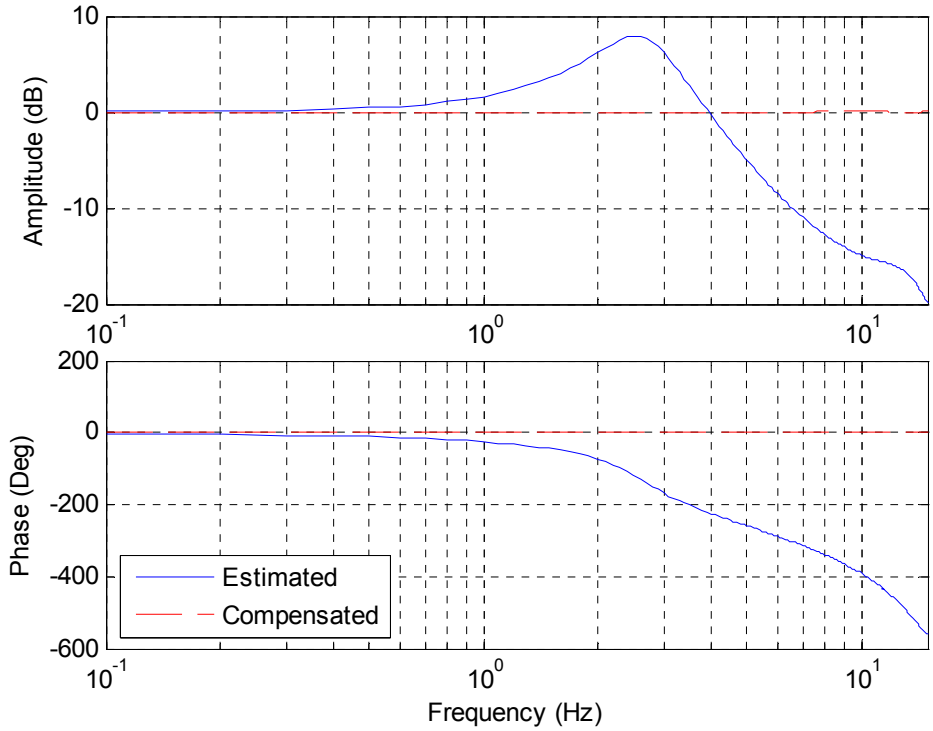

Figure 3-4 Simulated system response of output dynamometer speed control with and without feedforward controller

The designed feedforward controller was then implemented in the test. The experimental time responses for the actual response y and the demand signal y_d are shown in Figure 3-5.

Magnified views of Figure 3-5 at three locations are shown in Figure 3-6. As it can be seen from these results, the tracking performance in time domain was significantly improved. Almost perfect tracking was achieved without using future values of the input signal, which proved the effectiveness of proposed control method.

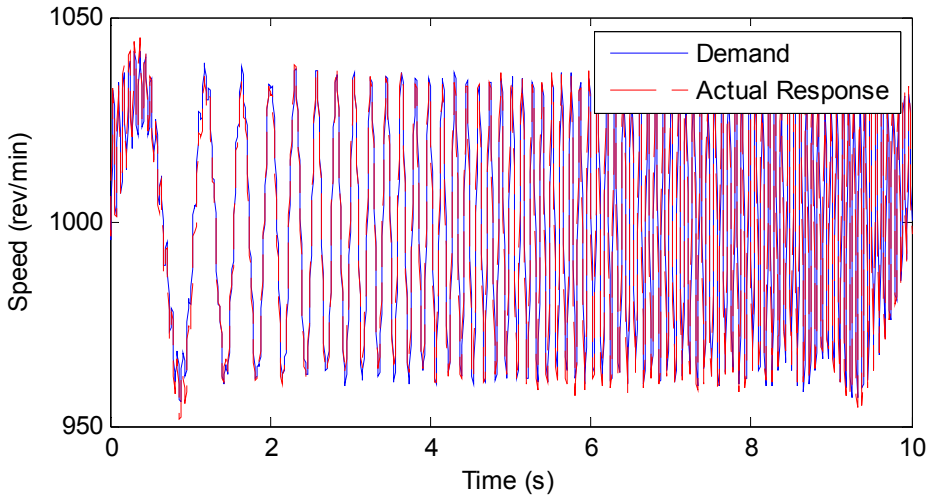

Figure 3-5 Actual response of output dynamometer speed control with and without feedforward controller

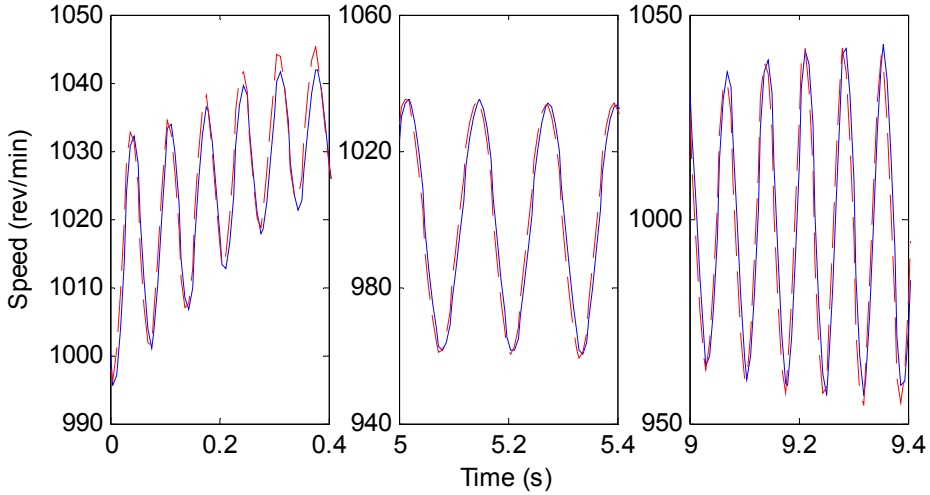

Figure 3-6 Magnified views of Figure 3-5

The frequency response of the system with feedforward controller is shown in Figure 3-7, and compared with the frequency response of the system with only feedback controller.

The frequency domain results clearly show that the amplitude and phase of the closed loop system are well compensated by the feedforward controller. A small phase error was observed in the high frequency range, where the actual speed response was leading the speed demand in phase. This error was examined and proved to correspond to half sampling interval delay. The reason could be due to the use of the zero order hold on the input when digitalising the estimated transfer function.

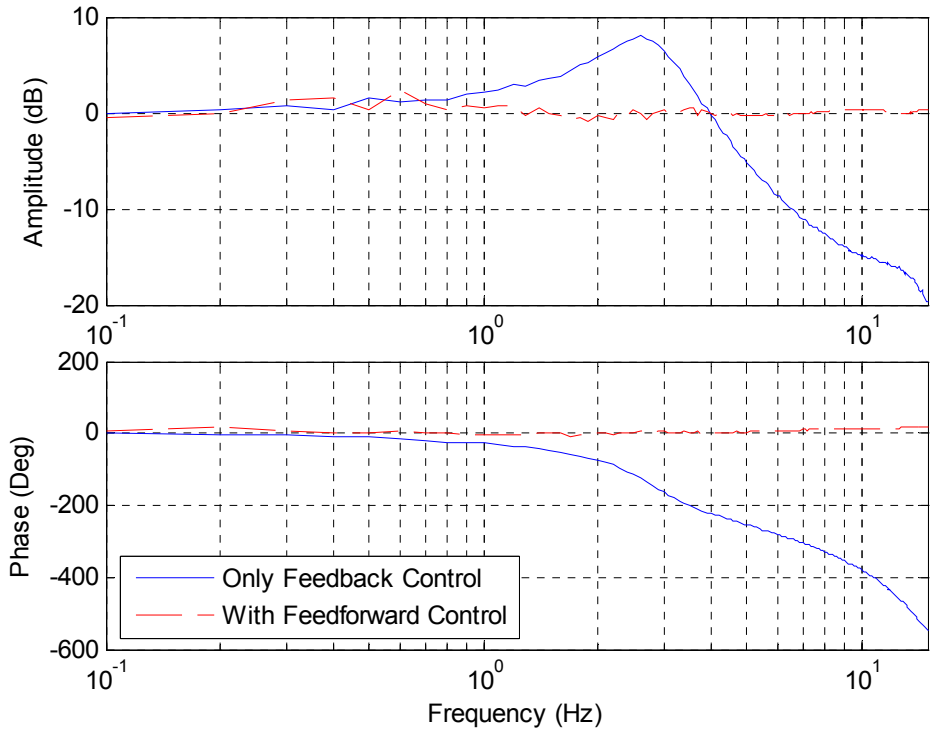

Figure 3-7 Frequency response of Figure 3-5

As discussed in precious section, the selection of the *D* value is very flexible. Greater *D* will not guarantee a better compensation performance. In the test, different numbers of manual delays were added to the feedback loop, to offer different *D* values. Transfer functions were estimated and feedforward controllers were designed for each estimated transfer function. The information for the estimation and feedforward controller design is summarised in Table 3-1. The frequency responses of the estimated transfer functions are shown in Figure 3-8, and the simulated frequency responses of the compensated systems are shown in Figure 3-9. It can be seen that zero phase shift was achieved in all the three cases. The amplitude compensation results are definitely improved by increasing the total number of the delays from 6 to 8, but not so obviously from 8 to 10. Hence, *D* equal to 8 was chosen and the designed feedforward controller was implemented in the test.

Table 3-1 Estimation and feedforward controller design with different *D* values

Total Delays (*D*)	Relative Order (*R*)	Preview Steps for *DPF* (*N*)	
		(*P*)	(*N-P*)
6	0 ($4^{th}/4^{th}$)	4	2
8	1 ($5^{th}/6^{th}$)	4	3
10	1 ($5^{th}/6^{th}$)	4	5

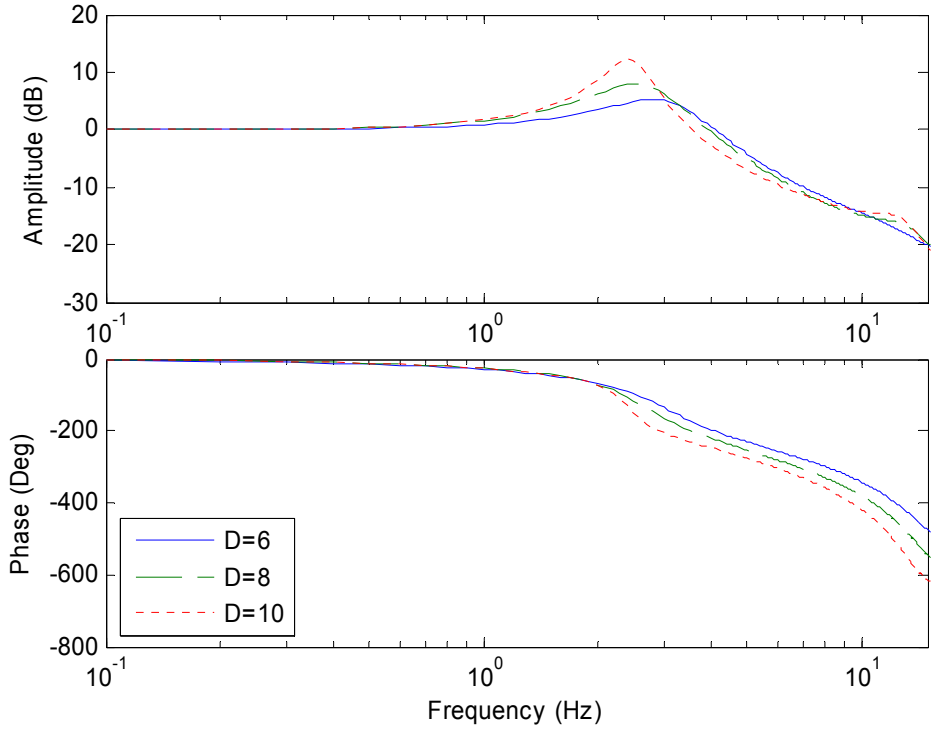

Figure 3-8 Frequency responses of the estimated transfer functions with different *D* values

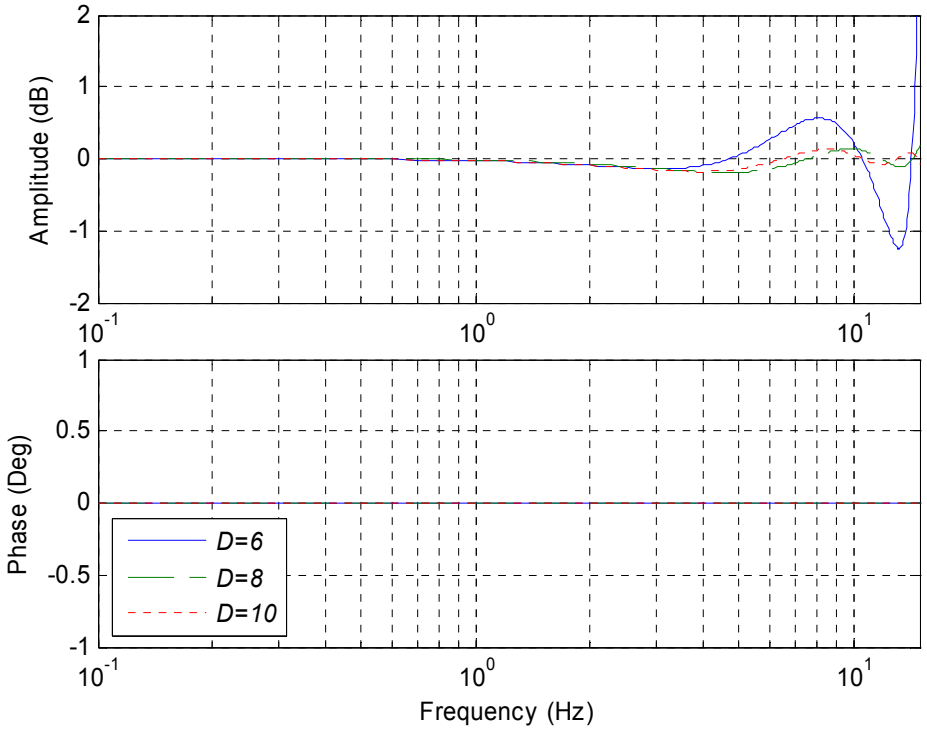

Figure 3-9 Simulated frequency responses of the compensated systems with different *D* values

3.3.2 Input Dynamometer Generated Torque Tracking Control

Different from speed control, motor torque control can be operated in open-loop. Torque demand can be converted into a percentage demand and sent directly to ABB drive system. The converting gain was calculated to be 0.2, i.e. 1000 Nm torque demand is equal to 200 percentage control signal demand. An open-loop control strategy is considered to be more suitable, because the motor and drive system possess relatively steady dynamics and are not affected by the external load and torque disturbances. The same process can be applied here to design a feedforward controller for the input dynamometer open-loop torque control system. Again 7 manual delays were added after the measured torque as shown in Figure 3-10. With one sample CAN bus delay, there were a total of 8 samples delay between the actual torque response output, *y*, and the delayed torque response, y_f.

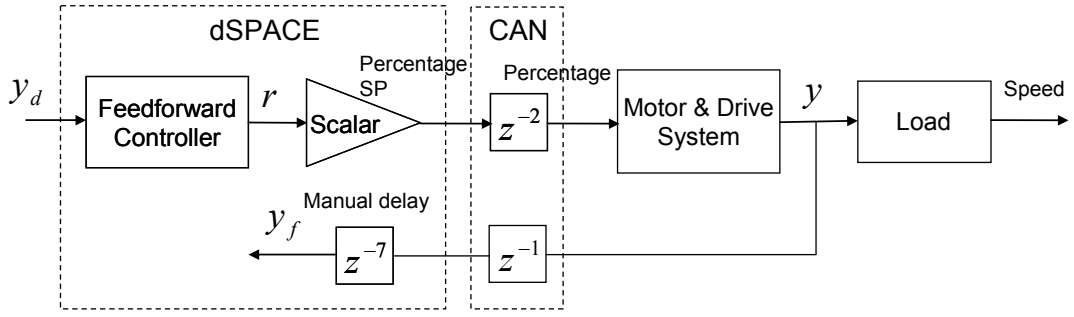

Figure 3-10 Torque control block diagram with manual delay

To design a feedforward controller for the system, a transfer function between the delayed torque response y_f and torque demand *r* is required, as shown in Figure 3-10. No new tests were necessary to identify this relationship. Instead, previous test results recorded in the closed loop speed control of the input dynamometer were used. The recorded percentage signal was divided by the gain factor of 0.2 and used as the torque setpoint signal, *r*. The recorded torque signal was shifted 7 samples backwards and used as the delayed torque response, y_f. After taking the FFTs, the measured and estimated frequency responses between the delayed torque response y_f and the torque demand *r* are shown in Figure 3-11. The relationship was estimated as a fourth order over fifth order transfer function, i.e. the relative order of 1, up to 15 Hz as follows:

$$G_{Torque}(s) = \frac{4.45s^4 - 1446s^3 + 1.988e5s^2 - 1.474e7s + 4.678e8}{s^5 + 114.7s^4 + 1.398e4s^3 + 7.474e5s^2 + 2.926e7s + 4.447e8} \quad \textbf{(3-38)}$$

This gives four unstable zeros.

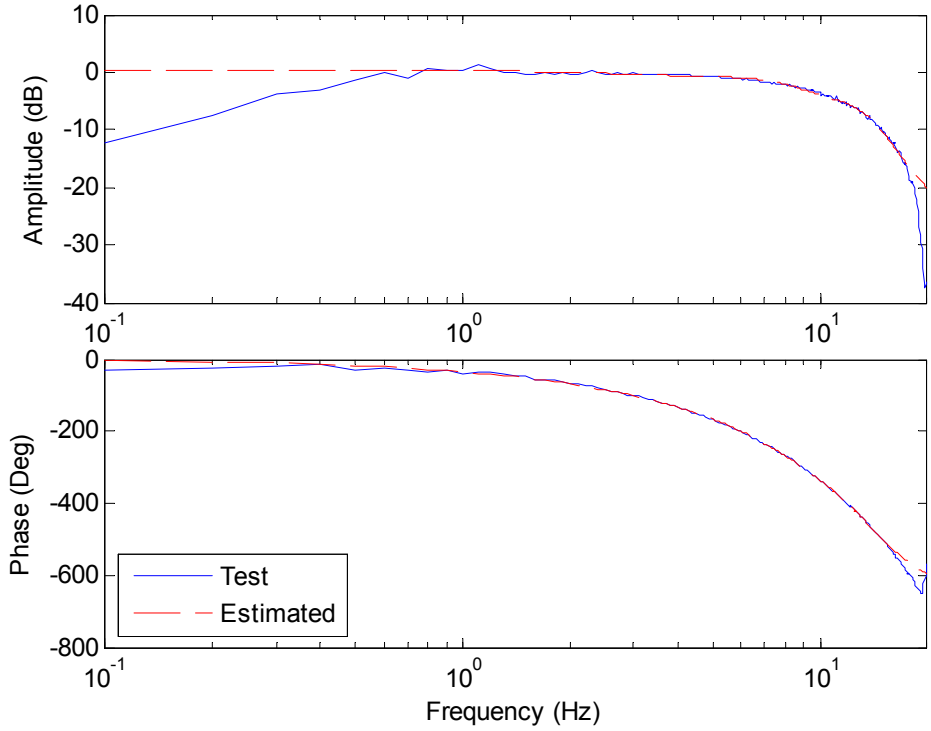

Figure 3-11 Delayed system response of input dynamometer torque control with 7 manual delay

The equivalent discrete transfer function can be obtained by using a zero order hold assumption on the input:

$$H_{Torque}(z^{-1}) = \frac{\begin{array}{c}0.002293z^{-1} - 0.022z^{-2} + 0.06542z^{-3} \\ - 0.0831z^{-4} + 0.04043z^{-5}\end{array}}{1 - 4.04z^{-1} + 6.766z^{-2} - 5.867z^{-3} + 2.632z^{-4} - 0.4884z^{-5}} \quad \textbf{(3-39)}$$

with four zeros outside the unit circle.

The same procedure used in previous section can be applied to design a feedforward controller for the input dynamometer torque control. There are a total of 8 sampling delays between the actual torque response signal y and delayed torque signal y_f, among which, one sampling delay is needed to invert the stable part of the estimated transfer function in Equation (3-39), and the remaining 7 samples delay can be used to design a digital preview filter to approximately invert the unstable part of the estimated transfer function. This gives:

$$H_a^{-1}(z^{-1}) = \frac{436.1 - 1762z^{-1} + 2951z^{-2} - 2559z^{-3} + 1148z^{-4} - 213z^{-5}}{z^{-1}} \quad \textbf{(3-40)}$$

$DPF_{\Phi}(z^{-1})$ can be calculated from Equation (3-6), which requires 4 preview steps because there are 4 unstable zeros:

$$DPF_{\Phi}(z^{-1}) = \frac{17.63 - 36.24z^{-1} + 28.53z^{-2} - 9.594z^{-3} + z^{-4}}{1.762z^{-4}} \quad \textbf{(3-41)}$$

With a uniform weighting function as before, the digital preview filter to compensate the amplitude was calculated from Equation (3-10), which requires 3 preview steps:

$$DPF_A(z^{-1}) = \frac{\begin{array}{r} -0.1131 + 2.692z^{-1} - 6.914z^{-2} + 9.67z^{-3} - 6.914z^{-4} \\ + 2.692z^{-5} - 0.1131z^{-6} \end{array}}{z^{-3}} \quad \textbf{(3-42)}$$

The above controller was first tested in simulation. The frequency response of the estimated transfer function with and without the designed feedforward controller is shown in Figure 3-12.

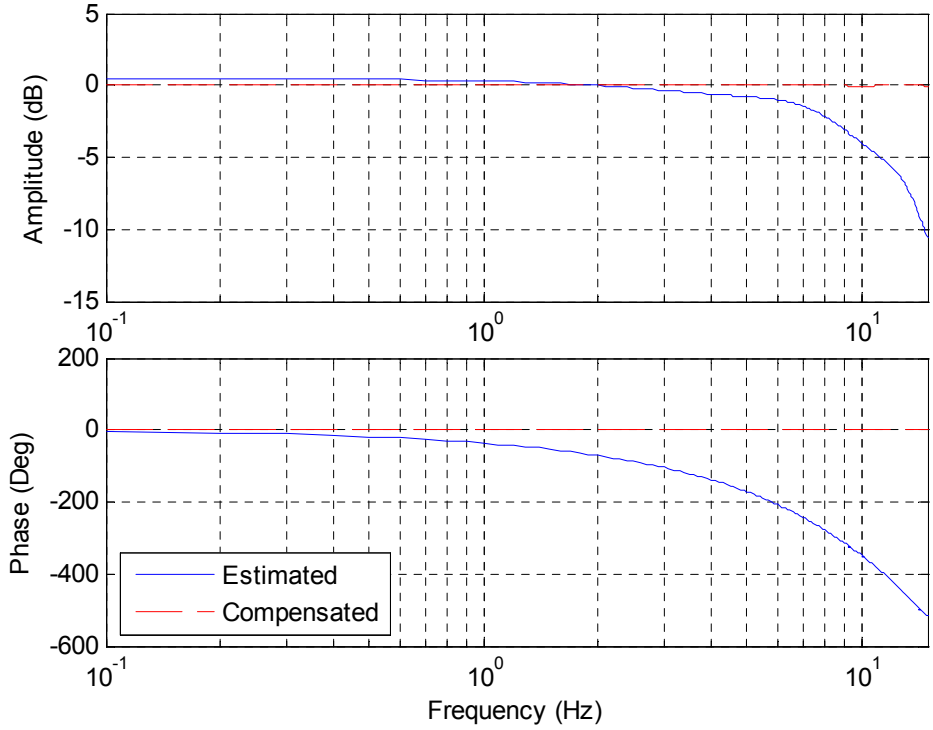

Figure 3-12 Simulated system response of input dynamometer torque control with feedforward controller

Again, simulation shows perfectly compensated system dynamics, with unity gain and zero phase shift for up to 15 Hz. There was a small steady state error of the original system, because 200% demand was not exactly equal to 1000 Nm as assumed from the motor rating. The steady state error was successfully corrected by the feedforward controller, and there was only slight fluctuation in the amplitude at high frequencies.

To test the designed feedforward controller with open-loop torque control, a care is needed when selecting the reference torque demand signal. In the test, the two motors were not coupled. Therefore the motor speed would keep increasing if a large constant torque component was demanded from the motor. Since the dynamic model was already identified for the input dynamometer and its drive system, including the motor inertia and damping ratio, a safe toque demand level for the test can be determined and tested in the simulation. Since the estimated damping ratio was 0.0432 for the input dynamometer, a constant torque of 5 Nm should make the motor speed settle at about 1000 rev/min. Therefore, the torque demand signal could comprise a constant torque of 5 Nm plus properly scaled SPHS signal, which was chosen to be 45 Nm. The experiments were carried out, and the demand signal y_d and the measured compensated system response y are shown in Figure 3-13. Magnified views of Figure 3-13 are shown in Figure 3-14. It can be seen in time domain that precisely torque tracking performance was achieved, and it was also realized without using future values of the demand torque signal.

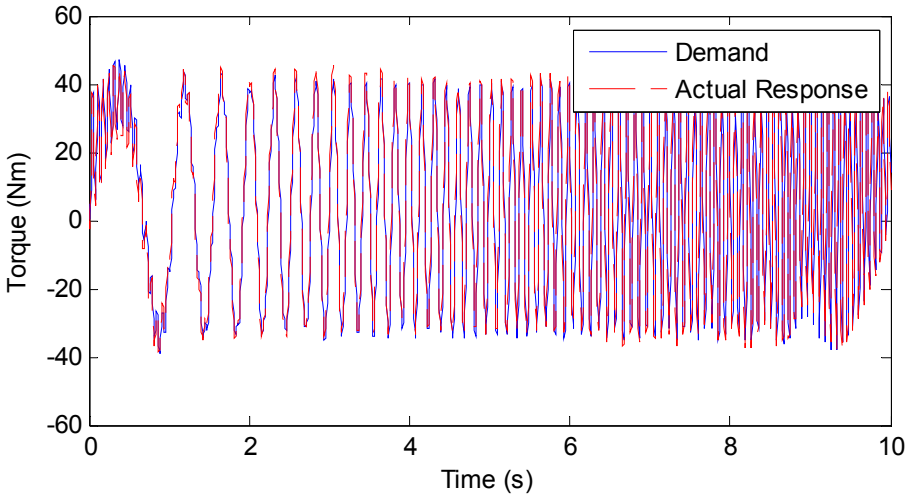

Figure 3-13 Actual response of input dynamometer torque control with feedforward controller

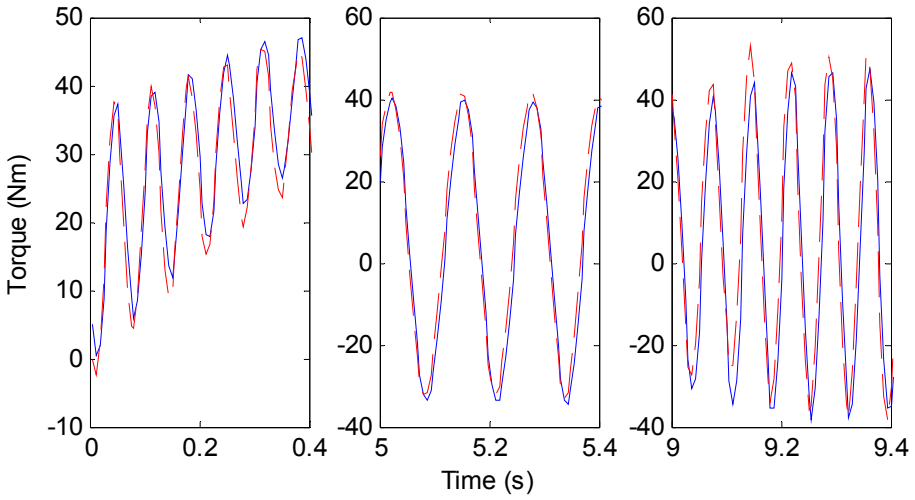

Figure 3-14 Magnified views of Figure 3-13

The frequency response of open-loop torque control of input dynamometer with and without the feedforward controller is shown in Figure 3-15.

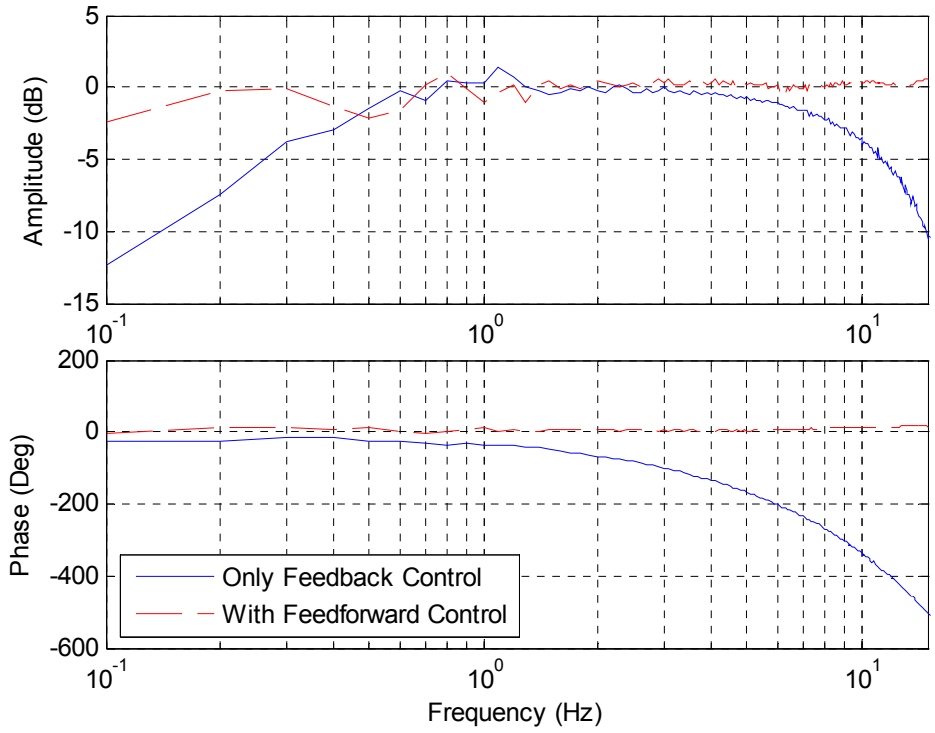

Figure 3-15 Frequency response of Figure 3-13

The frequency domain results illustrate the amplitude and phase are well compensated, although the results are not as good as in the simulation. These can be attributable to the nonlinearity and estimation errors. Fluctuations in the low frequency range for both original and compensated systems were due to measurement errors. Similar to the speed control results, the torque response leads

the torque demand signal by a half of sampling time, which may be due to the zero order hold approximation used in the digitalization of the estimated transfer function.

3.4 Conclusions

Excellent tracking was achieved by using the proposed causal digital preview filter as feedforward controller in both speed and torque control of the output and input dynamometers respectively.

The causality was achieved by adding manual delays to the original system after the actual response signal. Then the non-causal feedforward controller was designed for the delayed output signal, rather than the actual signal. If the total sampling delays between the delayed signal and actual signal can be made equal to the preview steps required by the non-causal feedforward controller, the actual response will exactly follow the demand signal without any delay. In that case the feedforward controller can be deemed as a causal controller and can be implemented to both motor speed and torque control when testing CVTs. Both simulation and experimental results are presented to demonstrate the effectiveness of the proposed control method.

The digital preview filter is one of the available techniques to design feedforward controllers. However, the proposed method can be applied to any other feedforward controller technique to make the controller causal. One of the reasons that DPF was implemented in this project was that a frequency domain weighting function can be incorporated into the optimization to emphasize a frequency range of interests. In this chapter, the weighting function was chosen to be uniform i.e. equal to one, over the frequency range up to 15 Hz. When the controller was designed to be used in CVT testing, the weighting function can be modified to emphasize good performance on a certain frequency range determined by the simulation results based on the real-time models.

The digital preview filter is designed to work within a defined frequency range. Hence, to implement the feedforward controller in the test, it was necessary to test the system with a reference signal, which does not include any frequency components higher than the design bandwidth. Normally, a low pass filter should be

employed for the reference signal when testing the CVT with real-time engine and vehicle models.

Another aspect of designing a feedforward controller was the selection of the sampling frequency. The fastest sampling frequency of 160 Hz was used in the tests. Using a lower sampling frequency in CP CADET, e.g. 80 Hz, would increase the time delay on the CAN bus, and it also made the stabilization of the system much harder by retuning the PID controller. Therefore the number of sampling delays that can be added to the feedback loop is reduced. This meant that fewer preview steps were available to design the digital preview filter, which could degenerate the compensation performance. For example, with 80 Hz control frequency, only 4 manual delays could be added to the feedback loop giving the same absolute time delay as 8 manual delays with 160 Hz control frequency, but the number of preview steps available to design the feedforward controller was halved. This would certainly degenerate the compensation performance.

Chapter 4

Feedforward Controller Robustness

Using a digital preview filter as part of a feedforward controller was demonstrated to be effective in the previous chapter, but the feedforward controller was sensitive to changes in the plant dynamics. It is not a problem for the generated torque control of the input dynamometer, as it is open-loop control and the dynamics of the motor and drive system is not affected by the other motor. However, for the output dynamometer speed control, not only the gear ratio change will result in the change of system dynamics, but also the torque generated by the input dynamometer will be perceived as a disturbance by the output dynamometer.

One way to tackle the problem of changing system dynamics is to make the feedforward controller adaptive to the plant dynamics. The plant dynamics could be continuously estimated on-line, and the feedforward controller parameters could be adjusted according to the updated system transfer function. The drawback of this kind of control scheme is that the estimation process will take finite duration before it converges, so it requires that the plant dynamics can only be slowly changing. Because the continuous change in the CVT gear ratio will result in fast changing closed loop dynamics, the performance of adaptive feedforward control may not be satisfactory.

Another way would be to ensure that the original system dynamics is the same as the one when the feedforward controller was designed. To achieve this, another compensator is added to the system to retain the original system dynamics when the gear ratio changes. The disturbance torque introduced by the input dynamometer is also compensated by demanding additional percentage control signal from the output dynamometer. In theory, the proposed gear ratio compensator can be updated at the feedforward controller sampling rate or even faster, which is an advantage over the existing adaptive method.

4.1 Gear Ratio Compensation of O/P Dynamometer Speed Control

The feedforward controller was designed in the last chapter according to the dynamics of the existing system, to approximate the inverse of the original system. It is only effective when the dynamics of original system is kept unchanged. In the case of speed control for the output dynamometer as shown in Figure 3-1, although the PID controller, motor and drive system dynamics are invariant, the load dynamics in terms of inertia and damping will vary with the gear ratio, when they are lumped into the output dynamometer dynamics by the square of the ratio. Thus the feedforward controller will fail to compensate the system dynamics if the gear ratio changes. This can be solved in two ways, either updating the feedforward controller to match the new system dynamics as a result of the gear ratio change, or updating the closed loop to compensate the change in gear ratio. As discussed at the beginning of the chapter, the latter would be a better choice, which can be achieved by adding another controller to the feedback loop of the original system as shown in Figure 4-1.

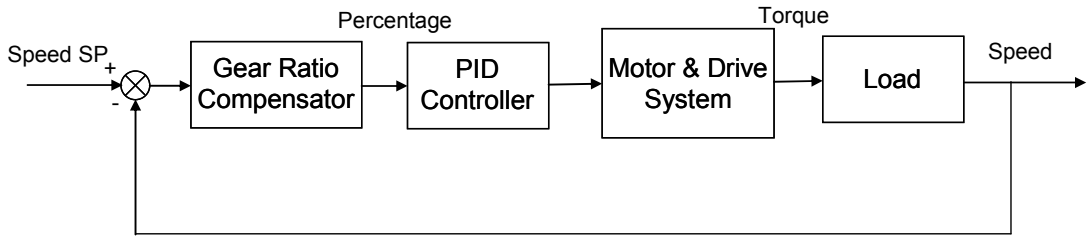

Figure 4-1 Output dynamometer closed loop speed control with gear ratio compensator

The purpose of the gear ratio compensator is to retain the dynamics of the original system when the gear ratio changes. The compensator can be formulated as follows:

$$G_{Ratio\_cmp}(s) = \frac{(J_O + \tau^2 \times J_I)s + (B_O + \tau^2 \times B_I)}{J_N s + B_N} \quad \textbf{(4-1)}$$

where τ is the gear ratio. J_I and B_I are the combined inertia and damping ratio of the input dynamometer and input shaft, and J_O and B_O are the combined inertia and damping ratio of the output dynamometer and output shaft. J_N and B_N are the nominal inertia and damping ratio of a virtual load, on which the feedforward

controller was originally designed. The nominal values were the inertia and damping ratio of the output dynamometer rotor. The main role of the numerator of the gear ratio compensator is to cancel the dynamics of the actual load, while the main role of the denominator is to retrieve the dynamics of the virtual load. The inertias and damping ratios were estimated in the previous chapter. The gear ratio τ can be updated as fast as the sampling frequency by dividing the speeds of the output and input dynamometers. Since only the actual ratio between the dynamometers is considered, the compensator will not be affected by the dynamics of the CVT.

The performance of the gear ratio compensator was examined by connecting the two dynamometers with a mechanical gear box. The gear box was set to neutral first and then to a 1:1 gear ratio.

4.1.1 Test with Neutral Gear

In a neutral gear, the output shaft was attached to the output dynamometer, where the inertia and damping ratios of the load were higher than the nominal values. With the same PID controller, the closed loop speed response is expected to be different. The test results are shown in Figure 4-2, with the gear in neutral position.

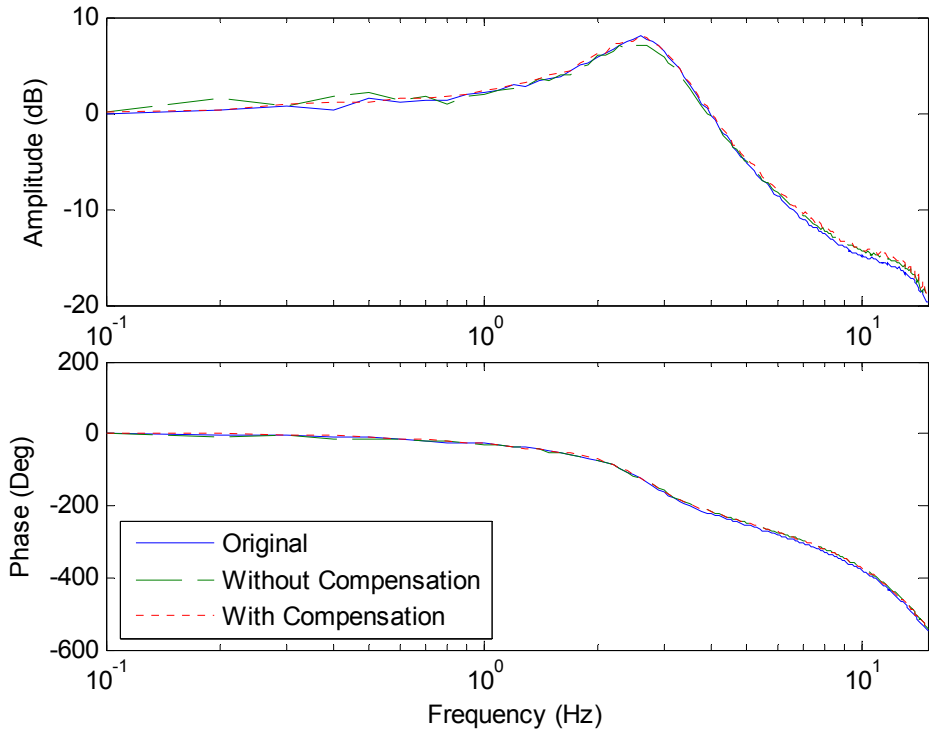

Figure 4-2 Closed loop speed responses of the output dynamometer on a neutral gear with and without the gear compensator

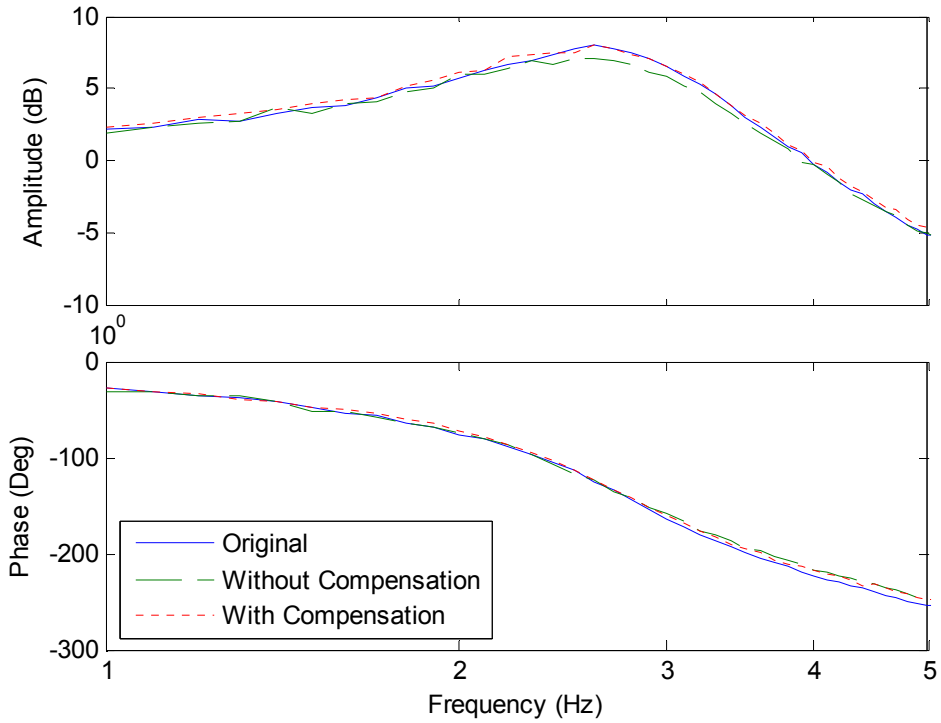

Figure 4-3 A magnified view of Figure 4-2

The solid line shows the closed loop speed response of only output dynamometer with added manual delays as in previous chapter in Figure 3-3. With a neutral gear ratio and the output shaft attached, and the same PID controller parameters there was only slight change in the amplitude, and the phase was almost the same as before, because the inertia and damping of the output shaft is relatively small compared to the output dynamometer. However, deviation from original dynamics can still be observed in the amplitude, especially in the middle frequency range, between 2 Hz and 4 Hz as shown in Figure 4-3. This was successful corrected by the gear ratio compensator, as shown by the dotted line.

If the feedforward controller designed in previous chapter was used here without any change in its parameters, the nominal load used in the gear ratio compensator would be the inertia and damping of the output dynamometer rotor. The speed demand consisted of a SPHS signal with a frequency range of up to 15 Hz and a scaled amplitude of 45 rev/min, superposed on a steady state speed of 1000 rev/min. The test results in the time domain are shown in Figure 4-4. Magnified views of Figure 4-4 are shown in Figure 4-5.

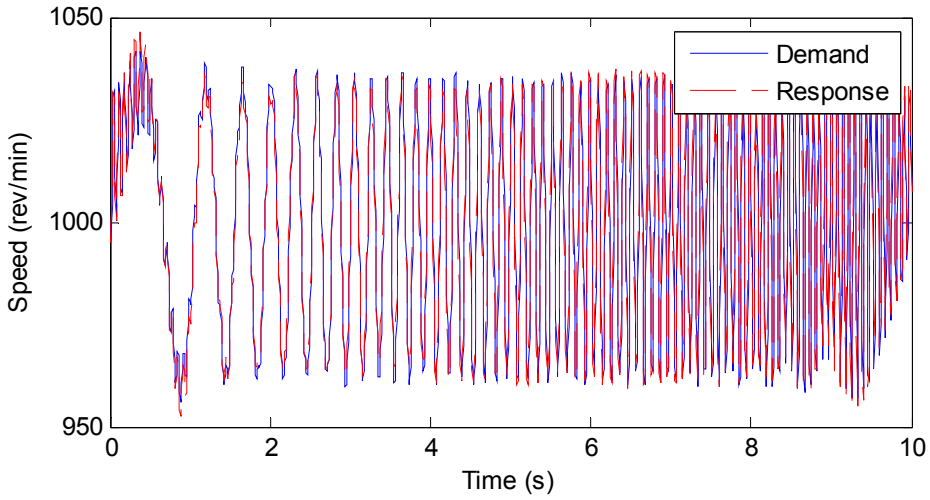

Figure 4-4 Output dynamometer speed control with a neutral gear, original PID and feedforward controllers, and gear compensator

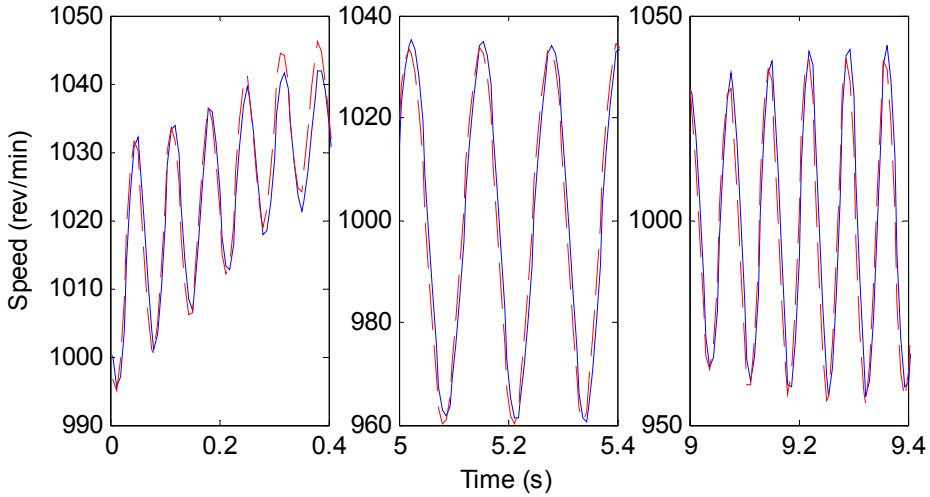

Figure 4-5 Magnified views of Figure 4-4

The frequency response of Figure 4-4 is shown in Figure 4-6, and is compared with the PID only control.

Good tracking performance is observed in both time and frequency domains, even slightly better performance in high frequency range than in the previous chapter (as shown in Figure 3-7). Since the dynamics of the original system was not significantly changed by the attached output shaft, this test does not provide clear evidence of the effectiveness of the gear compensator. Therefore, more tests were carried out with a 1:1 gear ratio and with the same speed demand.

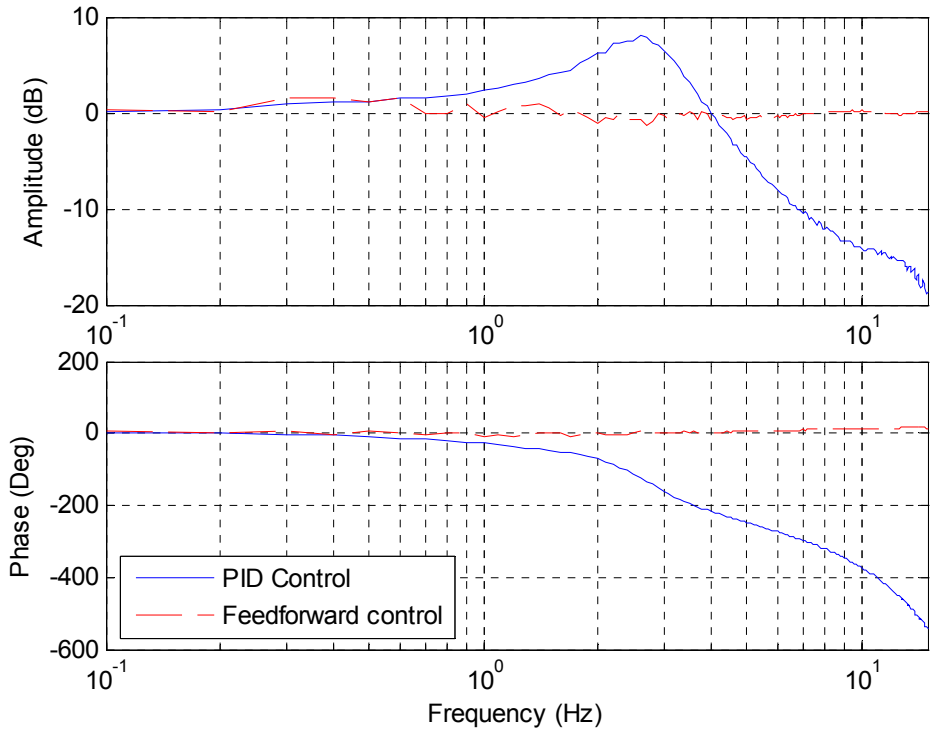

Figure 4-6 Frequency response of Figure 4-4

4.1.2 Test with 1:1 Gear Ratio

With the gear ratio set to 1:1, the responses of the closed loop PID speed control with and without the gear compensator are shown in Figure 4-7, and compared with the original system response of only the output dynamometer.

The solid line still shows the closed loop speed response of only output dynamometer. With a 1:1 gear ratio and the whole shaft including input dynamometer rotor attached to the output dynamometer, the closed loop speed response was significantly changed, as shown by the dashed line. With the gear compensator, the frequency response was successfully compensated to give the same response as the original system, as shown by the dotted line. It can be seen that perfect match was achieved for both amplitude and phase for the frequencies up to 6 Hz. Within this frequency range, the dynamics of the system with a 1:1 gear ratio was successfully made to match the original system by the gear compensator. Large discrepancies at high frequencies are due to the backlash between the gears, which were heard when running the motor in high frequency range.

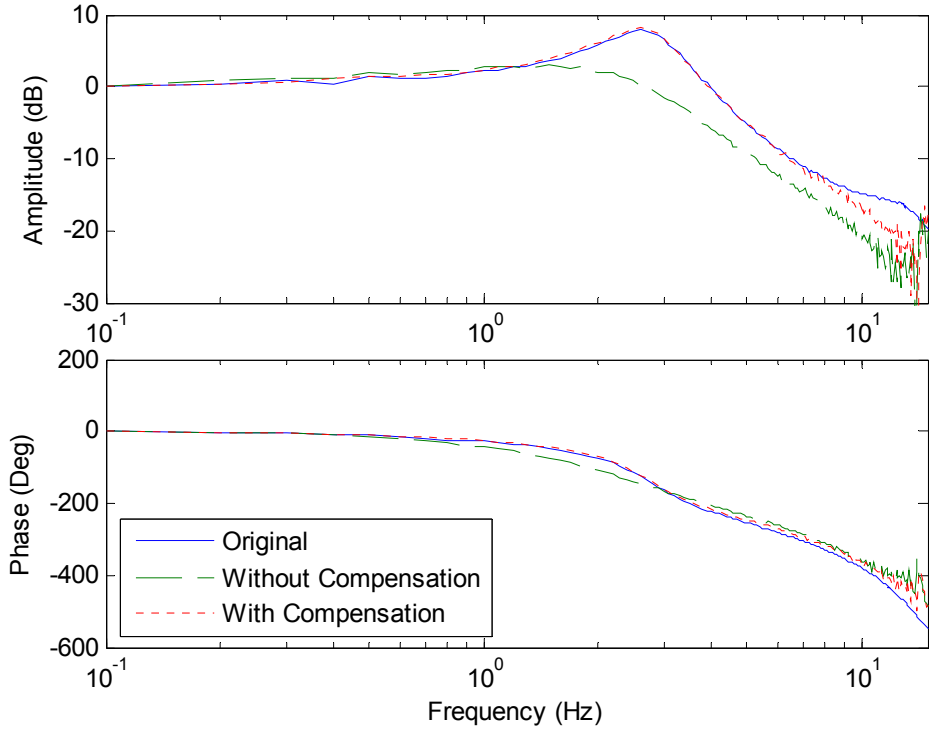

Figure 4-7 Closed loop speed control dynamics of output dynamometer with a 1:1 gear ratio

Since the compensated system with a 1:1 gear ratio matches the original system for frequencies only up to 6 Hz without noticeable effects of backlash, tests were carried out with a SPHS speed demand signal with frequency components up to 10 Hz. The test results are shown in Figure 4-8. Magnified views of Figure 4-8 are shown in Figure 4-9.

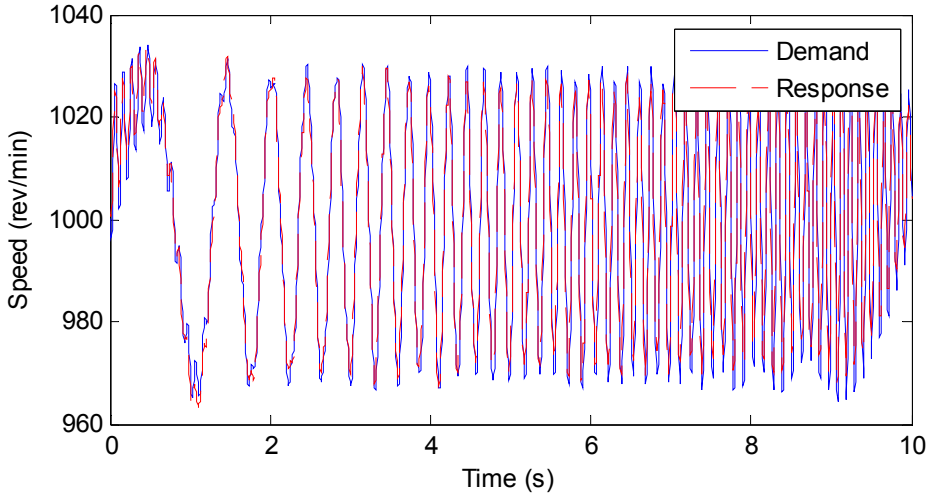

Figure 4-8 Output dynamometer speed control with a 1:1 gear ratio, original PID and feedforward controllers, and gear compensator

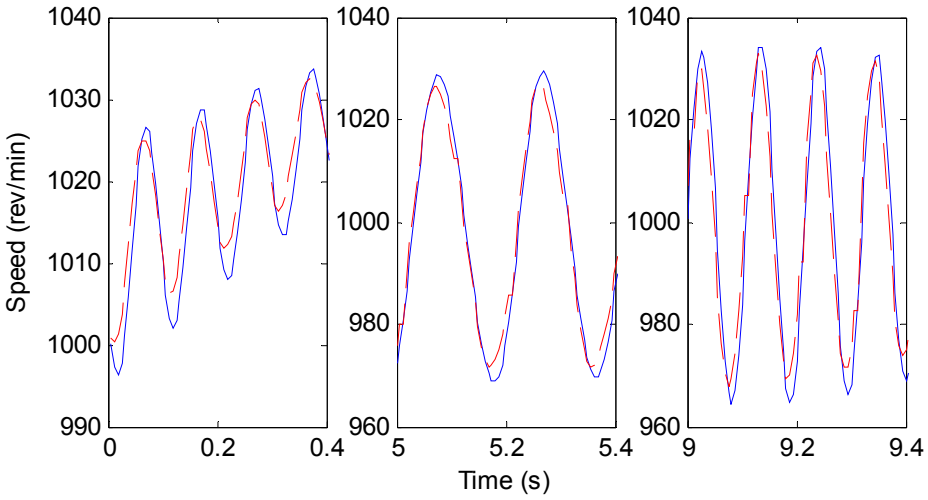

Figure 4-9 Magnified views of Figure 4-8

The frequency response of Figure 4-8 is shown in Figure 4-10, and compared with PID only control.

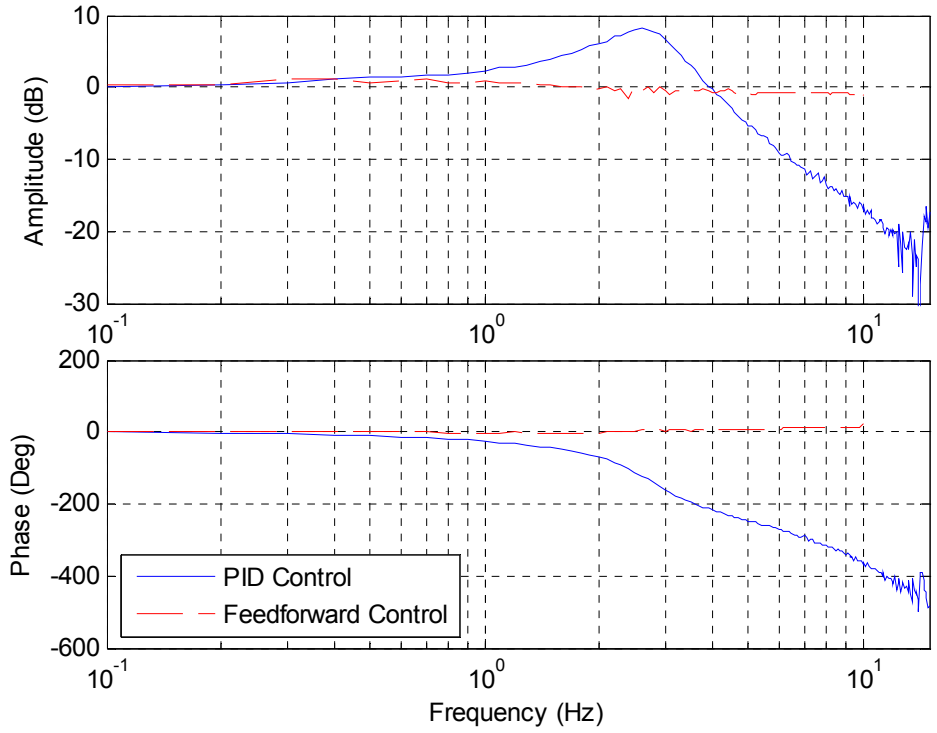

Figure 4-10 Frequency response of Figure 4-8

The speed tracking performance shown in Figure 4-10 can be further improved, especially in the high frequency range. The feedforward controller for the output dynamometer speed control can actually be designed according to the couple system instead of single motor. Then the compensated frequency range can be extended to 10 Hz when optimising the amplitude performance. In the way the backlash effects can also be included in the closed loop and regulated by the PID controller, which

will guarantee a better final control performance, whereas in here, the original feedforward controller was used to demonstrate the effectiveness of the gear compensator.

4.2 Compensation of Disturbance Torque for O/P Dynamometer

When the two motors are coupled, the interaction of the generated torques needs to be considered. For the input dynamometer, the generated torque is controlled to provide the torque demand in the previous chapter, and must not be affected by the torque generated by the output dynamometer. For the output dynamometer, the speed is controlled to follow the speed demand. In this case, the torque generated by the input dynamometer will act as a disturbance torque on the output dynamometer, and hence affect the output dynamometer speed controller. However, this disturbance torque is available from the input dynamometer demand at each sampling instant. In order to compensate for this torque, a compensating torque can be generated by the output dynamometer in the opposite direction. The compensation arrangement is shown in Figure 4-11.

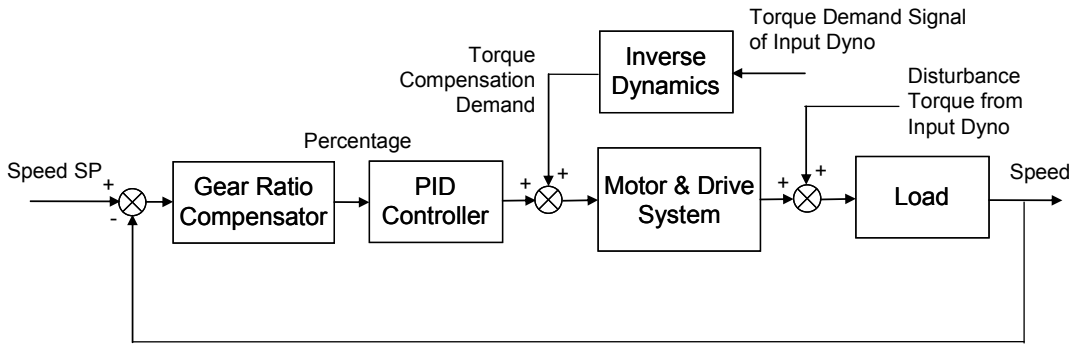

Figure 4-11 Disturbance torque compensation scheme for the output dynamometer

In order to generate an equivalent torque to cancel the disturbance torque, an additional percentage control signal is required for the output dynamometer. Due to the dynamics of the motor and drive system of the output dynamometer, the disturbance torque i.e. the torque demand of the input dynamometer is passed through another controller which possesses the inverse dynamics of the motor and

drive system of the output dynamometer. Thus if a disturbance torque is generated by the input dynamometer, an equal amount of torque will be generated by the output dynamometer to cancel each other. An inverse system had already been designed for the motor and drive system of the input dynamometer in the previous chapter when performing the generated torque tracking control. It is worthy to examine the dynamics of the motor and drive system for the input and output dynamometer. These are plotted in frequency domain in Figure 4-12.

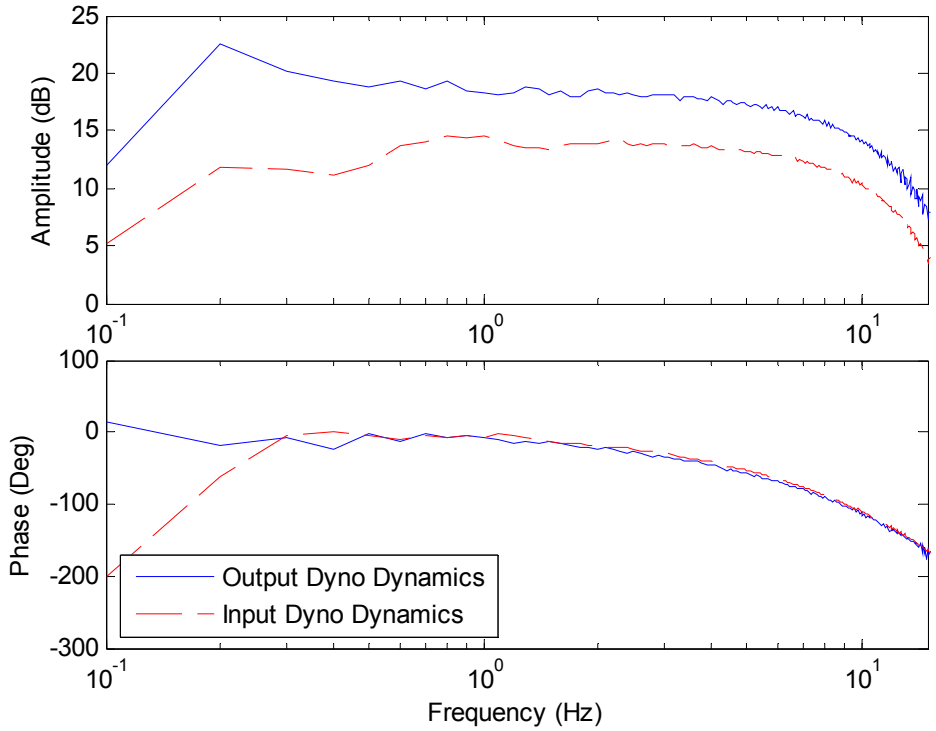

Figure 4-12 Transfer functions between generated torque and percentage control signal for output and input dynamometers

It can be seen from the figure that the dynamics of the motor and drive system for input and output dynamometers are in phase and the difference in amplitude is almost constant. To further prove this, the amplitude of output dynamometer was subtracted from input dynamometer and the result is shown in Figure 4-13, which shows an almost constant difference in amplitude, except in low frequency range and noise in high frequency range. The large errors in the low frequency range result from the measurement errors in the torque signals, which can also be seen in Figure 4-12. Since the dynamics of these two dynamometers were in phase and the difference between amplitudes was almost constant for the frequencies between 1 Hz and 10 Hz, the distinction in the dynamics can be easily corrected by a constant

scaling factor, without the need to design an inverse dynamics compensator for the output dynamometer. This factor was measured to be 0.636 for the frequencies between 1 Hz and 10 Hz.

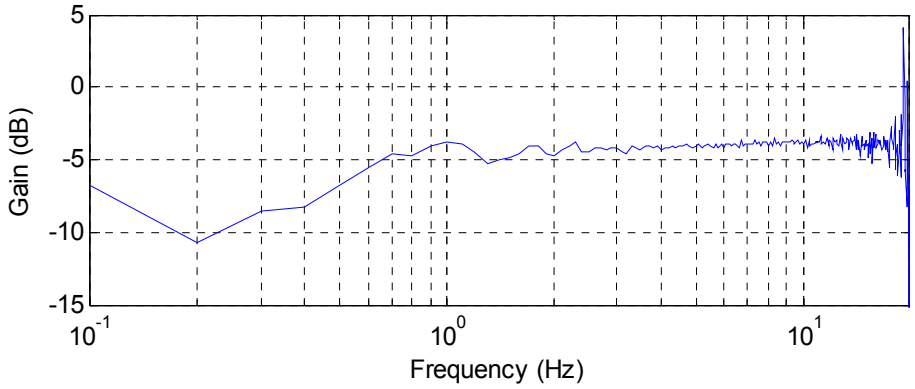

Figure 4-13 Difference in amplitude response of motor and drive system for input and output dynamometers

Therefore the compensation torque of the disturbance from the input dynamometer on the output dynamometer speed control can be structured as shown in Figure 4-14.

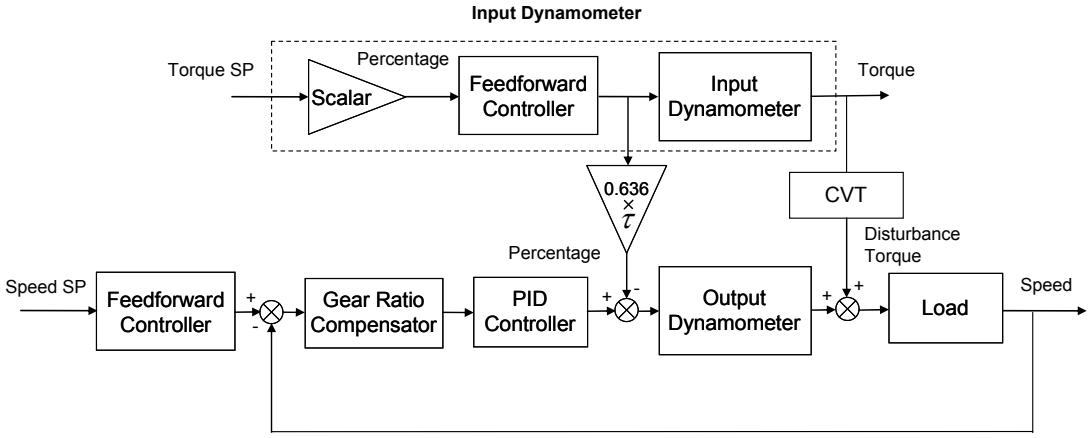

Figure 4-14 Block diagram of torque compensation scheme for output dynamometer speed control

To verify the proposed compensation scheme, both dynamometers were switched on. The output dynamometer was in speed control and input dynamometer was in torque control. Both feedforward controllers were kept the same as designed in the previous chapter. The output dynamometer speed demand consisted of a DC speed of 1000 rev/min plus a SPHS signal with a frequency range of up to 10 Hz, and a scaled amplitude to 35 rev/min. The input dynamometer torque demand consisted of a

SPHS signal with the same frequency range and amplitude. The test results are shown in the following figures.

The measured output dynamometer speed is shown in Figure 4-15. Magnified views of Figure 4-15 are shown in Figure 4-16.

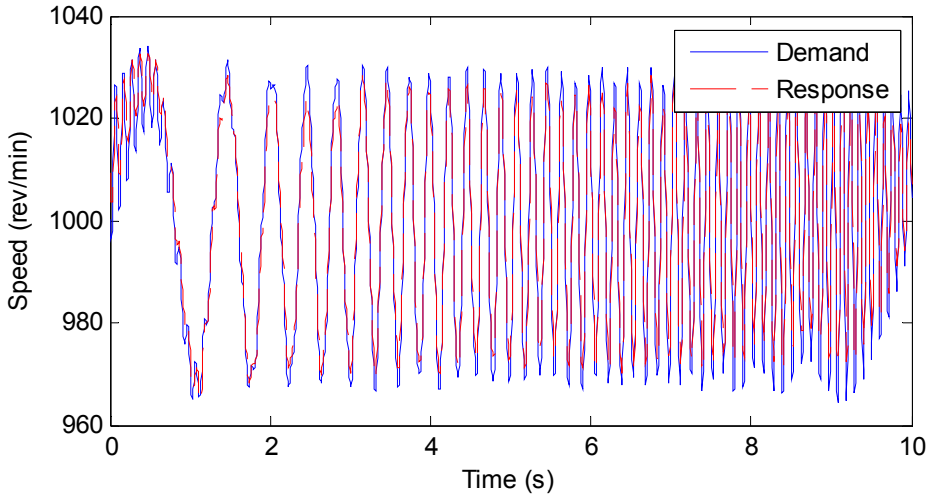

Figure 4-15 Output dynamometer speed with a 1:1 gear ratio

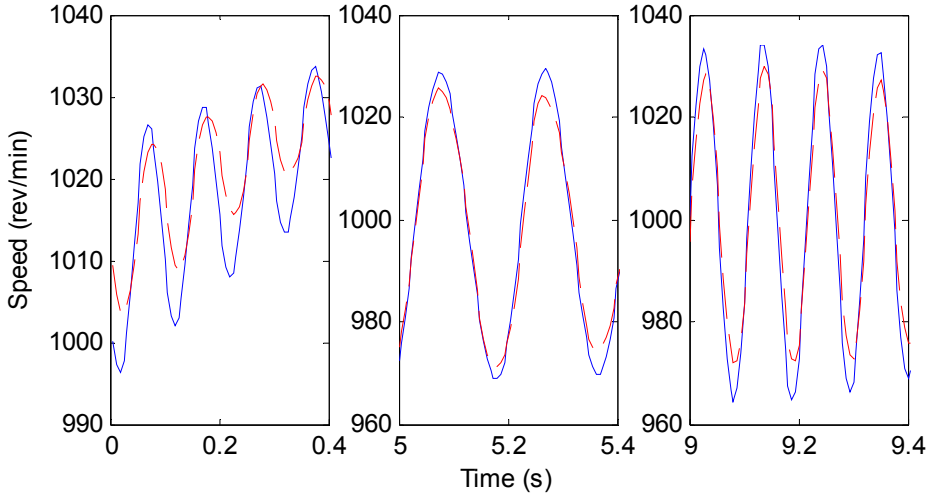

Figure 4-16 Magnified views of Figure 4-15

The frequency response of the system was shown in Figure 4-17, compared with the one without a torque disturbance, when the input dynamometer was switched off.

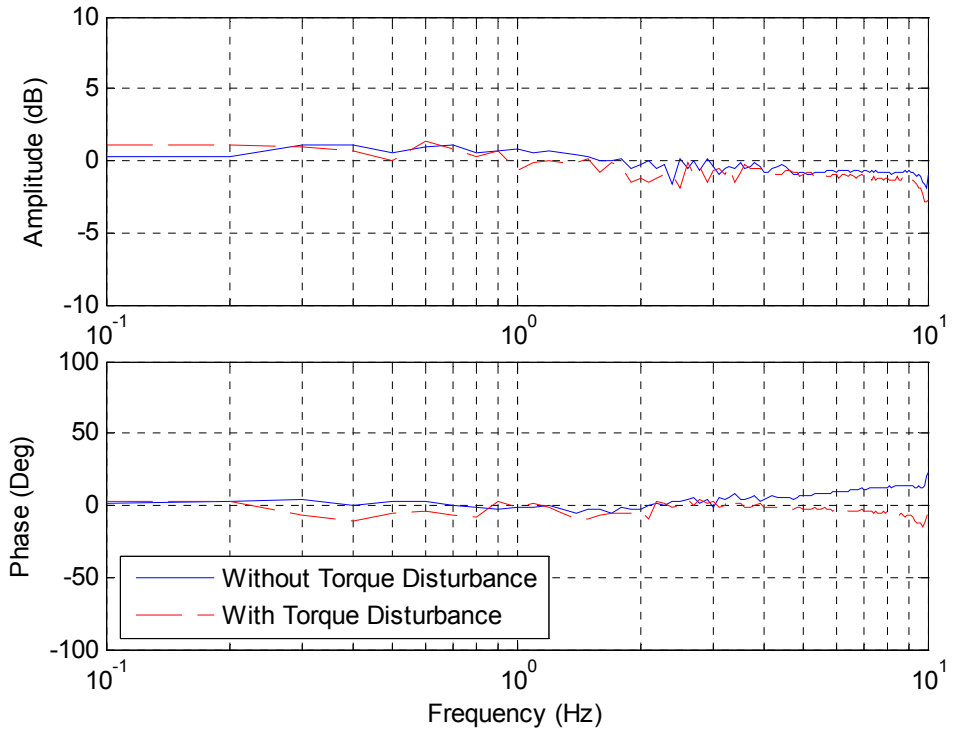

Figure 4-17 Frequency response of Figure 4-15 compared with the results shown in Figure 4-10

It can be seen that the speed was well controlled. If comparing with the speed response without external torque in Figure 4-10, the results were quite similar to each other, which verified the effectiveness of the disturbance torque compensation scheme for the output dynamometer. The compensation scheme was based on the differences between the dynamics the input and output dynamometers, as seen in Figure 4-13. The difference in amplitude response was not perfectly flat. The compensation factor used here was an averaged value, so there was a small discrepancy for the two speed control responses in the amplitude at high frequencies as shown in Figure 4-17. In other words, the speed control was still affected by the torque generated by the input dynamometer, but in a negligible way. The phase response was also delayed, but seemed to offer a better result. Difference in the responses at high frequencies with and without torque disturbance could result from the backlash effect. With the backlash between the gears, the torque generated by the input dynamometer will not be immediately cancelled by the torque generated by the output dynamometer, even if the compensation factor was accurate.

The proposed scheme is based on the dynamics difference of the dynamometers. It eliminates the need to design an additional feedforward controller, and also it is

based on the control signal rather than the measured torque value, which may be contaminated by significant noise.

The input dynamometer torque controller performance was also assessed by using the data obtained from the same test. The generated input dynamometer torque is shown in Figure 4-18, and compared with the torque demand. The generated torque was calculated by using Equation (2-31). Magnified views of Figure 4-18 is shown in Figure 4-19.

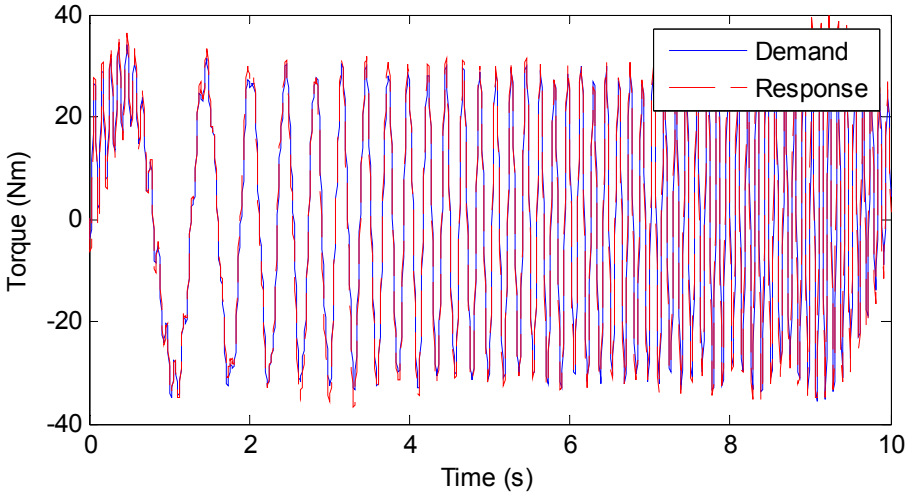

Figure 4-18 Demanded and generated input dynamometer torque with a 1:1 gear ratio

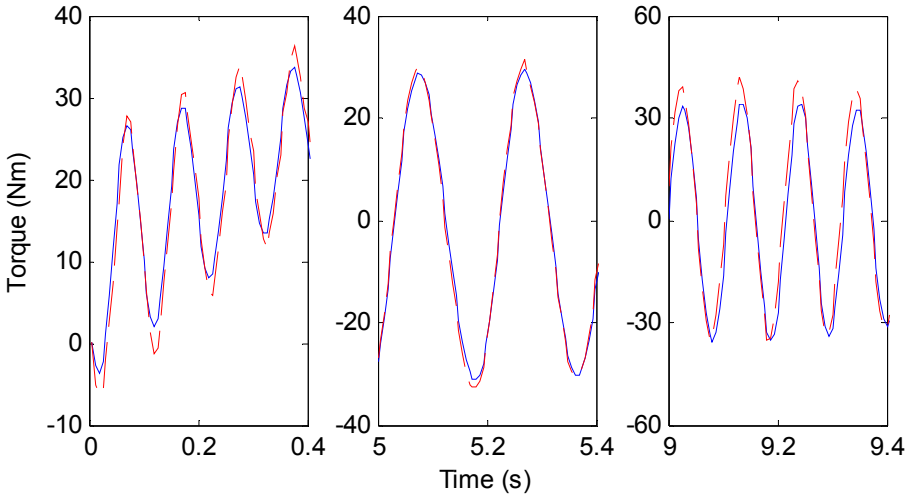

Figure 4-19 Magnified views of Figure 4-18

The frequency response of the torque control system is shown in Figure 4-20.

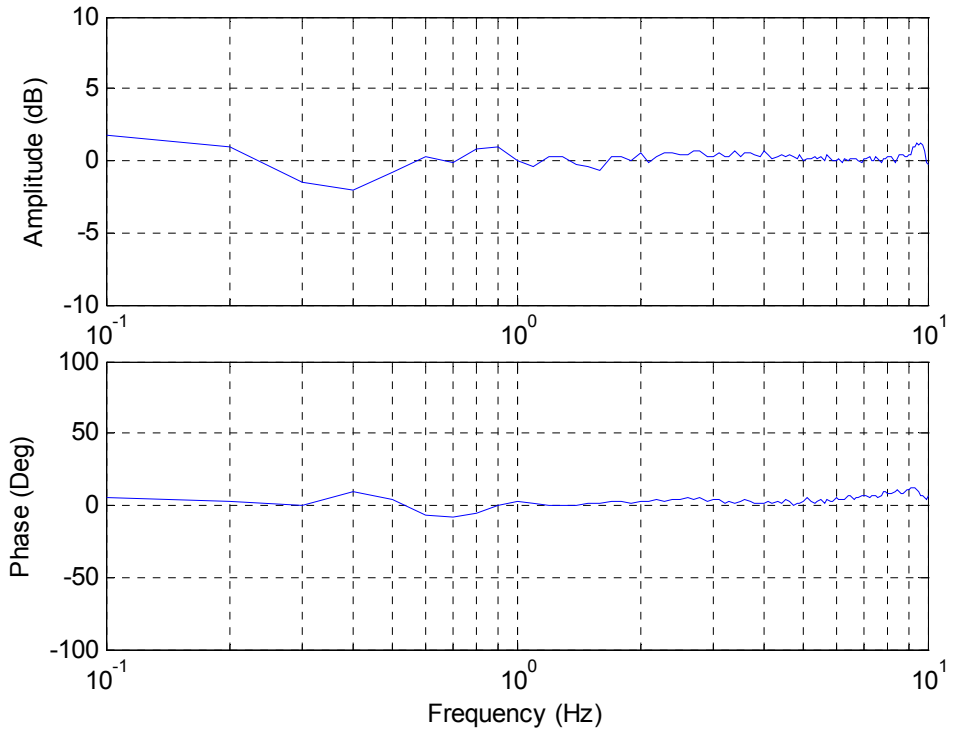

Figure 4-20 Frequency response of Figure 4-18

It can be seen from both time and frequency domain results that the generated input dynamometer torque was precisely controlled to track the torque demand, and was not affected by the coupling between the input and output dynamometers. A similar result to the one on single motor control as shown in previous chapter in Figure 3-15 was obtained. The control result was almost perfect except for the small error in high frequency, which was also seen in Figure 3-15.

4.3 Compensation of Inertia Torque for I/P Dynamometer

So far, the generated torque of the input dynamometer was controlled to track the torque demand, without jeopardising the speed control of the output dynamometer. When testing a CVT in a real vehicle, the torque applied on the input shaft of the CVT is the engine brake torque. Since the input shaft of the CVT was connected to the input dynamometer where the torque measurement was taken, it would be more realistic that the measured input dynamometer torque was controlled to track the simulated engine brake torque rather than the generated torque.

The difference between the generated torque and measured torque was the torque used to accelerate the input dynamometer rotor inertia and to overcome the damping inside the motor. This difference needs to be compensated to make the measured torque track the torque demand. Since the inertia and damping ratio had already been estimated for the input dynamometer in Chapter 2, they can be compensated by calculating the acceleration from the output dynamometer speed demand, the inertia and damping compensation scheme is shown in Figure 4-21.

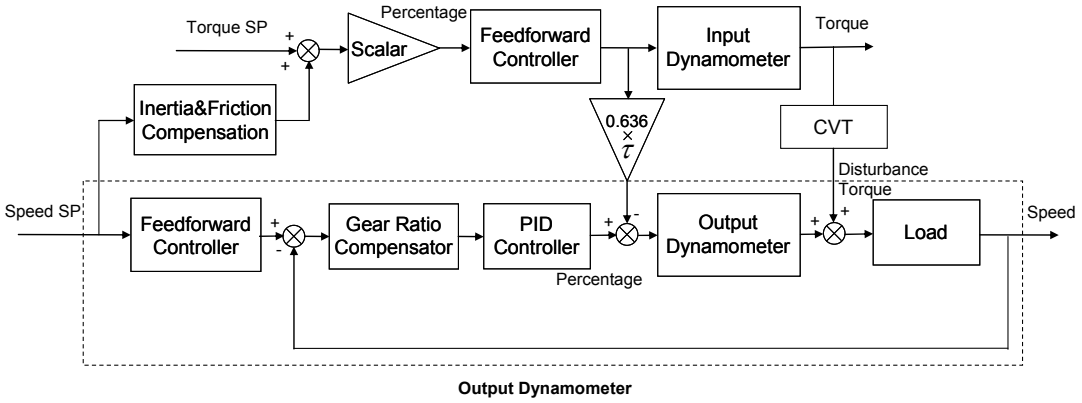

Figure 4-21 Inertia and damping torque compensation scheme for input dynamometer

Theoretically, the inertia and damping torque should be calculated from the measured speed response of the input dynamometer rather than the speed demand, but the measured speed contains noise and results in large errors when calculating the derivative. More importantly, it will introduce high frequency input signal to the feedforward controller of the torque control, which was designed for a specific frequency range. With near perfect speed control, the compensation calculated from the speed demand should give the same results as the one calculated from the actual speed.

4.3.1 Test with Inertia Torque Compensator

Tests were carried out to examine the proposed inertia and damping compensation scheme. The speed demand for the output dynamometer was the same as before. The torque demand for the input dynamometer consisted of a SPHS signal with frequencies up to 10 Hz and an amplitude of 45 Nm, superposed on a steady state of

torque demand of 100 Nm. The measured input dynamometer torque is shown in Figure 4-22. Magnified views of Figure 4-22 are shown in Figure 4-23.

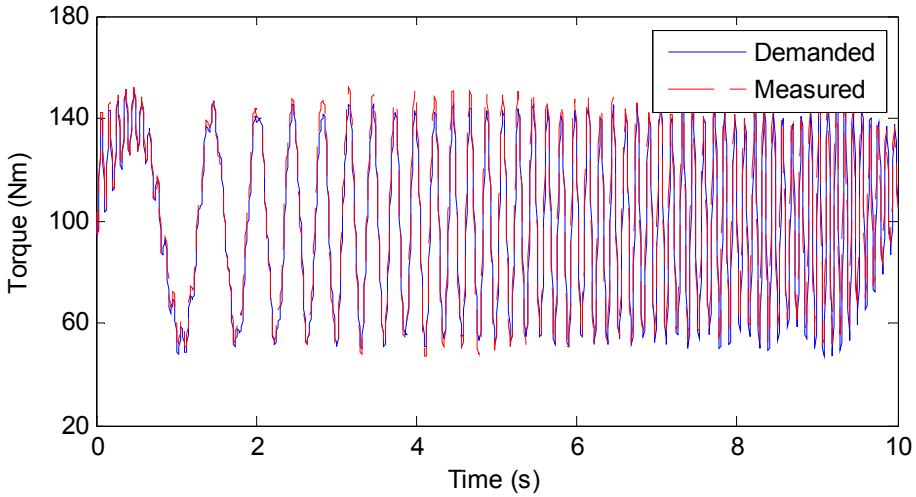

Figure 4-22 Measured torque of input dynamometer with inertia torque compensation

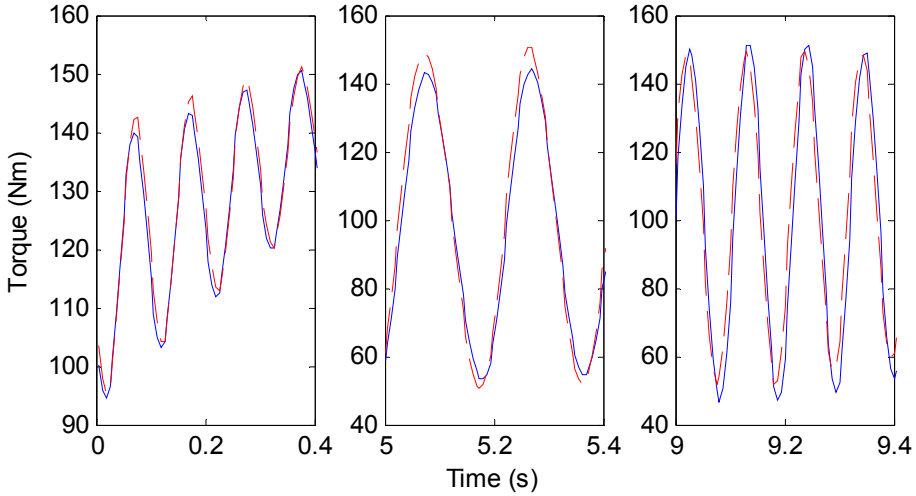

Figure 4-23 Magnified view of Figure 4-22

The frequency response is shown in Figure 4-24. It can be seen from the test results in both time and frequency domains that although the inertia and damping torque compensation for input dynamometer was simple, the compensation method is extremely effective. The amplitude of the measured torque in the middle frequency range was slightly higher than the demand. This could be due to the error in the output dynamometer speed control. As discussed, the error in speed control will lead to the errors in the calculation of inertia and damping torque.

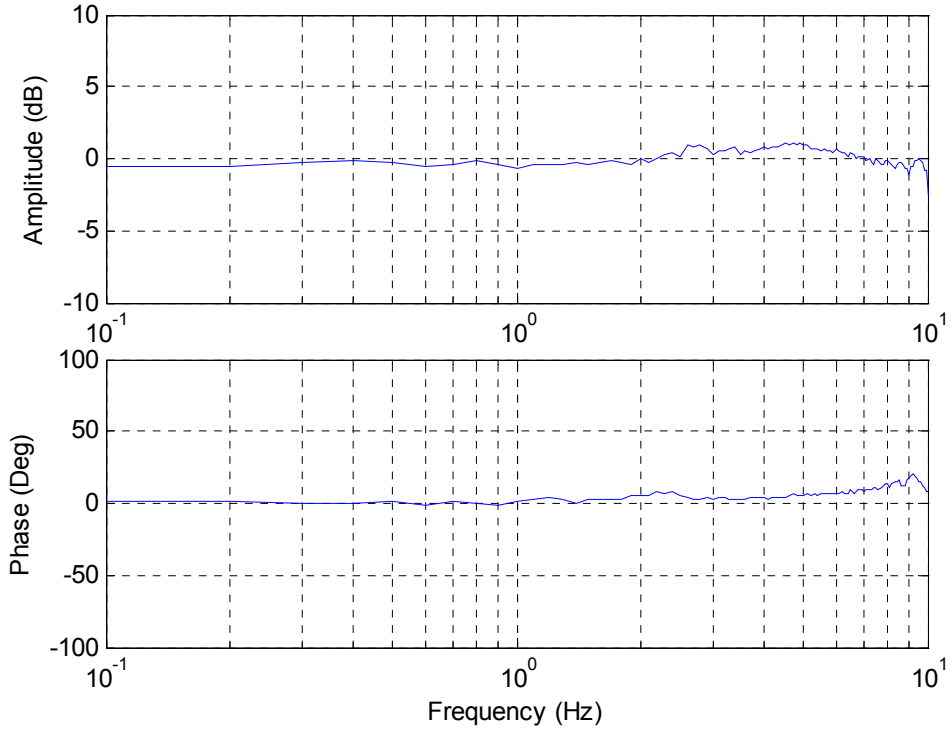

Figure 4-24 Frequency response of Figure 4-22

To further examine this, the speed response of the output dynamometer was also recorded, and the response in time domain is shown in Figure 4-25. Magnified views of Figure 4-25 is shown in Figure 4-26. The frequency response is shown in Figure 4-27.

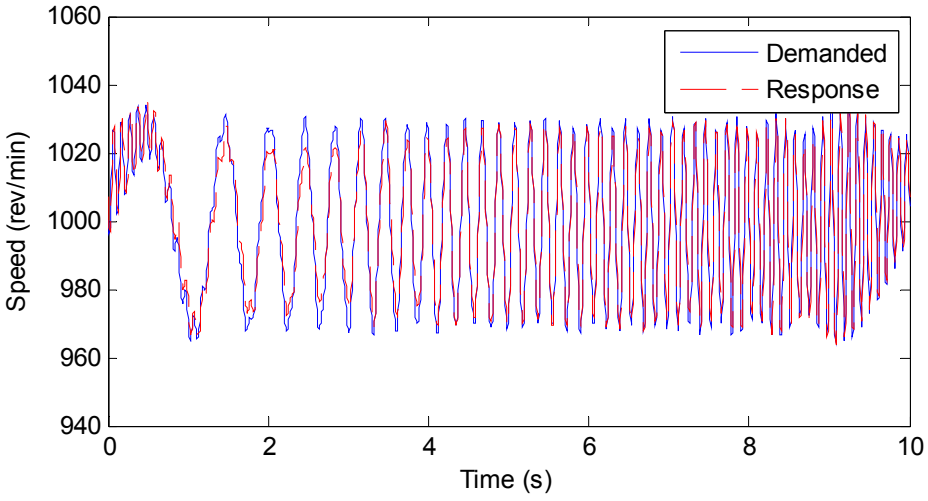

Figure 4-25 Speed response of output dynamometer with inertia torque compensation for input dynamometer

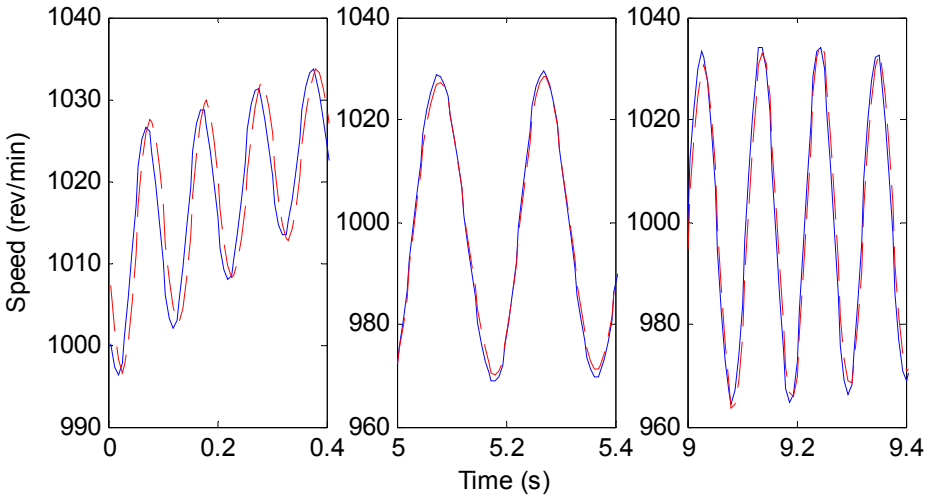

Figure 4-26 Magnified views of Figure 4-25

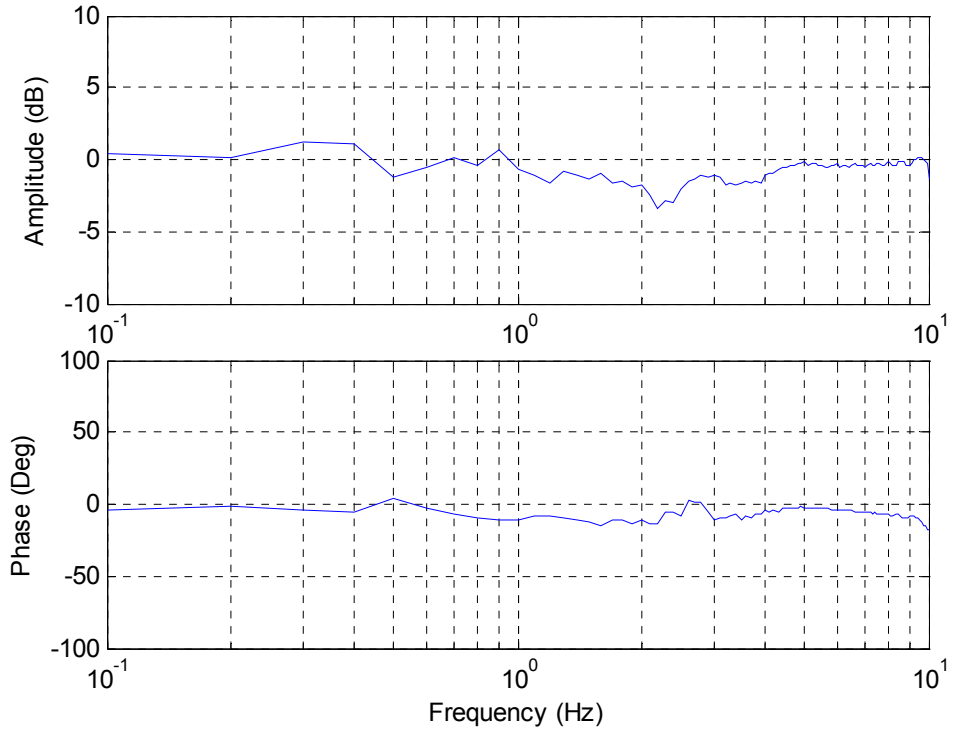

Figure 4-27 Frequency response of Figure 4-25

The output dynamometer speed performance shows errors in the middle frequency range. The backlash effect is always one of the factors that affect the control performance. Due to the backlash, even with a 1:1 gear ratio, the speed and torque will be different on the input and output shafts. Then the disturbance torque from the input dynamometer will not be exactly cancelled by the additional output dynamometer torque even though an exactly same among of torque is generated in the opposite direction. The speed of input dynamometer will also be different from the speed of output dynamometer. The calculation of inertia and damping torque

from speed demand will not be the same as calculated from the input dynamometer speed response even though the output dynamometer speed is equal to the speed demand.

4.3.2 Test with additional PID controllers

The control performance could be further improved if another PID controller is added for both output and input dynamometer controls on the outer loop to further correct the tracking error. Then the speed control will be in the form of structure (a) in Figure 1-9, and the torque control will be in the form of structure (b) in Figure 1-8. The overall block diagram with additional PID controllers is shown in Figure 4-28.

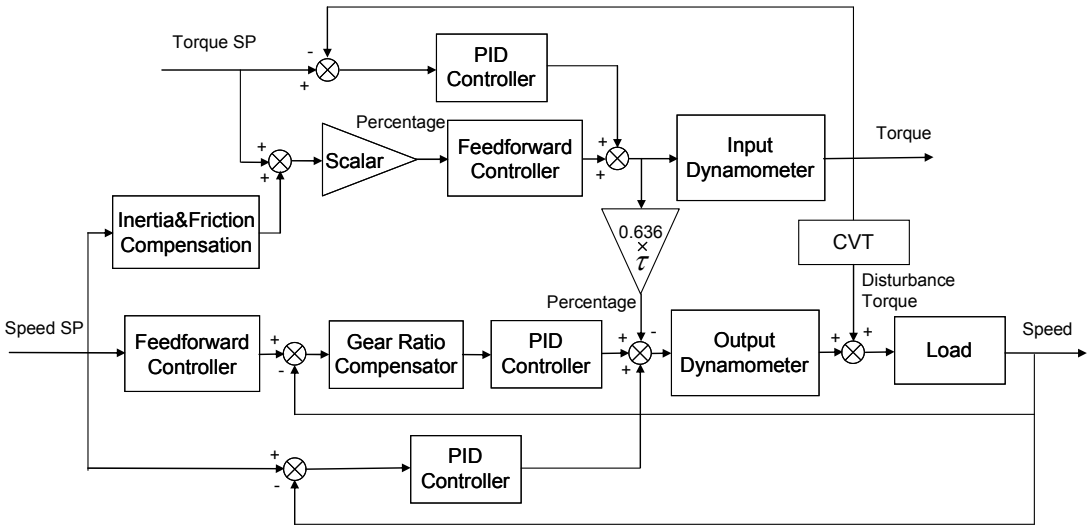

Figure 4-28 Overall control block diagram with additional PIDs

Tuning of the PID controller would be dependent on a specific application. If the feedforward controls for the motor torque and speed were nearly perfect, the torque and speed errors would be very small, and the added PID controllers will have minor effects on the original control systems. If the control errors were relatively large, the PID controllers will provide further correction on the errors. But using additional PID controllers will certainly introduce phase shift into the system, so better performance can not be guaranteed. Sometimes a compromise may need to be considered for the amplitude and phase when tuning the parameters of the PID controller.

Tests were carried out with the same speed and torque demand for the output and input dynamometers as the previous test. Two more PID controllers were added to

the outer loop of the speed and torque control. The PID parameters were tuned in dSPACE starting with 0.1 for both proportional and integral gains. The derivative gain was set to be 0 due to the noise. Then by running the test through SPHS cycles, the gains were adjusted to offer better time responses. Finally, the PID parameters for the speed control were tuned to be 0.08 for the proportional gain, 0.4 for the integral gain and 0 for the derivative gain, while for the torque control the parameters were 0.03 for the proportional gain, 0.3 for the integral gain and 0 for the derivative gain. With additional PID controllers, the measured input dynamometer torque is shown in Figure 4-29. Magnified views of Figure 4-29 is shown in Figure 4-30. The frequency response is shown in Figure 4-31, compared with the response without additional PID controller.

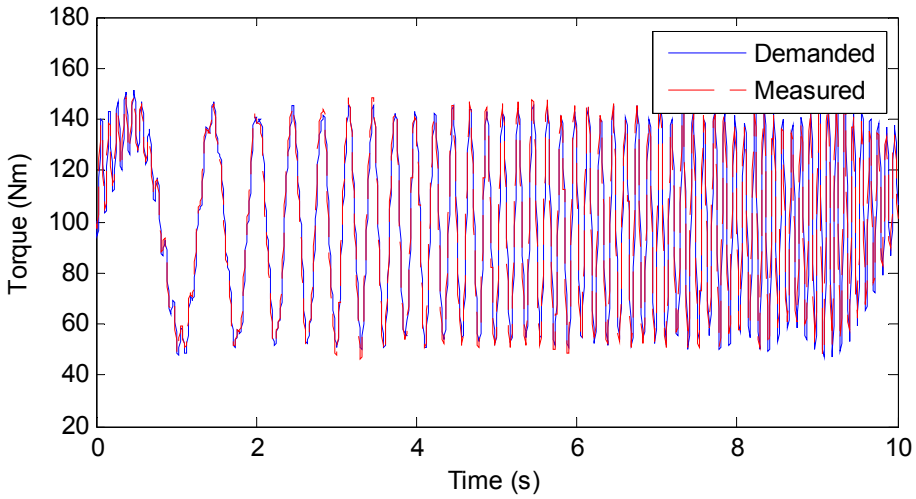

Figure 4-29 Measured input dynamometer torque with additional PID controller

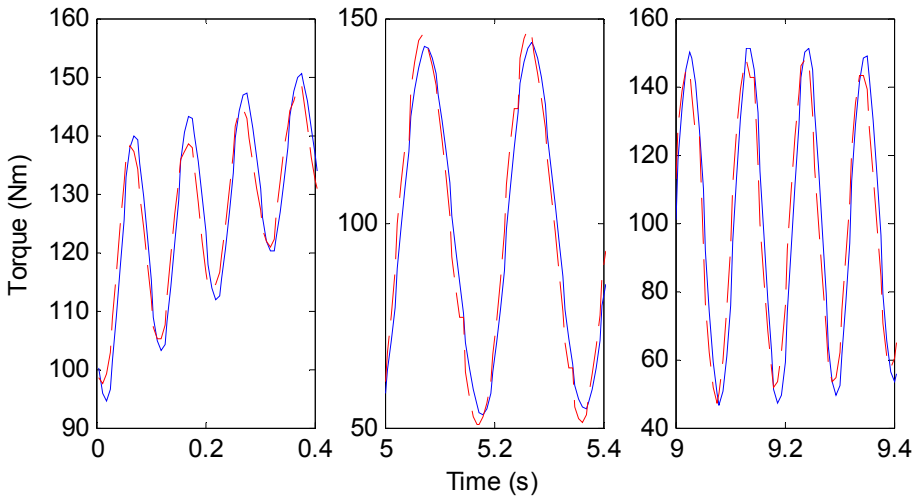

Figure 4-30 Magnified views of Figure 4-29

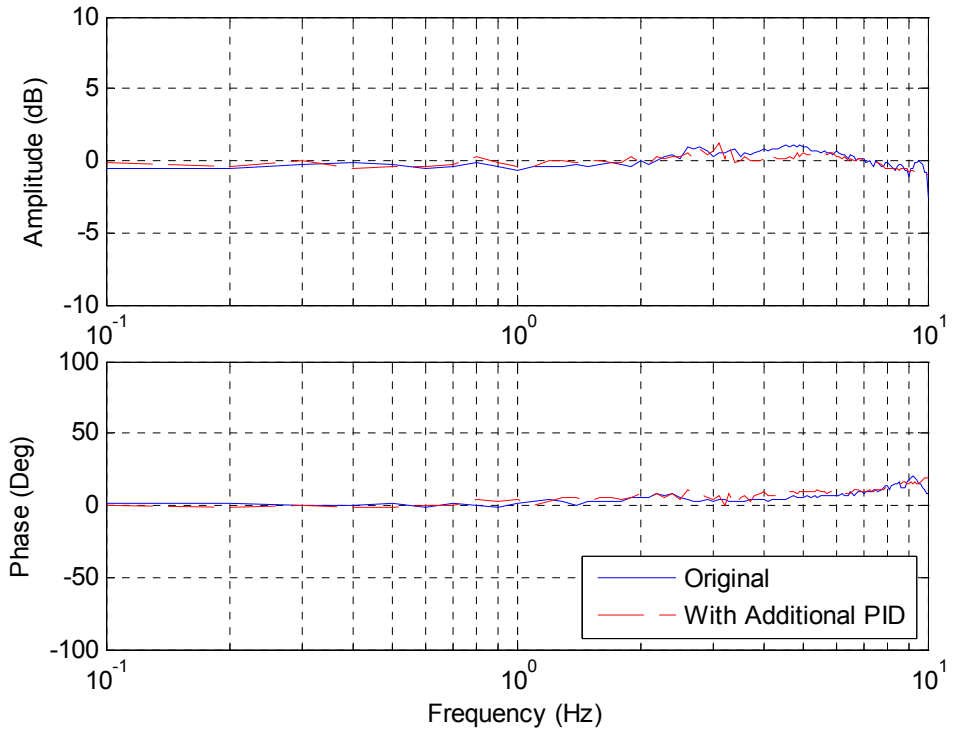

Figure 4-31 Frequency response of Figure 4-29 compared with the results shown in Figure 4-24

It can be seen from the amplitude response that the tracking error was reduced, especially in the middle frequency range. Meanwhile, the phase became slightly worse at the same frequency range. As discussed before, the PID controller will introduce phase shift into the system, and sometimes it is a compromise between amplitude and phase responses. However, the control results were already satisfactory without the additional PID controller, i.e. the additional PID controller did not show much improvement.

Relatively large control errors were observed on the output dynamometer speed control response in Figure 4-27. The response is significantly improved by the additional PID controller. The time domain response is shown in Figure 4-32. Magnified views of Figure 4-32 are shown in Figure 4-33. The frequency response is shown in Figure 4-34 compared with the response without additional PID controller.

Comparing Figures 4-25 and 4-32, the improvement in time domain is very obvious between 1 s and 3 s. In frequency domain, a definitely better result was observed for both amplitude and phase up to 2 Hz, due to the use of the PI controller, which has more effects in the low frequency range. Fluctuation occurs around 3 Hz for both amplitude and phase response, which was also observed in the torque control in

Figure 4-31, which is because of the interaction between the two motors. However, the result for the speed control still seems better around 3 Hz than without the additional PID controller. Above 4 Hz, the control result is generally not as good as before, in either amplitude or phase response, but the difference seems negligible. The overall performance is thus definitely improved by the additional PID controller.

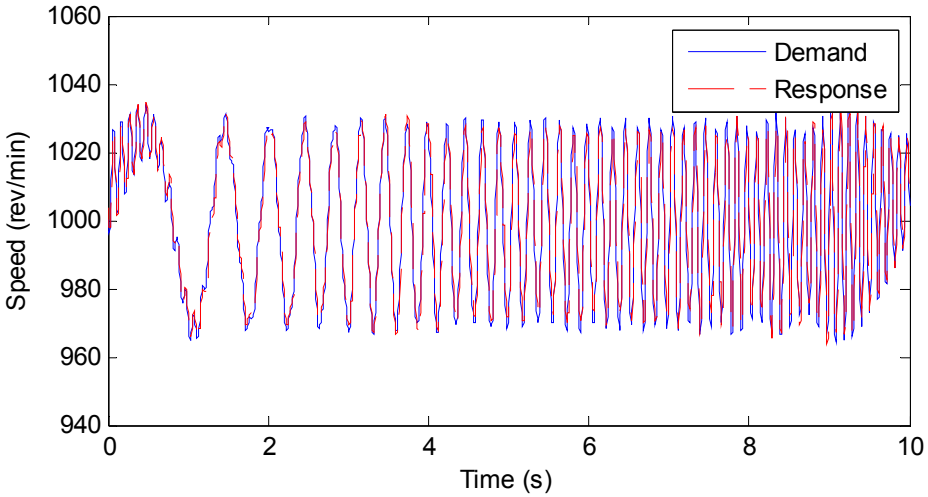

Figure 4-32 Measured output dynamometer speed with additional PID controller

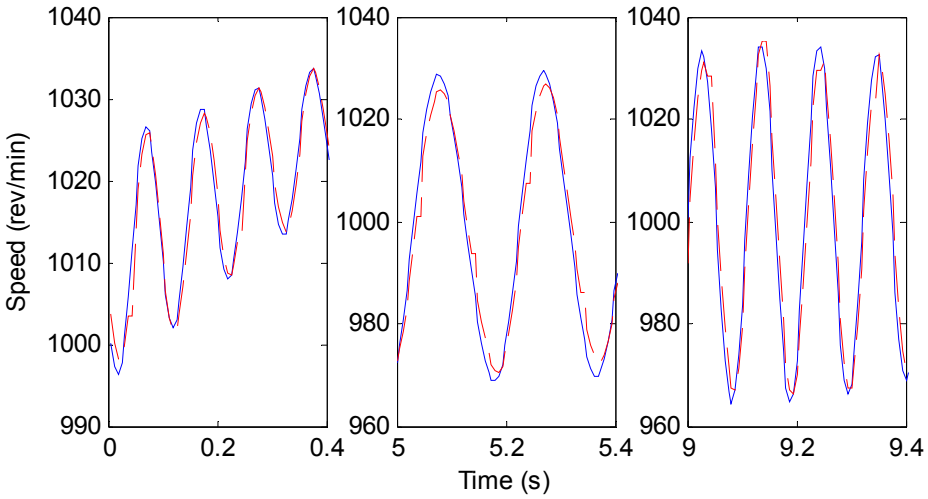

Figure 4-33 Magnified view of Figure 4-32

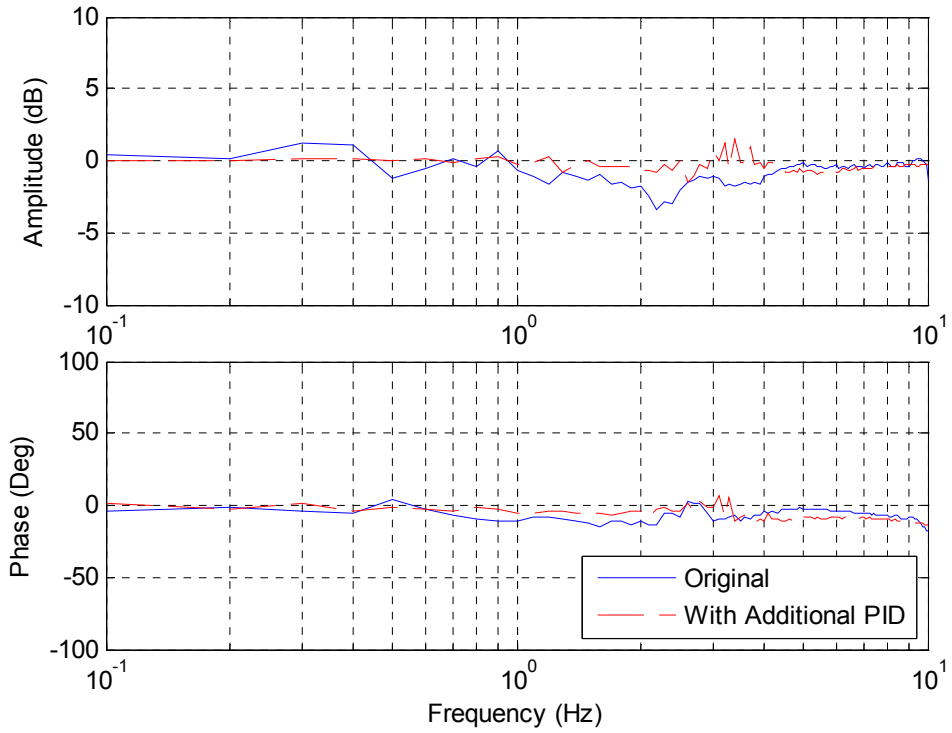

Figure 4-34 Frequency response of Figure 4-32

Hence, the performance of the additional PID controller is hard to predict, especially when the two motors are coupled. It could be a compromise on the performance between amplitude and phase responses, like the input dynamometer torque control, or between low and high frequency ranges, like the output dynamometer speed control. The utilization of additional PID controller and tuning its parameters will depend on the specific application. Normally the additional PID controller is not necessary or the parameters can be set to be relatively small, so that it will only act on relatively big errors. At the same time, it will not change the dynamics of the original system and affect the performance of the feedforward controller.

Chapter 5 Testing with Real Time Model

All the previous tests were carried out with SPHS multi frequency signal as input. Since it contains all the specified sub harmonics in one signal, it provides a challenging way to test the effectiveness of the proposed torque and speed tracking controllers, but this kind of signal was not expected when testing CVTs. More realistic signals are used to test the designed controllers in this section, which are the engine brake torque and vehicle speed simulated from real-time engine and vehicle models. Although the real-time model is constructed with a manual transmission rather than a CVT, the simulation results are still representing typical engine brake torques and vehicle speeds encountered in real driving conditions.

5.1 Engine and Vehicle model

The engine and vehicle model used in this section of the work were supplied by the Ford Motor company and for brevity and confidentiality reasons only their main attributes are described here.

The vehicle model is based on the standard vehicle road load equation, including speed dependent rolling resistance, aerodynamic drag, acceleration and gradient effects. It can be expressed by the equation as follows:

$$F_t = r_c m_v g + m_v a + m_v g \sin\theta_r + \frac{1}{2}\rho C_D A v_v^{\,2} \qquad \textbf{(5-1)}$$

The dynamics of tyre traction and stiffness and damping in the vehicle drive shafts are also embedded within the model.

The engine model is termed as a ‘mean value engine model’, the outputs from the model are the cycle averages for one complete engine cycle, as opposed to a crank angle based model where outputs are derived on a crank angle basis and thus include

phenomena such as torque pulsations on the crankshaft. The engine model is based on a neural-network representation of engine torque and exhaust gas temperature derived from data obtained from steady state testing undertaken with the engine on a dynamometer facility. Enhanced dynamics of the model are included by the addition of an 'emptying and filling' representation of the gas dynamics in the inlet and exhaust manifolds, the exhaust gas recirculation system and the turbocharger.

A model based representation of the engine electronic control unit (ECU) is also used to derive set points for the various engine actuators (e.g. exhaust gas recirculation (EGR), variable geometry turbocharger (VGT), fuel rail pressure, injection rate and timing), based on driver inputs (e.g. pedal position), and other powertrain states (e.g. engine boost pressure, mass air flow, engine speed, and engine temperature).

5.2 Testing with Simulation Results

The simulated vehicle speed and engine brake torque through a standard EUDC driving cycle are taken as the speed and torque demands for the output and input dynamometers respectively. The testing structure is shown in Figure 5-1. In the real time model, the reference speed is a EUDC driving cycle, and the simulated vehicle speed is fed back to the driver model to calculate the accelerator and brake pedal positions. The clutch position and the number of the gears are preset profiles with regards to real time.

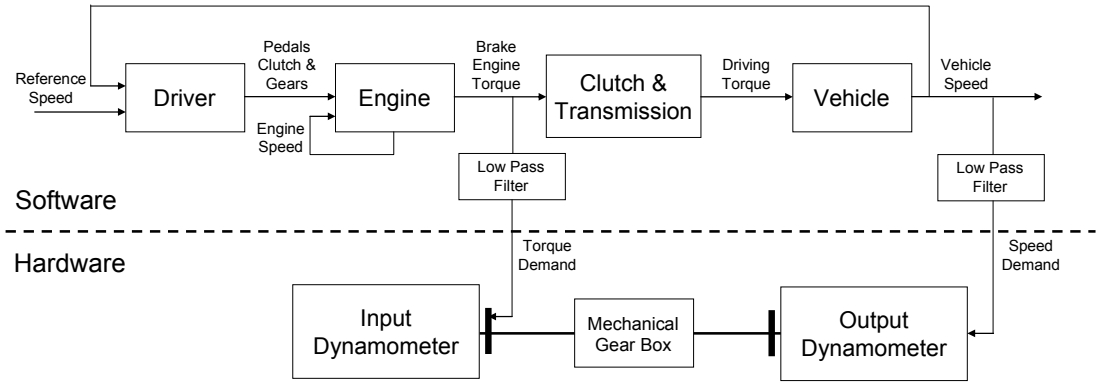

Figure 5-1 Testing structure with simulation results

The test results for the output dynamometer speed control are shown in Figure 5-2, while the test results for the input dynamometer torque control are shown in Figure 5-3.

Since the EUDC driving cycle consists of several small driving cycles, the simulated vehicle speed and engine brake torque also contains similar profiles for each individual cycle. Typical acceleration and braking processes are selected for a magnified view from Figure 5-2 for speed control, and shown in Figure 5-4. Meanwhile, the same regions are also selected from Figure 5-3 for torque control, magnified, and shown in Figure 5-5.

It can be seen from these test results that excellent tracking control was achieved for both torque and speed. The tracking errors were generally due to noise. As motioned before, the torque transducer has an accuracy of +/- 0.1% of full scale, i.e. +/- 1 Nm, so the measurement error will have more effects at low torque values. There is also some error from calibration of the torque transducer, e.g. it measuring between -1.2 and -0.8 Nm when the motors were switched off.

In fact, the simulated engine brake torque was not flat, e.g. between 250 s and 260 s shown in Figure 5-5 (b), there were small variations in the amplitude of the signal, which was normally less than 1 Nm, as shown in Figure 5-6. The feedforward controller will attempt to follow these fast but low amplitude signals, but the resultant response can not be accurately measured. This caused an error for the PID controller to further correct, thus a noisy response in torque was observed.

The most critical aspect in the overall control was not the behaviour of the feedforward controller, but the dynamic compensation for the output dynamometer when the two motors were coupled, such that torque generated by the input dynamometer will not have any effects on the output dynamometer. The speed control compensation was achieved by a dynamics factor as shown in Figure 4-13, which was almost constant, except for noise in the high frequency range. If the compensation failed due to the inaccuracy of the dynamics factor, the speed of output dynamometer will be pulled away from the speed demand by the input dynamometer torque, and the compensation of inertia and damping torque for the measured input dynamometer torque, which was calculated from the speed demand will also fail in this case.

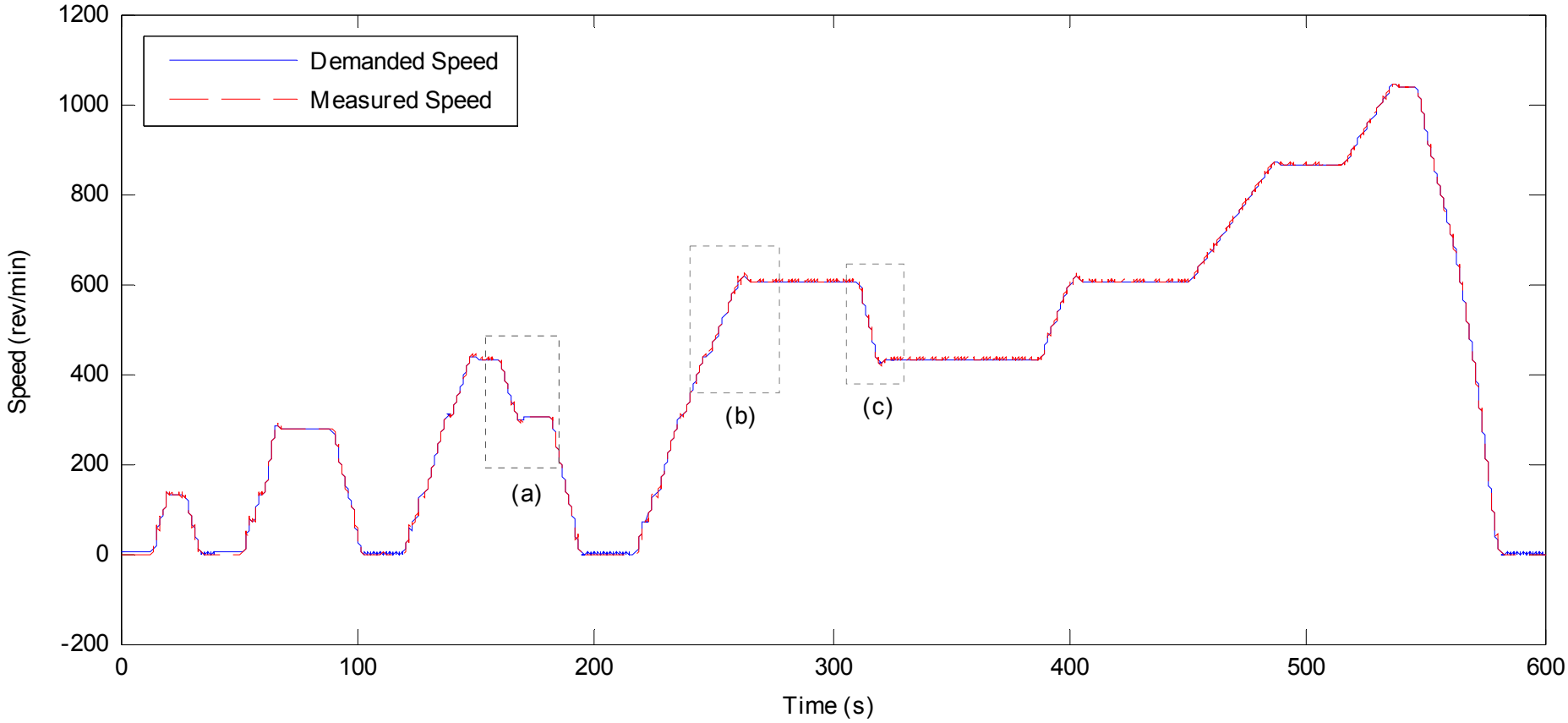

Figure 5-2 Measured output dynamometer speed again simulated vehicle speed

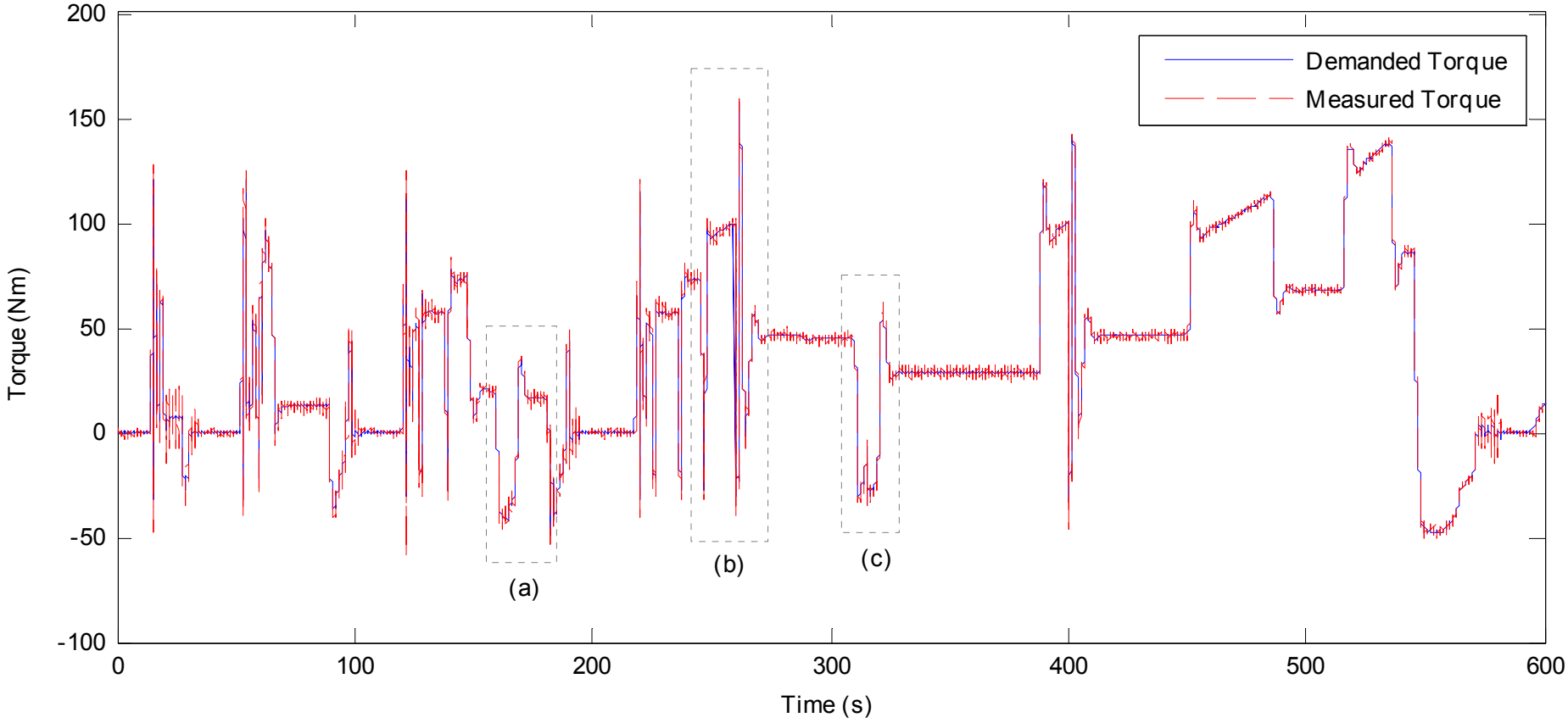

Figure 5-3 Measured input dynamometer torque against simulated engine brake torque

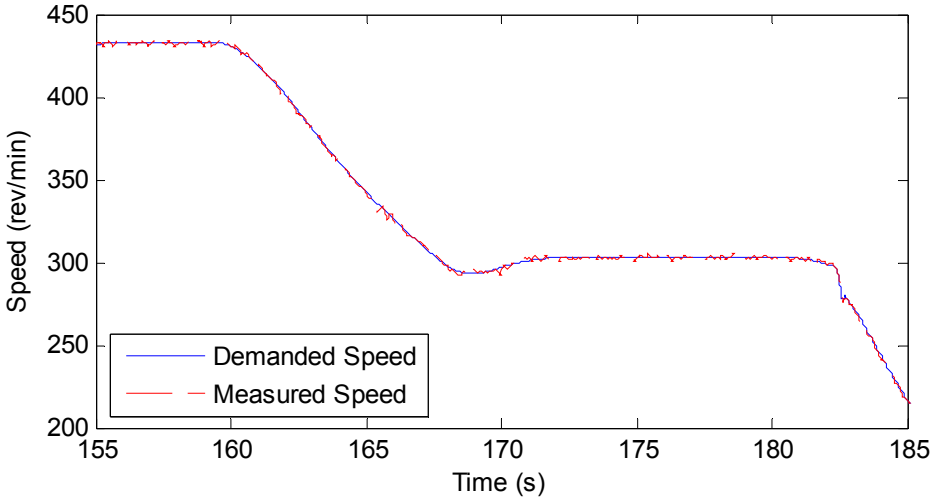

(a)

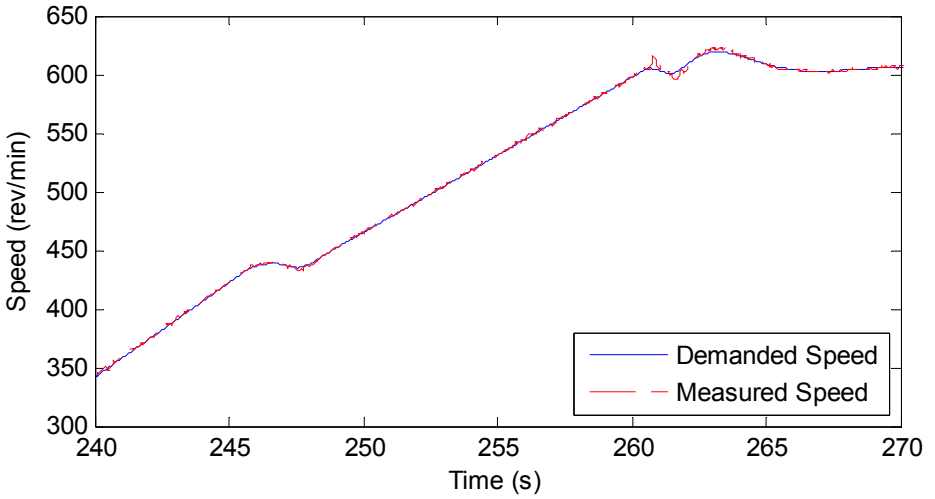

(b)

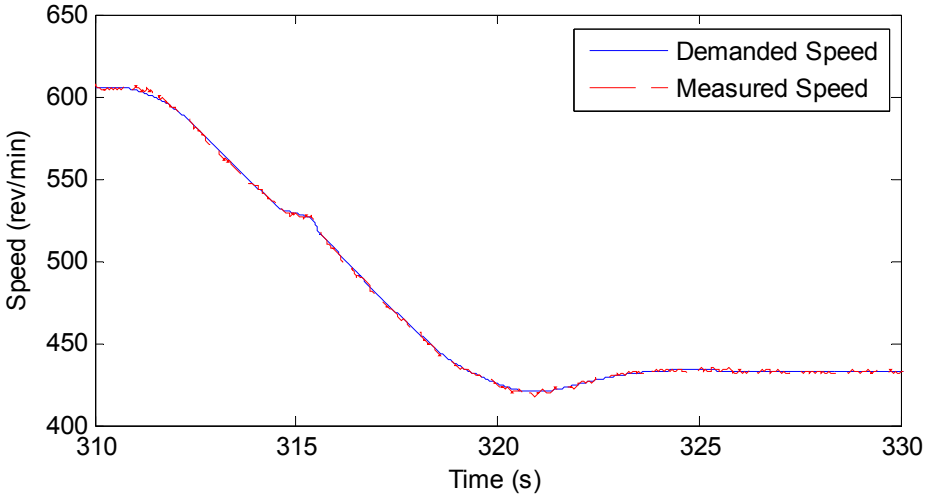

(c)

Figure 5-4 Magnified views of Figure 5-2

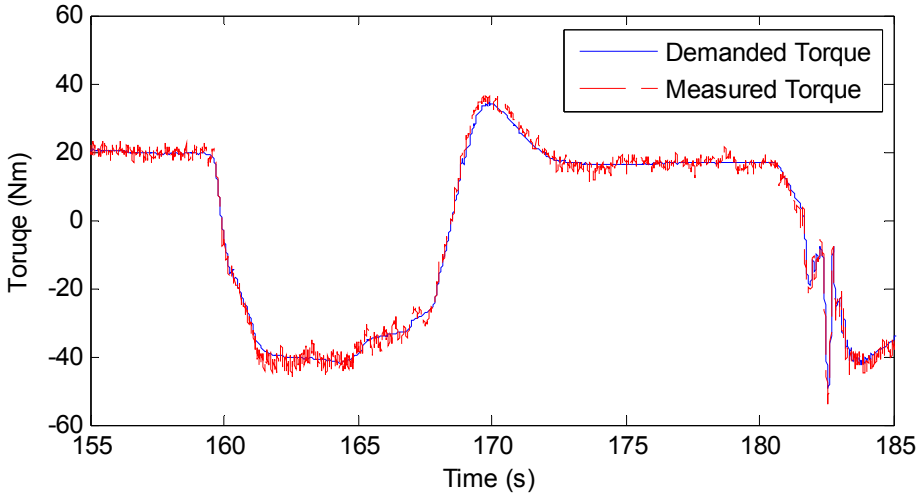

(a)

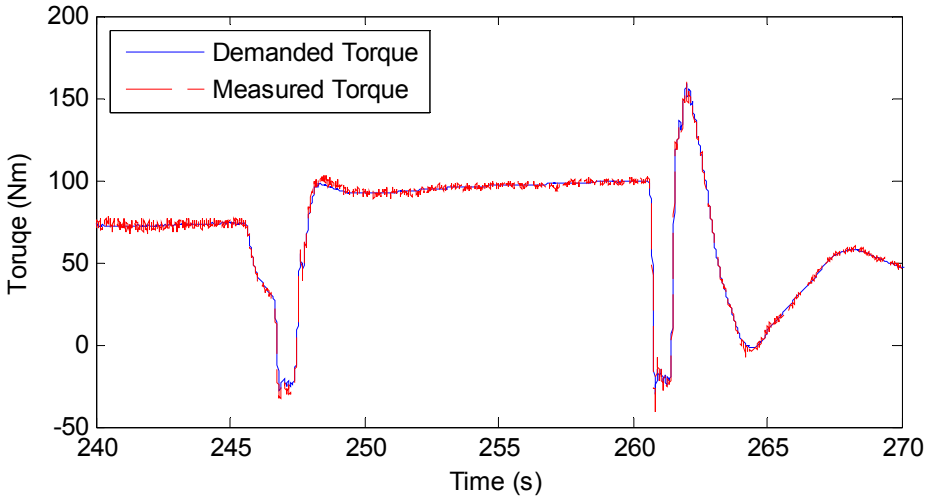

(b)

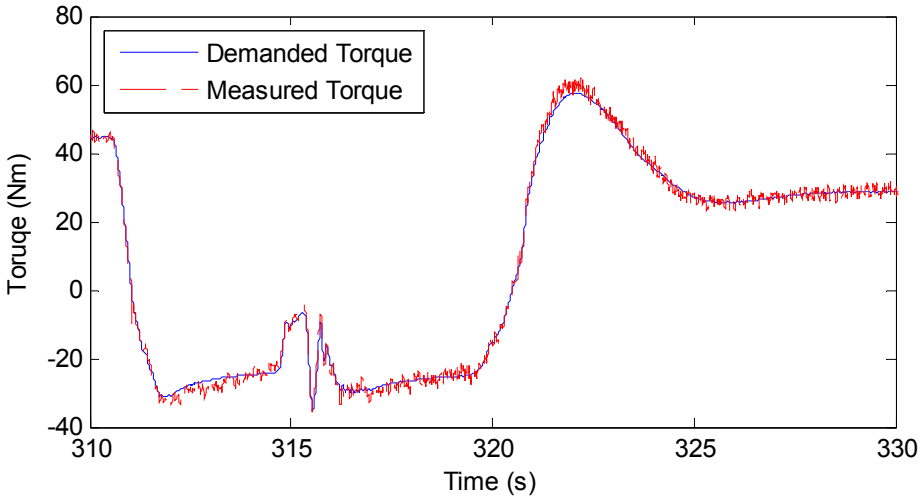

(c)

Figure 5-5 Magnified views of Figure 5-3

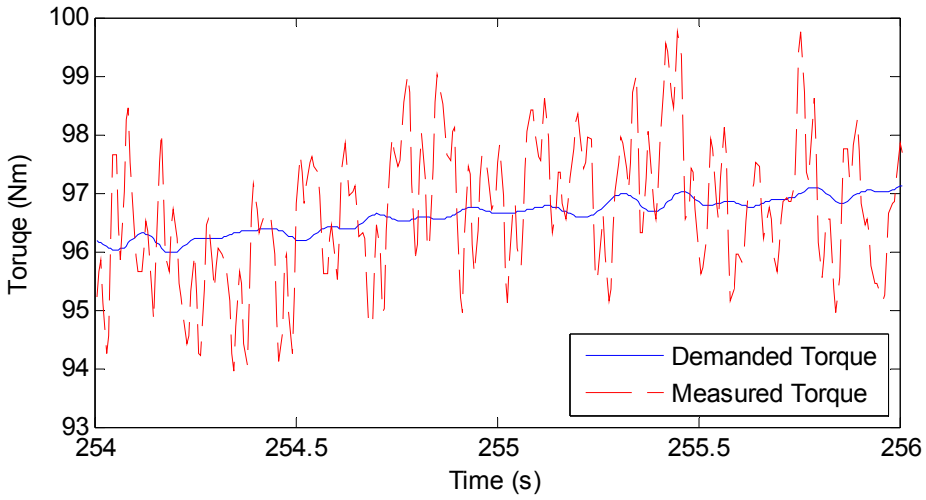

Figure 5-6 Fluctuations in simulated engine brake torque as input dynamometer torque demand

For example in Figures 5-4 (b) and 5-5 (b), there was a sudden drop in the brake engine torque around 261 s because of a gear change and the associated lift off of the accelerator pedal. As the dynamics compensation is not perfect, and the fast change of the generated input dynamometer torque was not exactly repeated by the output dynamometer in the opposite direction, the output dynamometer speed deviated from the speed demand. Since the inertia torque was still calculated from the speed demand, an error was caused on the measured input dynamometer torque. The error in speed shown here was already improved by the additional PID controller, the situation was worse before the PID controller was added.

When testing the CVT in a real vehicle, even with a robot driver, the speed tracking accuracy needs to be within +/-1 km/h, i.e. +/-10 rev/min. The speed tracking error shown in the test results is normally only +/-2 rev/min, and +/-10 rev/min on very rare occasions, like shown in Figure 5-4 (b) around 261 s. When testing the CVT with a real engine, the measured engine brake torque will also oscillate significantly during an engine cycle for the firing and pumping processes, e.g. a peak value of 70 Nm for a mean brake torque of 30 Nm. The torque tracking error shown in the results is normally +/-5 Nm, and +/-10 Nm for the worst situation. Hence, the control results can sufficiently meet with the requirements to test a CVT.

In order to show the success of designed controllers for speed and torque control, a new test was carried out on the input and output dynamometer running through the simulation results, with the original PID controllers provided by the CP CADET

system. The test was only run up to 200 s, covering the first three small cycles. The test results are shown in Figure 5-7 for measured output dynamometer speed and in Figure 5-8 for measured input dynamometer torque.

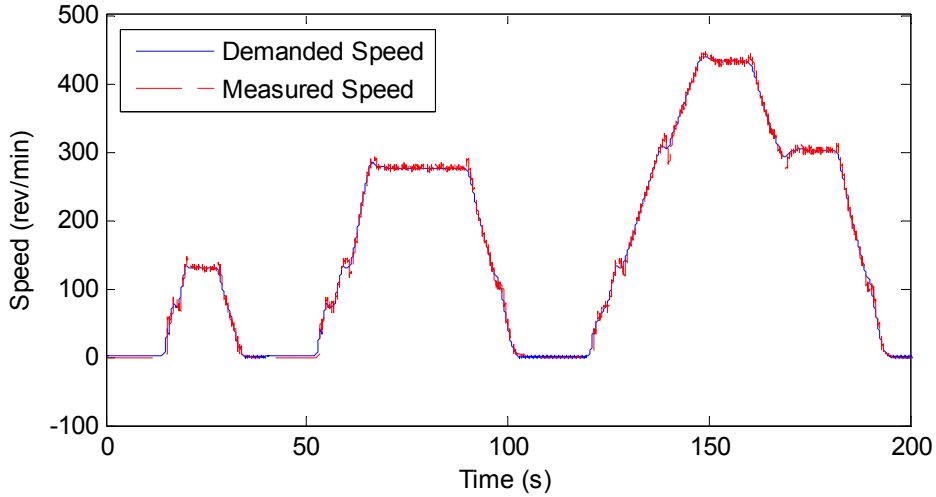

Figure 5-7 Measured output dynamometer speed with PID controllers in the CP CADET system

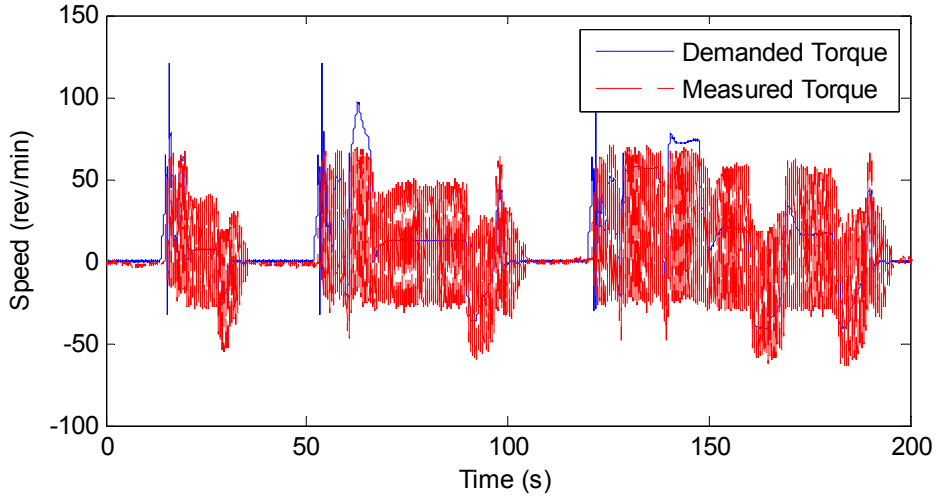

Figure 5-8 measured input dynamometer torque with PID controllers in the CP CADET system

The same region as shown in Figures 5-4 (a) and 5-5 (a) was selected for a magnified view, which is shown in Figures 5-9 and 5-10 for speed and torque control respectively.

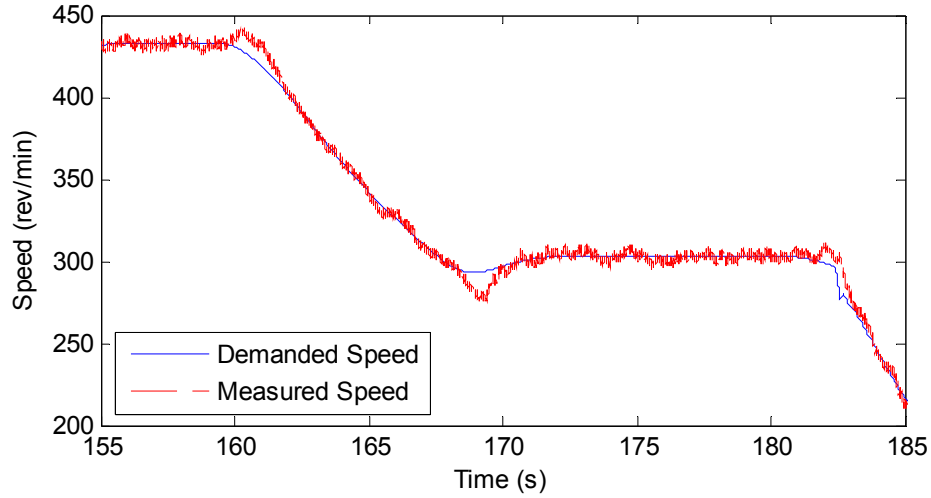

Figure 5-9 A magnified view of Figure 5-7

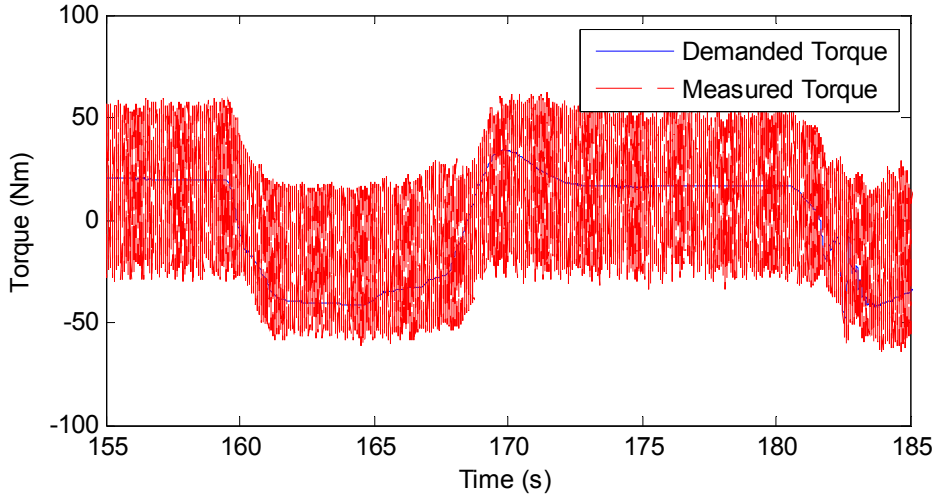

Figure 5-10 A magnified view of Figure 5-8

Because there is no compensation for the interaction between the two motors when they are coupled, the PID controllers have to be tuned to emphasize good performance on one control, either speed or torque. Otherwise the two PID controllers will function against each other and damage the shaft. As seen from the test results, the speed control was tuned to be stiff, and torque control to be loose. In this case, the torque control performance is sacrificed, but even so the speed control is still much worse than before as shown in Figure 5-4 (a). Moreover, the PID controller is tuned for a specific gear ratio. Therefore, the performance will be worse if the gear ratio changes.

As these results suggest, the proposed controllers improved the system response significantly compared with the PID controllers as implemented by the manufacture of the system. The interaction between these two motors was successfully

compensated by the proposed controllers, e.g. the gear ratio compensator and the disturbance torque compensator. Along with the designed speed and torque controllers, the measured speed and torque of the output and input dynamometer are precisely controlled to track the real-time simulation results.

5.3 HIL Testing

Final tests were carried out on HIL testing. The testing structure is shown in Figure 5-11. Compared with Figure 5-1, the clutch and transmission components are removed from the real time model. The measured input dynamometer speed is fed back to the engine model as the engine speed and the measured output dynamometer torque is fed back to the vehicle model as the driving torque. Since the mechanical gear box was fixed with a 1:1 gear ratio, the measure signals were amplified by the current overall gear ratio instead of the final drive ratio when fed back to the real time model. In this way, the gear box can be deemed as a transmission with final drive mechanisms.

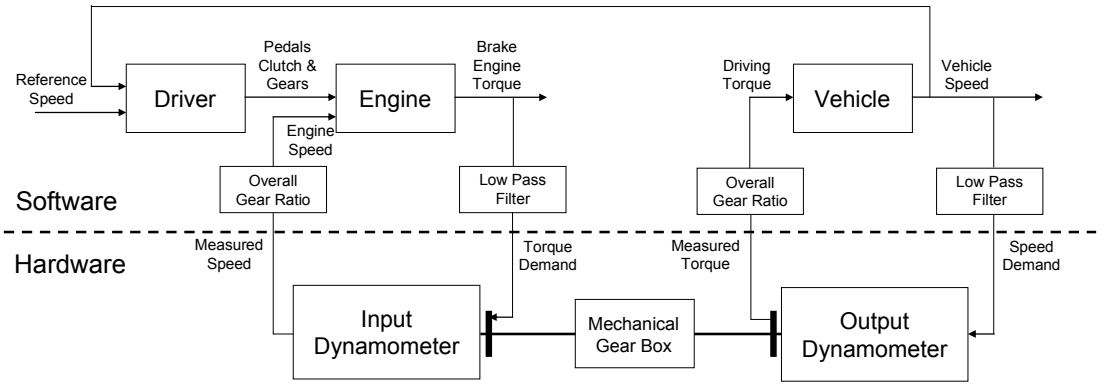

Figure 5-11 HIL testing structure

Since the clutch and transmission components were removed from the real time model, tests were carried out with a period of the speed profile when there is no operation on the gear lever and clutch, i.e. fixed overall ratio between the engine and wheels. Tests were carried out between 136 s and 176 s of the EUDC driving cycle, when the engine and vehicle models are running on third gear and the clutch is fully engaged. The speed profile contains typical acceleration, steady speed and deceleration processes.

The output dynamometer speed control test results are shown in Figure 5-12, and three magnified views are shown in Figure 5-13, while the input dynamometer torque control test results are shown Figure 5-14 and three magnified views are shown in Figure 5-15. Because of the use of low pass filters, there are phase shifts between the outputs of the real time models and the dynamometer demands for both speed and torque control. The outputs of the engine and vehicle models are shown by solid lines. After low pass filter, the dynamometer demands are shown by dotted lines and the dynamometer responses are shown by dashed lines.

It can be seen that both speed and torque responses of the dynamometers are very noisy. The fluctuations are even more significant than the errors introduced by the low pass filters. However, phase shifts are still observed between the dynamometer responses and the real time model outputs. Since the simulated vehicle speed is quite smooth, the phase shift is more obvious on the output dynamometer speed control. Actually, because of the large mass of the vehicle and the damping in the tyres, the vehicle model will have low pass filter behaviours, which will not response to the noises in the torque signal. Meanwhile the simulated engine brake torque is much noisier than the vehicle speed, which makes the phase shift even less significant. For example, the input dynamometer torque response between 164 s and 166 s shown in Figure 5-15 can be considered to closely follow the simulated engine brake torque.

Apart from the phase shifts introduced by the low pass filters, the dynamometer responses are successfully controlled to track the filtered real time model outputs without any phase shifts which can be seen in Figures 5-13 and 5-15.

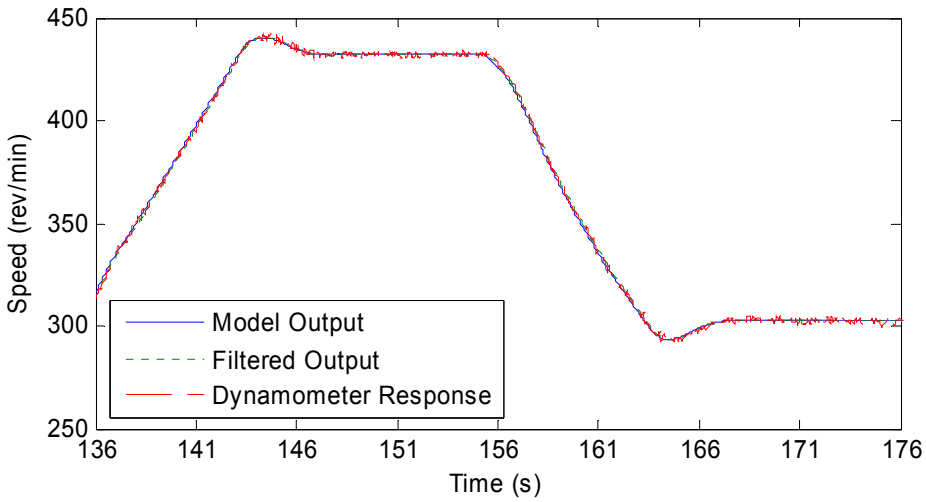

Figure 5-12 HIL output dynamometer speed control results

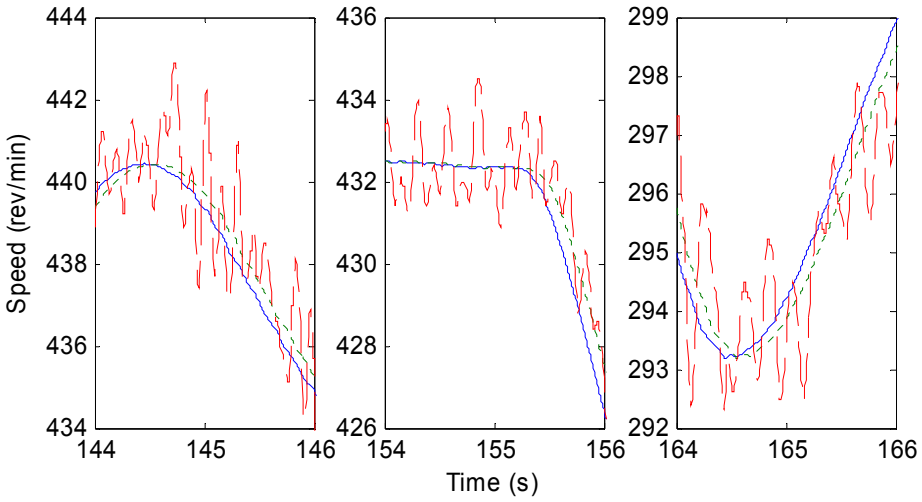

Figure 5-13 magnified views of Figure 5-12

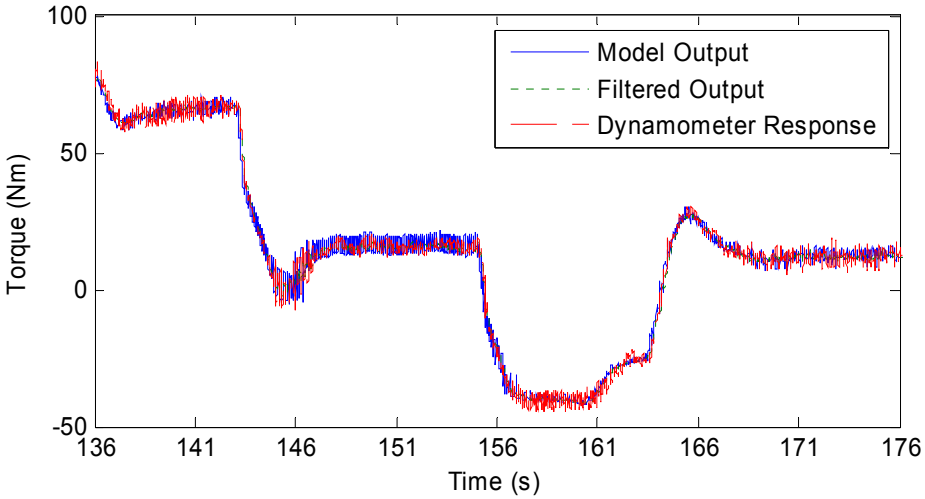

Figure 5-14 HIL input dynamometer torque control results

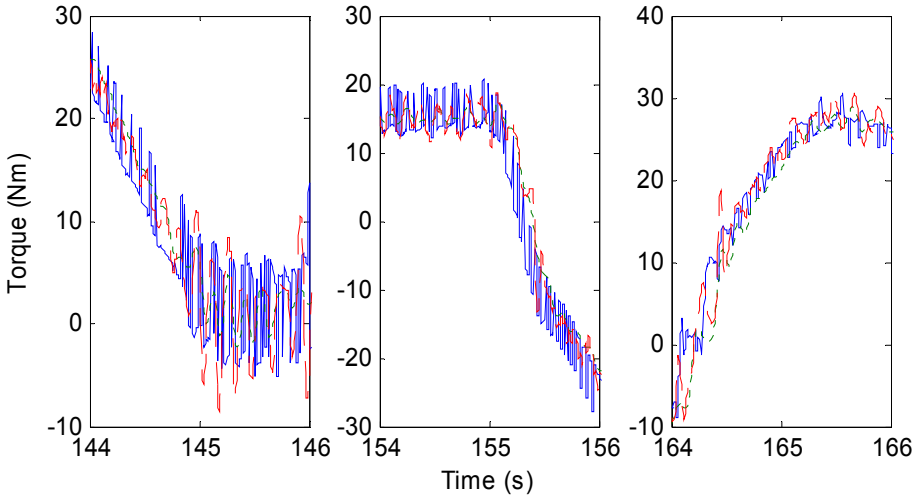

Figure 5-15 Magnified views of Figure 5-14

As discussed in Section 4.3.2, additional PID controllers may further improve the compensation results. Therefore, further tests were carried out with additional PID controllers for both input and output dynamometers. The control errors are derived from the dynamometer responses and the real time model outputs as the inputs of the PID controllers. The same PID parameters are used here as in Section 4.3.2. The proportional, integral and derivative gains are 0.08, 0.4 and 0 for the output dynamometer speed control and 0.03, 0.3 and 0 for the input dynamometer torque control.

The output dynamometer speed control results are shown in Figure 5-16, and three magnified views are shown in Figure 5-17, while the input dynamometer torque control results are shown in Figure 5-18 and three magnified views are shown in Figure 5-19. Compared with the magnified views shown in Figures 5-13 and 5-15, phase responses are further improved for both speed and torque control, e.g. between 164 s and 166 s for the speed control and between 154 s and 156 s for the torque control. There is no obvious change in the speed amplitude with additional PID controller. The torque amplitude is sometimes slightly worse than before, e.g. between 164 s and 166 s shown in Figures 5-15 and 5-19. The control errors are made within +/- 3 rev/min for the output dynamometer speed control and +/- 5 Nm for the input dynamometer torque control. Therefore, the use of additional PID controllers is reasonable in this case. Except for the noises in the measured speed and torque signals, the input and output dynamometer responses are controlled to follow the simulation results of the real time engine and vehicle models.

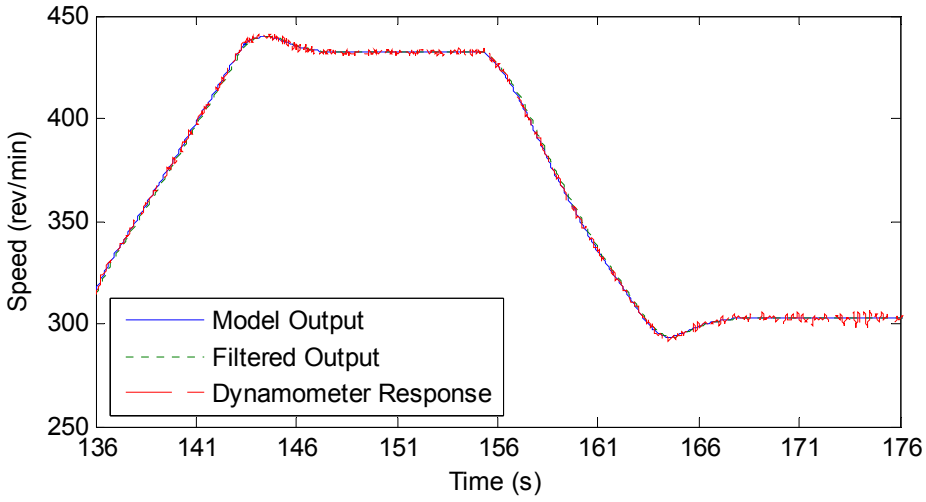

Figure 5-16 HIL output dynamometer speed control with additional PID

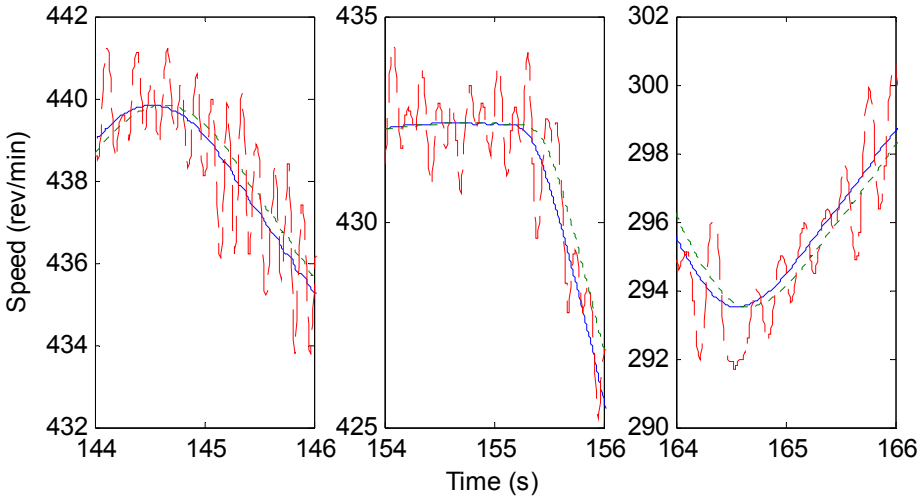

Figure 5-17 Magnified views of Figure 5-16

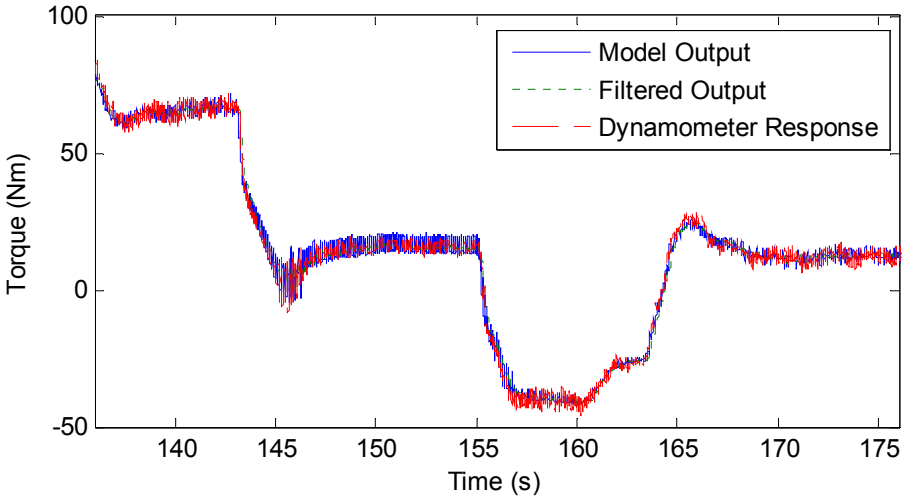

Figure 5-18 HIL input dynamometer torque control with additional PID

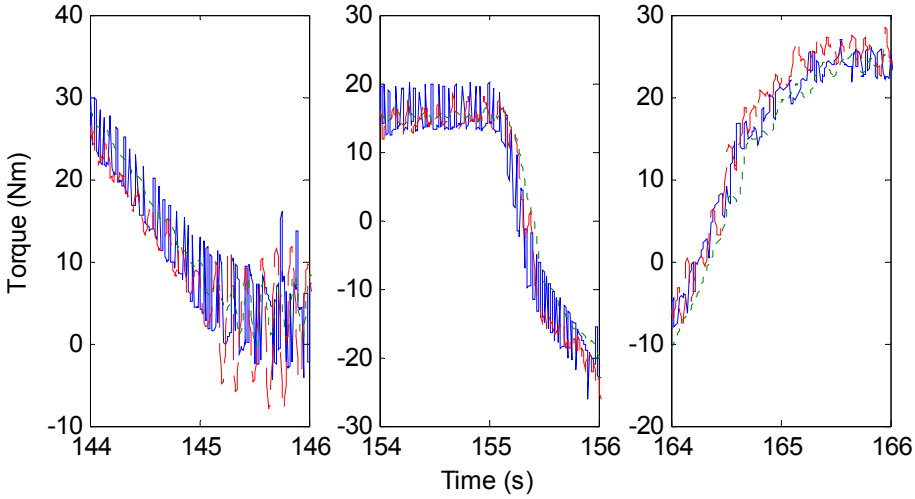

Figure 5-19 Magnified views of Figure 5-18

Chapter 6 Conclusions

In this chapter conclusion is drawn for the programme of research, and potential future work is also described.

6.1 Conclusions

In this programme of research, a hardware in the loop test facility has been developed for automotive powertrains, with a particular interest in testing CVTs. Two electric motors were utilized to substitute the real engine and vehicle and test CVTs installed in between. In order to provide the same testing environment as in a real engine and vehicle, real-time engine and vehicle models can be employed to demand virtual driving torque and vehicle speed from the dynamometers. In this thesis, digital controllers were designed for the input and output dynamometers to accurately track these demands

A feedforward control scheme based on the input-output inverse technique was employed to achieve a perfect tracking. First of all, linearized system models for the original plant were identified. Since there were unstable zeros in the identified models, direct inversion was not possible. Among the reviewed literature, ZPETC was used as the initial design of the feedforward controller to achieve zero phase shift for all frequencies. Then the design of the feedforward controller mainly focused on four aspects: (a) the further improvement of gain characteristics, (b) the optimal design, (c) the causality and (d) the enhancement of robustness to parameter variations.

For the first two aspects, a digital preview filter (DPF) was designed to approximate the inverse of the unstable zeros. The gain characteristics were improved by adding more zeros into the controllers. A penalty function was formulated within the desired frequency range and minimized by Lagrange method.

Since the DPF was non-causal, to implement it, future information of the input trajectory was required, which can not be provided by the real-time model in advance during the test. Causal application of DPFs was realized by adding manual delays into the feedback loop. Using system identification techniques, transfer functions with small relative orders were identified for the delayed systems in order to reduce the number of the preview steps required to invert the stable part of the transfer functions. As long as the total number of the preview steps required in the feedforward controller was designed to be equal to the total number of delays between the measured and delayed system responses, the feedforward controller can be implemented causally.

The designed feedforward controllers possess certain dynamics and will fail to compensate for the plant dynamics when there are external disturbances or changes in the plant parameters, especially for the output dynamometer speed control. The robustness of the feedforward controller was improved by maintaining the dynamics of the original plant in an adaptive manner. When the two dynamometers were coupled, torque generated by the input dynamometer was compensated for the output dynamometer by demanding additional torque from the output dynamometer. An additional controller was also designed for the output dynamometer speed control system to retain the original load characteristics, when the gear ratio is changed.

The designed feedforward controllers were tested and verified experimentally by using a manual gearbox before recommending its use for a CVT testing. A multi-frequency test signal as well as simulation results of a whole vehicle model were used as torque and speed demand signals in the experiments. A HIL case was also presented. Frequency and time domain results showed the effectiveness of the feedforward controllers under both testing procedures to fully compensate for the dynamics of both actuators.

6.2 Future Work

In this project, the proposed control scheme was tested and verified by using a manual gear box, because of the lack of technical information and support on the CVT. To test the available CVT with varying gear ratios, CAN bus communication

needs to be set up between the CVT ECU and the engine ECU, where the CVT can gather information about the driving condition and determine the optimal gear ratio. To set up the communication, real-time engine and ECU models with a proper level of simulation complexity are required. The models need to provide all the required interfaces to the CVT ECU. Alternatively, the engine ECU can exist in the hardware form and interface with real-time engine model and the CVT ECU.

The design of the feedforward controller in this project was based on the trial of adding different delays to the feedback loop and estimating the transfer functions with low relative orders. Generally speaking, the feedforward controller would offer better performance with more future values, which means more delays needed to be added to the feedback loop to make the feedforward controller causal. But adding more delay may make the feedback control unstable, and also may not give good fit when estimating the transfer function. Hence, future work is required to find an optimal number of manual delays added to the feedback loop and optimal orders for the numerator and denominator of the estimated transfer functions, to offer the best fit and at the same time the best compensation.

References

[1] L.Fel, "Development of the Ball Toroidal Continuously Variable Transmission," *SAE Technical Paper 981479*, 1998.

[2] Y.Ono, M.Goto, R.Yamashita, Y.Hasuda, and S.Yasuhara, "The Durability and Reliability of Variators for a Dual-cavity Full-toroidal CVT," *SAE Technical Paper 2000-01-0826*, 2000.

[3] H.Aitzetmüller, "Steyr S-Matic~The future CVT system," *SAE Technical Paper 2000-05-0129*, 2000.

[4] P.Kanphet, P.Jirawattana, and B.Direcksataporn, "Optimal Operation and Control of a Hydrostatic CVT Powertrain," *SAE Technical Paper 2005-01-1467*, 2005.

[5] C.J.Brace, M.Deacon, N.D.Vaughan, R.W.Horrocks, and C.R.Burrows, "An Operation Point Optimizer for the Design and Calibration of an Integrated Diesel/Continuously variable Transmission Powertrain," *Proceedings of the Institution of Mechanical Engineers. Part D, Journal of Automobile Engineering*, vol. 213 1999.

[6] K.Osamura, H.Itoyama, and H.Iwano, "Study of an Integrated Diesel Engine-CVT Control Algorithm for Improving Drivability and Exhaust Emission Performance," *SAE Technical Paper 2001-01-3452*, 2001.

[7] S.Sakaguchi, E.Kimura, and K.Yamamoto, "Development of an Engine-CVT Integrated Control System," *SAE Technical Paper 1999-01-0754*, 1999.

[8] T.Kim and H.Kim, "Performance of Integrated Engine-CVT Control Considering Powertrain Loss and CVT Response Lag," *Proceedings of the Institution of Mechanical Engineers. Part D, Journal of Automobile Engineering*, vol. 216 2002.

[9] K.Osamura, H.Itoyama, and H.Iwano, "Improvement of Drive Torque Response by Applying an Integrated Control Algorithm for a Diesel Engine and CVT," *JSAE Review 22*, 2001.

[10] M.Yasuoka, M.Uchida, S.Katakura, and T.Yoshino, "An Integrated Control Algorithm for an SI Engine and a CVT," *SAE Technical Paper 1999-01-0752*, 1999.

[11] S.Takahashi, "Fundamental Study of Low Fuel Consumption Control Scheme Based on Combination of Direct Fuel Injection Engine and Continuously Variable Transmission," 1998.

[12] S.Liu and B.Paden, "A Survey of Today's CVT Controls," 1997.

[13] M.A.Kluger and D.M.Long, "An Overview of Current Automatic, Manual and Continuously Variable Transmission Efficiencies and Their Projected Future Improvements," *SAE Technical Paper 1999-01-1259*, 1999.

[14] F.Sluis, T.Dongen, G.Spijk, A.velde, and A.Heeswijk, "Efficiency Optimization of the Pushbelt CVT," *SAE Technical Paper 2007-01-1457*, 2007.

[15] R.Kataoka, K.Okubo, T.Fujii, and S.Kanehara, "A Study on a Metal Pushing V-belt type CVT - A Novel Approach to Characterize the Friction Between Blocks and a Pulley, and Shifting Mechanisms," *SAE Technical Paper 2002-01-0697*, 2002.

[16] H.Nishizawa, H.Yamaguchi, H.Suzuki, M.Osawa, K.Iwatuki, and Y.Oshiumi, "Friction Characteristics Analysis for Clamping Force Setup in Metal V-Belt Type CVT," *SAE Technical Paper 2005-01-1462*, 2005.

[17] H.Yamaguchi, H.Nishizawa, H.Suzuki, K.Iwatuki, and K.Hoshiya, "Development of Belt Saturation Detection Method for V-Belt Type CVT," *SAE Technical Paper 2004-01-0479*, 2004.

[18] H.Lee and H.Kim, "Analysis of Primary and Secondary Thrusts for A Metal Belt CVT Part 1: New Formula for Speed Ratio-Torque-Thrust Relationship Considering and Tension and Block Compression," *SAE Technical Paper 2000-01-0841*, 2000.

[19] S.Akehurst, D.A.Parker, and N.D.Vaughan, "Potential for Fuel Economy Improvements by Reducing Frictional Losses in a Pushing Metal V-Belt CVT," *SAE Technical Paper 2004-01-0481*, 2004.

[20] M.Drogen and M.Laan, "Determination of Variator Robustness Under Macro Slip Conditions for a Push Belt CVT," *SAE Technical Paper 2004-01-0480*, 2004.

[21] T.Saito and A.D.Lewis, "Development of a Simulation Technique for CVT Metal Pushing V-Belt with Feedback Control," *SAE Technical Paper 2004-01-1326*, 2004.

[22] A.Ohashi, Y.Sato, K.Kajikawa, S.Sakuma, J.Urano, M.Yamaguchi, and A.Shibahara, "Development of High-efficiency CVT for Luxury Compact Vehicle," *SAE Technical Paper 2005-01-1019*, 2005.

[23] H.Takahara, H.Yasue, R.Habuchi, T.Ishihara, S.Tsuzuki, and J.Maeda, "Continuously Variable Transmission Control System for Toyota Intelligent Idling Stop System," *SAE Technical Paper 2004-01-1635*, 2004.

[24] T.H.Bradley, B.R.Huff, and A.A.Frank, "Energy Consumption Test Methods and Results for Servo-Pump Continuously Variable Transmission Control System," *SAE Technical Paper 2005-01-3782*, 2005.

[25] E.A.Solik, A.A.Frank, and P.A.Erickson, "Design Improvements on a Vee Belt CVT and Application to a New In-line CVT Concept," *SAE Technical Paper 2005-01-3459*, 2005.

[26] J.Jantos, "Control of the Transmission Ratio Derivative in Passenger Car Powertrain with CVT," *SAE Technical Paper 2001-01-1159*, 2001.

[27] A.F.A.Serrarens, S.Shen, and F.E.Veldpaus, "Control of a Flywheel Assisted Driveline with Continuously Variable Transmission," *Journal of Dynamic System, Measurement, and Control*, 2003.

[28] J.E.Mahoney, J.M.Maguire, and S.Bai, "Ratio Changing the Continuously Variable Transmission," *SAE Technical Paper 2004-01-1634*, 2004.

[29] A.F.A.Serrarens and F.E.Veldpaus, "Powertrain Control of a Flywheel Assisted Driveline with CVT," *Proceedings of the International Congress on Continuously Variable Transmissions, Eindhoven (1999)*, 1999.

[30] V.Wicke, C.J.Brace, M.Deacon, and N.D.Vaughan, "Preliminary Results from Driveability Investigations of Vehicles with Continuously Variable Transmission," *Int. Congress on Continuously Variable Power Transmission CVT'99*, 1999.

[31] D.Patel, J.Ely, and M.Overson, "CVT Drive Research Study," *SAE Technical Paper 2005-01-1459*, 2005.

[32] D.F.Pick, D.Yuan D.Wang, R.W.Proctor, and D.Patel, "Dead Pedal and the Perception of Performance of a Continuously Variable Transmission," *SAE Technical Paper 2005-01-1596*, 2005.

[33] V.Wicke, C.J.Brace, and N.D.Vaughan, "The Potential for Simulation of Driveability of CVT Vehicles," *SAE Technical Paper 2000-01-0830*, 2000.

[34] K.Abo, M.Kobayashi, and M.Kurosawa, "Development of a Metal Belt-Drive CVT Incorporating a Torque Converter for Use with 2-Liter Class Engines," *SAE Technical Paper 980823*, 1998.

[35] M.S.Castiglione, G.Stecklein, R.Senseney, and D.Stark, "Development of Transmission Hardware-in-the-loop Test System," *SAE Technical Paper 2003-01-1027*, 2003.

[36] A.Wagener, H.Kabza, C.Koerner, and P.Seger, "Model-based Drivetrain Development and Rapid Prototyping For a Hybrid Electric Car," *Automotive and Transportation Technology Congress and Exhibition*, 2001.

[37] M.Adenmark, M.Deter, and T.Schulte, "Testing Networked ECUs in a HIL Based Integration Lab," *SAE Technical Paper 2006-01-3495*, 2006.

[38] A.Wanpal, M.G.Babu, and N.Kankariya, "ECU Testing and Verification Using Hardware-in-the-Loop," *SAE Technical Paper 2006-01-1444*, 2006.

[39] M.B.Ganesh, "Hardware in the Loop Simulation (HIL) for Vehicle Electronics Systems Testing and Validation," *SAE Technical Paper 2005-26-304*, 2005.

[40] J.Gehring and H.Schutte, "A Hardware-in-the-Loop Test Bench for Validation of Complex ECU Networks," *SAE Technical Paper 2002-01-0801*, 2002.

[41] S.Kohl and D.Jegminat, "How to Do Hardware-in-the-Loop Simulation Right," *SAE Technical Paper 2005-01-1657*, 2005.

[42] P.J.Gawthrop, D.W.Virden, S.A.Neild, and D.J.Wagg, "Emulator-based Control for Actuator-based Hardware-in-the-Loop Testing," *Control Engineering Practice*, vol. 16, no. 8, pp. 897-908, 2008.

[43] M.Velardocchia and A.Sorniotti, "Hardware-in-the-Loop to Evaluate Active Braking Systems Performance," *SAE Technical Paper 2005-01-1580*, 2005.

[44] W.E.Misselhorn, N.J.Theron, and P.S.Els, "Investigation of Hardware-in-the-Loop for Use in Suspension Development," *Vehicle System Dynamics*, vol. 44, no. 1, pp. 65-81, 2006.

[45] A.Blakeborough, M.S.Williams, A.P.Darby, and D.M.Williams, "The Development of Real-Time Substructure Testing," *Philosophical Transactions: Mathematical, Physical and Engineering Sciences*, vol. 359, no. 1786, pp. 1869-1891, 2001.

[46] A.P.Darby, M.S.Williams, and A.Blakeborough, "Stability and Delay Compensation for Real-Time Substructure Testing," *Journal of Engineering Mechanics*, vol. 128, no. 12, pp. 1276-1284, 2002.

[47] M.Tomizuka, "Zero Phase Error Tracking Algorithm for Digital Control," *Journal of Dynamic Systems, Measurement and Control*, vol. 109, no. 1, pp. 65-68, 1987.

[48] J.A.Butterworth, L.Y.Pao, and D.Y.Abramovitch, "The Effect of Nonminimum-phase Zero Locations on the Performance of Feedforward Model-inverse Control Techniques in Discrete-time Systems," *2008 American Control Conference*, 2008.

[49] B.Haack and M.Tomizuka, "The Effect of Adding Zeros to Feedforward Controllers," *Journal of Dynamic Systems, Measurement and Control*, vol. 113, no. 1, pp. 6-10, 1991.

[50] C.Menq and J.Chen, "Precision Tracking Control of Discrete Time Nonminimum-Phase Systems," *Journal of Dynamic Systems, Measurement and Control*, vol. 115, no. 2A, pp. 238-245, 1993.

[51] J.Z.Xia and C.Menq, "Precision Tracking Control of Non-minimum Phase Systems with Zero Phase Error," *International Journal of Control*, vol. 61, no. 4, pp. 791-807, 1995.

[52] S.Yeh and P.Hsu, "An Optimal and Adaptive Design of the Feedforward Motion Controller," *IEEE/ASME Transactions on Mechatronics*, vol. 4, no. 4, pp. 428-439, 1999.

[53] E.Gross, M.Tomizuka, and W.Messner, "Cancellation of Discrete Time Unstable Zeros by Feedforward Control," *Journal of Dynamic Systems, Measurement and Control*, vol. 116, no. 1, pp. 33-38, 1994.

[54] E.Gross and M.Tomizuka, "Experimental Flexible Beam Tip Tracking Control with a Truncated Series Approximation to Uncancelable Inverse Dynamics," *IEEE Transactions on Control Systems Technology*, vol. 2, no. 4, pp. 382-391, 1994.

[55] B.Choi and C.Choi, "A Feedforward Controller by Modified Series Approximation," *IEEE/ASME Transactions on Mechatronics*, vol. 3, no. 3, pp. 249-251, 1998.

[56] D.Torfs, J.Swevers, and J.De Schutter, "Quasi-perfect Tracking Control of Non-minimal Phase Systems," *Proceedings of the 30th Conference on Decision and Control*, 1991.

[57] D.Torfs, J.De Schutter, and J.Swevers, "Extended Bandwidth Zero Phase Error Tracking Control of Nonminimal Phase Systems," *Journal of Dynamic Systems, Measurement and Control*, vol. 114, no. 3, pp. 347-351, 1992.

[58] M.M.Mustafa, "Trajectory-adaptive Digital Tracking Controllers for Non-minimum Phase Systems without Factorisation of Zeros," *IEE Proceedings: Control Theory and Applications*, vol. 149, no. 2, pp. 157-162, 2002.

[59] M.Yamada, Y.Funahashi, and S.Fujiwara, "Zero Phase Error Tracking System with Arbitrarily Specified Gain Characteristics," *Journal of Dynamic System, Measurement, and Control*, vol. 119, no. 2, pp. 260-264, 1997.

[60] M.Yamada, Y.Funahashi, and Z.Riadh, "Generalized Optimal Zero Phase Error Tracking Controller Design," *Journal of Dynamic Systems, Measurement and Control*, vol. 121, no. 2, pp. 165-170, 1999.

[61] G.Marro and L.Marconi, "Using the Diophantine Equation in the Design of a Digital Perfect Tracking Compensator," *Proceedings of 16th Benelux Meeting on Systems and Control*, 1997.

[62] L.Marconi, G.Marro, and C.Melchiorri, "A Solution Technique for Almost Perfect Tracking of Non-minimum-phase, Discrete-time Linear System," *International Journal of Control*, vol. 74, no. 5, pp. 496-506, 2001.

[63] T.Tsao and M.Tomizuka, "Adaptive Zero Phase Error Tracking Algorithm for Digital Control," *Journal of Dynamic Systems, Measurement and Control*, vol. 109, no. 4, pp. 349-354, 1987.

[64] B.Widrow and M.Bilello, "Adaptive Inverse Control," *Proceedings of the 1993 IEEE International Symposium on Intelligent Control*, 1993.

[65] Y.Gu and M.Tomizuka, "Multi-rate Feedforward Tracking Control for Plants with Nonminimum Phase Discrete Time Models," *Proceedings of the American Control Conference*, vol. 6, pp. 4290-4294, 1999.

[66] C.R.Burrows and M.N.Sahinkaya, "Frequency-Domain Estimation of Linearized Oil-Film Coefficients," *ASME Joint Lubrication Conference*, 1981.

[67] M.N.Sahinkaya, M.O.T.Cole, and C.R.Burrows, "On the Use of Schroeder Phased Harmonic Sequences in Multi-Frequency Vibration Control of Flexible Rotor/Magnetic Bearing Systems," *8th International Symposium on Magnetic Bearings*, 2002.

[68] M.R.Schroeder, "Synthesis of Low-Peak-Factor Signals and Binary Sequences with Low Autocorrelation," *IEEE Transactions on Information Theory*, 1969.

[69] T.Tsao, "Optimal Feed-Forward Digital Tracking Controller Design," *Journal of Dynamic System, Measurement, and Control*, vol. 116, no. 4, pp. 583-592, 1994.

[70] M.M.Mustafa, N.R.Yaacob, and N.A.Nik Mohamed, "Adaptive Zero-Phase Error-Tracking Controller with Advanced Learning," *Control and Intelligent Systems*, vol. 32, no. 2, pp. 116-125, 2004.